

INVESTIGATION OF THE ELECTROMAGNETIC PROPERTIES OF SINGLE
WALLED CARBON NANOTUBE THIN FILMS

A THESIS SUBMITTED TO
THE GRADUATE SCHOOL OF NATURAL AND APPLIED SCIENCES
OF
MIDDLE EAST TECHNICAL UNIVERSITY

BY

ŞEYDA KÜÇÜKYILDIZ

IN PARTIAL FULFILLMENT OF THE REQUIREMENTS
FOR
THE DEGREE OF MASTER OF SCIENCE
IN
METALLURGICAL AND MATERIALS ENGINEERING

JULY 2013

Approval of the thesis:

**INVESTIGATION OF THE ELECTROMAGNETIC PROPERTIES OF SINGLE
WALLED CARBON NANOTUBE THIN FILMS**

submitted by **ŞEYDA KÜÇÜKYILDIZ** in partial fulfillment of the requirements for the degree of **Master of Science in Metallurgical and Materials Engineering Department, Middle East Technical University** by,

Prof. Dr. Canan ÖZGEN

Dean, Graduate School of **Natural and Applied Sciences**

Prof. Dr. Cemil Hakan GÜR

Head of Department, **Metallurgical and Materials Engineering**

Assoc. Prof. Dr. Arcan Fehmi DERİCİOĞLU

Supervisor, **Metallurgical and Materials Eng. Dept., METU**

Assoc. Prof. Dr. Hüsnü Emrah ÜNALAN

Co-Supervisor, **Metallurgical and Materials Eng. Dept., METU**

Examining Committee Members:

Prof. Dr. Tayfur ÖZTÜRK

Metallurgical and Materials Engineering Dept., METU

Assoc. Prof. Dr. Arcan Fehmi DERİCİOĞLU

Metallurgical and Materials Engineering Dept., METU

Prof. Dr. Cemil Hakan GÜR

Metallurgical and Materials Engineering Dept., METU

Assist. Prof. Dr. Yunus Eren KALAY

Metallurgical and Materials Engineering Dept., METU

Assoc. Prof. Dr. Ali ÇIRPAN

Chemistry Dept., METU

Date: 12.07.2013

I hereby declare that all information in this document has been obtained and presented in accordance with academic rules and ethical conduct. I also declare that, as required by these rules and conduct, I have fully cited and referenced all material and results that are not original to this work.

Name, Last Name: Şeyda KÜÇÜKYILDIZ
Signature :

ABSTRACT

INVESTIGATION OF THE ELECTROMAGNETIC PROPERTIES OF SINGLE WALLED CARBON NANOTUBE THIN FILMS

Küçükyıldız, Şeyda

M.Sc., Department of Metallurgical and Materials Engineering

Supervisor: Assoc. Prof. Dr. Arcan Fehmi Dericioğlu

Co-Supervisor: Assoc. Prof. Dr. Hüsnü Emrah Ünalın

July 2013, 82 Pages

The work presented in this thesis can be divided in two parts. First part discusses the dispersion and deposition routes of single walled carbon nanotube (SWNT) thin films. Two different types of SWNTs and several dispersing agents were examined to achieve a homogeneous SWNT solution. A tip-sonicator and an ultrasonic bath was compared and it has been found that tip-sonicator increases the efficiency of SWNT dispersions. Vacuum filtration and spray coating techniques were utilized for the deposition of SWNT thin films. Optoelectronic properties of the films were examined for different SWNT densities. Moreover, SWNT thin film functionalization with acid treatment was investigated in order to improve the electrical conductivities of the thin films. Centrifugation of SWNT solutions provided higher optical transmittance at a given wavelength of 550 nm and lower sheet resistance values. It has also been found that, 150 Ω/\square sheet resistance can be achieved at an optical transmittance of 90 % for SWNT thin films on glass substrates that were deposited via vacuum filtration method. The second part investigated the electromagnetic interference shielding properties of the SWNT films. For this purpose, glass fiber woven fabrics were coated with SWNT thin films by spray coating method. Different densities of SWNT films were investigated and the electromagnetic wave reflection and transmission values were analyzed through the utilization of free-space method within a frequency range of 18 – 40 GHz. Our results indicated that the electromagnetic wave reflection properties of the samples were not satisfactory despite their conductivities within the investigated frequency range.

Keywords: single walled carbon nanotube thin films, spray-coating, vacuum filtration method, free-space method, glass fiber woven fabrics.

ÖZ

KARBON NANOTÜP İNCE FİLMLERİN ELEKTROMAGNETİK ÖZELLİKLERİNİN İNCELENMESİ

Küçükyıldız, Şeyda

Yüksek Lisans, Metalurji ve Malzeme Mühendisliği Bölümü

Tez Yöneticisi: Doç. Dr. Arcan Fehmi Dericioğlu

Ortak Tez Yöneticisi: Doç. Dr. Hüsnü Emrah Ünal

Temmuz 2013, 82 Sayfa

Bu tez çalışması iki bölümden oluşmaktadır. İlk bölüm, tek duvarlı karbon nanotüp (KNT) çözeltilerinin hazırlanması ve tek duvarlı KNT ince filmlerin oluşturulmasını incelemektedir. Homojen bir KNT çözeltisi elde edebilmek için, iki farklı tip tek duvarlı KNT ve farklı yüzey aktif madde kombinasyonları denenmiştir. Uç tipi karıştırıcı ve ultrasonic banyo yöntemleri karşılaştırılmış ve uç tipi karıştırıcının KNT çözelti kalitesini arttırdığı gözlenmiştir. KNT ince filmlerin üretiminde vakum filtrasyon ve spreyle kaplama yöntemleri kullanılmıştır. Farklı KNT yoğunluklarında hazırlanan filmlerin optoelektronik özellikleri incelenmiştir. Bunlara ek olarak, asit banyolarının KNT ince filmlerin elektriksel iletkenliklerine olan etkisi araştırılmıştır. Santrifüj uygulanan KNT çözeltileri ile hazırlanan filmlerin 550 nm dalga boyunda daha düşük düzlemsel direnç değerlerine karşılık daha yüksek optik geçirgenlik sağladığı gözlenmiştir. Cam altlık üzerine vakum filtrasyon yöntemi ile kaplanan bir KNT ince film % 90 optik geçirgenlikte, $150 \Omega/\square$ düzlemsel direnç değerine sahiptir. Vakum filtrasyon ve spreyle kaplama yöntemlerinin her ikisi de, farklı altlıklar üzerinde geniş yüzey alanlarının kaplanmasında kullanılmıştır. Bu çalışmanın ikinci amacı, tek duvarlı KNT ince filmlerin elektromagnetik özelliklerinin incelenmesidir. Spreyle kaplama yöntemi kullanılarak, cam fiber dokumaların yüzeylerinde KNT filmler oluşturulmuştur. Farklı yoğunluklarda hazırlanan KNT filmlerin elektromagnetik dalga yansıtma ve geçirim özellikleri serbest uzay yöntemi kullanılarak 18 – 40 GHz frekans aralığında incelenmiştir. Sonuçlara göre, elektriksel iletkenliklerine rağmen KNT film kaplanmış cam fiber dokumaların elektromagnetik dalga yansıtma özellikleri gelişmemiştir.

Anahtar kelimeler: tek duvarlı karbon nanotüp ince filmler, spreyle kaplama yöntemi, vakum filtrasyon yöntemi, serbest-uzay yöntemi, SiC-bazlı dokumalar.

To My Precious Family...

ACKNOWLEDGEMENTS

This graduate study was financed by METU-BAP under the contact number of BAP-03-08-2011-004. Also, I want to acknowledge TÜBİTAK for their financial support in the last year of the study.

I would like to thank my advisor Assoc. Prof. Dr. Arcan Fehmi Dericiođlu for his support throughout the whole time I have worked on this project and I would like to express my gratitude to Assoc. Prof. Dr. Hüsnu Emrah Ünalan for giving me the opportunity to occupy all the facilities in NANOLAB and for his invaluable encouragement, advice and guidance throughout the research. I feel so lucky to have met those great advisors and have the opportunity to work with them.

I am deeply thankful to my lab-mates and my dearest friends Şahin Coşkun, Elif Selen Ateş, Ayşegül Afal, Barış Özdemir, Burcu Aksoy, Emre Mülazımođlu and Recep Yüksel for their infinite support and kindness. I also appreciate the great moral support and patience from Ayşe Merve Genç, Tuba Demirtaş, Güher Kotan, Evren Tan and Başak Aysin. I can never forget the time we had together. Besides being wonderful friends, all these brilliant people have an extra mission like being my personal life coaches when it is appropriate. Without their friendship, the research period would have been a complete disaster. I especially want to mention and thank Anıl Kantarcıođlu for giving me the strength to keep going at the hardest times. Thank you for always being there for me.

Finally, I would like to thank my mom and dad for their infinite love and support over the years. They were the best and I owe so much to them. Thank you for everything...

TABLE OF CONTENTS

| | |
|------------------------|------|
| ABSTRACT..... | v |
| ÖZ..... | vi |
| ACKNOWLEDGEMENTS..... | viii |
| TABLE OF CONTENTS..... | ix |
| LIST OF TABLES..... | xii |
| LIST OF FIGURES..... | xiii |

CHAPTERS

| | |
|--|----|
| 1. INTRODUCTION..... | 1 |
| 2. SINGLE WALLED CARBON NANOTUBE THIN FILMS..... | 3 |
| 2.1. Introduction..... | 3 |
| 2.1.1. Carbon Allotropes..... | 3 |
| 2.1.2. Carbon Nanotubes..... | 5 |
| 2.1.2.1. Multi Walled Carbon Nanotubes (MWNTs)..... | 6 |
| 2.1.2.2. Single Walled Carbon Nanotubes (SWNTs)..... | 6 |
| 2.1.3. SWNT Synthesis..... | 10 |
| 2.1.3.1. Arc Discharge..... | 10 |
| 2.1.3.2. Laser Ablation..... | 11 |
| 2.1.3.3. Chemical Vapor Deposition (CVD)..... | 12 |
| 2.1.4. Potential Applications of SWNTs..... | 12 |
| 2.1.5. Properties of SWNT Thin Films..... | 13 |
| 2.1.6. SWNT Thin Film Fabrication..... | 16 |
| 2.1.6.1. Dispersion..... | 17 |
| 2.1.6.2. Deposition..... | 20 |
| 2.1.6.2.1. Dip Coating..... | 20 |
| 2.1.6.2.2. Spray Coating..... | 21 |
| 2.1.6.2.3. Spin Coating..... | 23 |

| | |
|---|----|
| 2.1.6.2.4. Vacuum Filtration..... | 24 |
| 2.1.7. Applications of SWNT Thin Films | 26 |
| 2.2. Experimental Details | 27 |
| 2.2.1. SWNT Thin Film Fabrication | 27 |
| 2.2.2.1. Substrate Cleaning..... | 27 |
| 2.2.2.2. Vacuum Filtration Method | 28 |
| 2.2.1.2.1. Dispersion of SWNTs | 28 |
| 2.2.1.2.2. Deposition Process | 28 |
| 2.2.2. Post Deposition Acid Treatments..... | 28 |
| 2.2.3. Spray Coating Method | 30 |
| 2.3. Characterization Methods..... | 30 |
| 2.3.1. Scanning Electron Microscope (SEM)..... | 30 |
| 2.3.2. Optical Transmittance Measurements | 31 |
| 2.3.3. Sheet Resistance Measurements..... | 31 |
| 2.4. Results | 32 |
| 2.4.1. Effect of Sonication..... | 32 |
| 2.4.2. Effect of SWNT Type | 32 |
| 2.4.3. Effect of Density | 34 |
| 2.4.4. Effect of Surfactant | 37 |
| 2.4.5. Effect of Post Deposition Treatments | 38 |
| 2.4.6. Effect of Centrifugation..... | 39 |
| 2.4.7. Large Area Applications | 42 |
| 2.4.8. Mechanical Stability of SWNT Thin Films..... | 43 |
| | |
| 3. CHARACTERIZATION OF ELECTROMAGNETIC PROPERTIES OF SWNT FILM COATED GLASS FIBER WOVEN FABRICS..... | 45 |
| | |
| 3.1. Introduction | 45 |
| 3.1.1. Electromagnetic Waves..... | 45 |
| 3.1.1.1. Microwave Band Applications..... | 48 |
| 3.1.2. Electromagnetic Wave – Matter Interactions..... | 50 |
| 3.1.2.1. Shielding Theory | 50 |

| | |
|--|----|
| 3.1.2.2. Electromagnetic Loss Mechanisms..... | 51 |
| 3.1.2.2.1. Dielectric Loss | 52 |
| 3.1.2.2.2. Magnetic Loss | 54 |
| 3.1.2.2.3. Reflection Loss and Absorption Loss | 55 |
| 3.1.3. Characterization Methods of the EMI Shielding | 57 |
| 3.1.3.1. SOLT (Short- Open- Load- True) Calibration | 58 |
| 3.1.3.2. TRL (True- Reflect- Line) Calibration | 58 |
| 3.1.4. EMI Shielding Materials..... | 59 |
| 3.1.5. EM Wave Absorbing Materials | 60 |
| 3.2. Experimental Details | 62 |
| 3.2.1. General Procedure..... | 62 |
| 3.2.2. Spray Coating of SWNT Films | 63 |
| 3.2.3. Characterization Methods | 64 |
| 3.2.3.1. Scanning Electron Microscope (SEM) | 64 |
| 3.1.3.2. Free Space Technique | 64 |
| 3.3. Results | 66 |
| | |
| 4. CONCLUSIONS and FUTURE RECOMMENDATIONS | 71 |
| | |
| 4.1. Conclusions | 71 |
| 4.2. Future Recommendations..... | 72 |
| | |
| REFERENCES | 73 |

LIST OF TABLES

TABLES

| | |
|--|----|
| <u>Table 2.1.</u> The comparison between ITO and other alternative transparent conductors including CNT thin films [61]..... | 15 |
| <u>Table 3.1.</u> Radar bands and their application fields [109]..... | 48 |

LIST OF FIGURES

FIGURES

| | |
|---|----|
| <u>Figure 2.1.</u> (a) sp^3 , (b) sp^2 , (c) sp hybridized carbon atoms. | 3 |
| <u>Figure 2.2.</u> Models of carbon allotropes: (a) diamond, (b) graphite, (c) single walled carbon nanotube and (d) C_{60} fullerene [3] | 4 |
| <u>Figure 2.3.</u> Quantized and the continuous electron wave vectors, k_{\perp} and k_{\parallel} . Adopted from [10]..... | 5 |
| <u>Figure 2.4.</u> (a) Schematic of a MWNT, (b) a transmission electron microscopy (TEM) image of MWNTs [4, 12]... .. | 6 |
| <u>Figure 2.5.</u> Schematic representations of a SWNT and a chiral vector: (a) Graphene sheet rolled into a seamless tube [2]. (b) Illustrating the vectors a_1 and a_2 , the chiral vector C_h shown as OA, the translation vector T is shown as OT which is perpendicular to C_h and the wrapping angle θ . Also possible zigzag and armchair patterns are demonstrated [10].. .. | 8 |
| <u>Figure 2.6.</u> (a) Graphene network showing all the possible indices [15]. (b) Atomic structures of zigzag, armchair and chiral SWNTs. Taken from reference [16]..... | 8 |
| <u>Figure 2.7.</u> Band structures of SWNTs with indices (a) (5, 5), (b) (10, 0) and (c) (9, 0) (derived by zone-folding of the band structure of the graphene sheet) [3]..... | 9 |
| <u>Figure 2.8.</u> Schematic representation of an arc discharge set-up [19]..... | 10 |
| <u>Figure 2.9.</u> Schematic representation of a laser ablation set-up [20]..... | 11 |
| <u>Figure 2.10.</u> Schematic representation of the experimental set-up for CVD process [36]. ... | 11 |
| <u>Figure 2.11.</u> (a) Optical transmittance versus wavelength in the visible regions. The inset shows a SWNT thin film on a flexible substrate. (b) Sheet resistance versus optical transmittance at 550 nm wavelength for different nanotube densities [37]..... | 13 |
| <u>Figure 2.12.</u> Bending (a) and tensile (b) test results comparing SWNT thin films and ITO on PET substrates [60]..... | 14 |
| <u>Figure 2.13.</u> (a) Schematic representation of how surfactants may adsorb onto the SWNT surface [62]. (b) Hemispherical adsorption of surfactant micelles on energetically favorable positions on the SWNT. Additional schematic representation shows the hydrophilic and hydrophobic ends [66]. (c) Aqueous dispersions prepared by SDS, triton X-100, and NaDDBS [62]..... | 17 |

| | |
|---|----|
| <u>Figure 2.14.</u> Schematic representation of the debundling process via sonication and surfactant adsorption. Adopted from reference [68]..... | 18 |
| <u>Figure 2.15.</u> (a) Schematic illustration of the dip coating process. (b) Photograph of SWNT thin films after 1, 3, 5 and 10 dipping cycles. (c) Variation in optical transmittance and sheet resistance as a function of the number of coatings. Green line shows the results from NMP-SWNT solution, red line belongs to SDS aided SWNT dispersion and the black line represents the Triton x-100 dispersed SWNT solutions. Adopted from [75]..... | 20 |
| <u>Figure 2.16.</u> (a) Schematic illustration of the spray coating set-up. (b) Film thickness versus optical transmittance plot of spray coated SWNT networks [77]. (c) Resistivity versus optical transmittance plot for spray coated CNT networks and ITO [77]. (d) Spray coated SWNT thin film on glass substrate [77]..... | 21 |
| <u>Figure 2.17.</u> Schematic illustration of spin coating process..... | 22 |
| <u>Figure 2.18.</u> (a) Photograph of the filtration set-up utilized for the fabrication of SWNT thin films. (b) Schematic illustration of vacuum filtration process..... | 23 |
| <u>Figure 2.19.</u> Illustration of the film transfer process..... | 24 |
| <u>Figure 2.20.</u> SEM images of the SWNT thin films deposited on silicon substrates utilizing various concentrations and filtration volumes [15]..... | 25 |
| <u>Figure 2.21.</u> SWNT thin film fabrication process. (a) Sonication process. (b) SWNT solution after the dispersion step. (c) Vacuum filtration set-up and the SWNT network on MCE membrane. (d) Film transfer process. (e) Removal of the MCE membrane with acetone. (f) SWNT thin film deposited on glass substrate..... | 28 |
| <u>Figure 2.22.</u> SWNT thin film spray coating process..... | 29 |
| <u>Figure 2.23.</u> Schematic of the two probe sheet resistance measurement set up..... | 30 |
| <u>Figure 2.24.</u> Digital photographs of the SWNT solutions after (a) 3 hours of ultrasonic bath sonication and (b) 5 minutes of tip-sonication. Red circle on (a) indicates the aggregates formed by SWNT bundles..... | 31 |
| <u>Figure 2.25.</u> Sheet resistance vs. optical transmittance plot for P2 and P3 SWNT thin films. Lines are for visual aid..... | 32 |
| <u>Figure 2.26.</u> Photograph of SWNT thin films deposited on glass substrates by vacuum filtration method at the same concentration and five different filtration volumes..... | 33 |
| <u>Figure 2.27.</u> SEM images of the SWNT thin films prepared from filtration volumes of (a) 2.5 ml and (b) 12.5 ml..... | 34 |
| <u>Figure 2.28.</u> (a) Transmittance of the SWNT films prepared with different filtration volumes. (b) Sheet resistance vs. optical transmittance plot for SWNT thin films..... | 35 |

| | |
|---|----|
| <u>Figure 2.29.</u> Photograph of vials (10 ml) containing SDBS, SDS and Triton x-100 assisted SWNT dispersions taken 5 minutes after sonication..... | 36 |
| <u>Figure 2.30.</u> Sheet resistance vs. optical transmittance plot for the SWNT thin films prepared with different surfactants. Lines are for visual aid..... | 37 |
| <u>Figure 2.31.</u> Sheet resistance vs. optical transmittance plot for post deposition treated acid functionalized SWNT thin films. Lines are for visual aid.. | 38 |
| <u>Figure 2.32.</u> Improved optical transmittance data of the SWNT films deposited after centrifugation for four different filtration volumes..... | 39 |
| <u>Figure 2.33.</u> Sheet resistance vs. optical transmittance plot for various SWNT thin films. Lines are for visual aid..... | 39 |
| <u>Figure 2.34.</u> SEM images of the SWNT thin films deposited by vacuum filtration on glass from (a) centrifuged SWNT solution, (b) regular SWNT solution..... | 40 |
| <u>Figure 2.35.</u> Photographs of SWNT thin films deposited on 10 cm x 10 cm (a) glass and (b) PET substrates using vacuum filtration method. | 41 |
| <u>Figure 2.36.</u> Photographs of SWNT thin films deposited on 10 x 10 cm ² glass substrates using spray coating method. | 42 |
| <u>Figure 2.37.</u> Mechanical stability of SWNT films on PET substrates. (a) Sheet resistance vs. bending radius plot. ITO data was obtained from [103]. (b) SWNT thin film deposited on PET substrate. | 43 |
| <u>Figure 3.1.</u> Propagation of an EM wave at (a) near field and (b) far field. (c) Representation of transverse oscillating EM wave with the electric and magnetic field components [104].. | 46 |
| <u>Figure 3.2.</u> Electromagnetic spectrum [105]..... | 46 |
| <u>Figure 3.3.</u> Atmospheric window [106]..... | 47 |
| <u>Figure 3.4.</u> Interaction of electromagnetic radiation with the shielding material. Adopted from [112]. | 51 |
| <u>Figure 3.5.</u> (a) Polar dipoles and (b) their polarization in the presence of an electric field.. | 52 |
| <u>Figure 3.6.</u> Dielectric constant and loss dispersion of dielectric materials with respect to frequency [116]..... | 53 |
| <u>Figure 3.7.</u> Dipole configuration in the existence of an external magnetic field (H) for (a) diamagnetic materials and (b) paramagnetic materials..... | 54 |
| <u>Figure 3.8.</u> Free-space method set-up. | 57 |

| | |
|--|----|
| <u>Figure 3.9.</u> TRL calibration method (a) thru, (b) reflect and (c) line standards adopted from [130]. | 58 |
| <u>Figure 3.10.</u> Schematic of electromagnetic wave absorbing materials (a) Salisbury screens, (b) Dallenbach layer, (c) Jaumann absorbers and (d) performance of multi-layered Jaumann absorbers; all adopted from [119]. | 61 |
| <u>Figure 3.11.</u> (a) Uniaxial, (b) ± 90 biaxial, (c) ± 45 biaxial and (d) quadraaxial weaving textures in glass fiber woven fabrics [107]..... | 62 |
| <u>Figure 3.12.</u> Schematic view of quadriaaxial glass fiber woven fabric.. | 63 |
| <u>Figure 3.13.</u> Free-space measurement set-up and the network analyzer. | 64 |
| <u>Figure 3.14.</u> Photograph of spray coated SWNT films on glass fiber woven fabrics for (a) 25 ml, (b) 50 ml and (c) 100 ml sprayed dispersion volumes. | 66 |
| <u>Figure 3.15.</u> SEM images of spray coated SWNT films on glass fiber woven fabrics for (a) 25 ml, (b) 100 ml sprayed dispersion volumes..... | 66 |
| <u>Figure 3.16.</u> Reflection loss versus frequency plot for the SWNT film coated glass fiber woven fabrics with different spraying volumes. | 67 |
| <u>Figure 3.17.</u> Transmission loss versus frequency plot for the SWNT film coated glass fiber woven fabrics with different spraying volumes. | 68 |
| <u>Figure 3.18.</u> % EM wave absorption versus frequency plot for the SWNT film coated glass fiber woven fabrics with different spraying volumes..... | 69 |

CHAPTER 1

INTRODUCTION

Nanomaterials have received a lot of interest due to their novel properties and application areas, in the last decades. Among nanomaterials, single walled carbon nanotubes (SWNTs) are one of the most promising candidates. They possess unique physical, mechanical and chemical properties. SWNTs can be utilized individually or in a network form. A two dimensional (2D) network which is composed of randomly distributed metallic and semiconducting SWNTs are novel materials for many electronic device applications. They exhibit high optical transmittance and electrical conductivity depending on the SWNT density and the network continuity. Depending on the film thickness (density), application areas show variety. They can be used in many electronic devices such as supercapacitors, organic photovoltaic devices, field emission displays or conductive composites.

Fabrication of SWNT thin films can be done by direct growth or solution based deposition techniques such as vacuum filtration, spin coating, dip coating or spray coating. Solution based deposition techniques are cheaper and applicable over large areas and various substrates. However, those deposition techniques require homogeneous SWNT dispersions. SWNTs have large aspect ratio; thus, they can easily agglomerate in the form of cylindrical bundles under van der Waals forces. In order to separate SWNTs, anionic, cationic and non-ionic surfactants or organic solvents are being used. These surfactants provide an electrostatic repulsion at the outer surface areas of the SWNTs and keep them apart from each other. It is important to utilize an effective and nondestructive surfactant at the same time. Removal of the surfactant from the deposited SWNT thin films is also a critical point, which is directly proportional to the improvement in the quality of the optoelectronic properties of the thin films. Dispersion process includes sonication steps for surfactant aided SWNT solutions. Sonication activates the unzipping behavior of the SWNT bundles. However, sonication type, time and power can damage and shorten SWNTs due to heat generation. Optimizations of sonication and dispersion parameters directly affect the stability of the dispersion and the SWNT thin film quality.

Optoelectronic properties of the SWNT thin films can be improved by functionalization. Acid functionalization is a very common post deposition technique, which removes the residual surfactant from the SWNT side walls. Nitric acid (HNO_3) baths increase the electrical conductivity of the SWNT thin films. Additional acid treatments such as thionyl chloride (SOCl_2) can also be utilized for reducing the sheet resistance of thin films.

Transparent and conductive electrodes are being utilized in solar cells, organic light emitting diodes (OLEDs), touch panels and many other optoelectronic devices. Among them indium tin oxide (ITO) is one of the most common materials. However, flexible, cost effective, conductive and robust SWNT thin films can be preferred as an alternative to ITO electrodes. In addition, SWNT thin film coating process does not need a vacuum system

that can be applied at low temperatures via all solution based methods on several substrates over large areas. Spray coating method, especially, is the most suitable deposition technique for larger area applications. SWNT thin films can easily be scaled up by utilizing a practical spray coating setup for making transparent electrodes or thick SWNT layers for other applications.

Chapter 2 investigates SWNT thin film fabrication from many aspects including dispersion, deposition and post-deposition procedures in detail. Optoelectronic properties of the SWNT thin films were altered and examined for various SWNT densities. Effects of the sonication, SWNT type, surfactant and centrifugation were discussed. Furthermore, SWNT thin films were also applied over larger areas on both glass and polyethylene terephthalate (PET) substrates. Mechanical stability of the films, which were deposited on flexible PET substrates, was also evaluated.

Chapter 3 shifts the focus to discuss the electromagnetic wave properties of SWNT film coated glass fiber woven fabrics. Electromagnetic wave absorption, reflection and transmission measurements and analysis were done by utilizing a free-space method within 18 – 40 GHz frequency range. Electromagnetic interference (EMI) has been a common problem for many industries in the recent years. Increasing usage and pervasiveness of the electromagnetic wave based devices cause electromagnetic wave interference and results in electromagnetic radiation leakage. This leakage can harm human health or cause information and quality loss in various engineering applications. Therefore, EMI shielding material design became a new and mandatory research area. The main mechanism of shielding depends on reflection. Conductive materials like metal sheets or grids were widely utilized in EMI shielding designs. However, conductive polymers and other carbon-based alternatives also became popular alternatives due to their light weights. Carbon nanotubes (CNT) were utilized as conductive fillers in various composites and CNT thin films EMI shielding properties were investigated through different frequency ranges before. It is found that, shielding effectiveness (SE) is frequency dependent. Higher frequencies cause larger skin depths and penetration; thus, thickness of the shielding material needs extra layers in order to maintain the same SE. EM wave absorbing materials are also very common in military applications for radio detection and ranging (RADAR). Therefore, suppressing the EM energy and controllable energy storage is another challenge for researchers.

To sum up, in this thesis, first the fabrication and characterization of the SWNT thin films were achieved. Then, the EM wave properties of the films on glass fiber woven fabrics were examined and analyzed using a network analyzer and a free- space method at a given frequency range.

CHAPTER 2

SINGLE WALLED CARBON NANOTUBE THIN FILMS

2.1. INTRODUCTION

2.1.1 Carbon Allotropes

Carbon can have very different and important properties depending on its bonding structure and possible atomic configuration. Each carbon atom has six electrons, which are occupying $1s^2$, $2s^2$ and $2p^2$ orbitals. Electrons which are strongly bounded by the core, fill the $1s^2$ orbital, thus the remaining four electrons in the valence orbitals are relatively weaker. Because of these four valence electrons occupied at $2s^2$ and $2p^2$ orbitals, several covalent bonds can be easily formed. The combination of these atomic orbitals is called hybridization, where that the mixing of a $2s$ electron with one, two or three $2p$ electrons is called sp^n hybridization with $n=1, 2, 3$ [1, 2]. Common carbon allotropes such as diamond, graphite, nanotubes or fullerenes have different bonding structures due to these hybrids as shown in Figure 2.1.

sp^3 hybrid structure demonstrated in Figure 2.1 (a) has a tetrahedral geometry and composed of three p orbitals and the s orbital, making strong covalent sigma (σ) bonds between them. sp^2 hybridized atoms shown in Figure 2.1 (b) have trigonal geometries combining the s orbital with two of the p orbitals and making σ bonds. Rest of the p orbitals, can make π bonds, which are weaker than σ bonds. sp hybrid structure is a combination of the s orbital and a p orbital that has a linear geometry as shown in Figure 2.1 (c). sp hybridized atoms also have π bonds in addition to σ bonds.

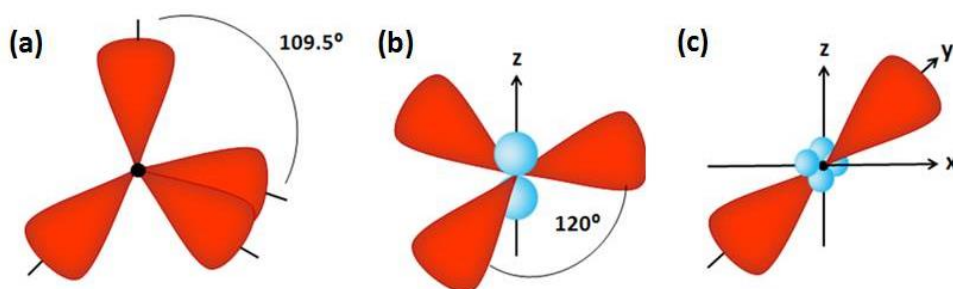


Figure 2.1 (a) sp^3 , (b) sp^2 , (c) sp hybridized carbon atoms.

In diamond, carbon atoms having four valence electrons occupy the sp^3 hybrid orbital so that hybridized atoms make strong covalent σ bonds with neighboring atoms through a tetrahedral geometry as shown in Figure 2.2 (a). Diamond is the hardest naturally occurred material because of this firmly constructed arrangement. Diamonds are electrical insulators because electrons are tightly held within the covalent σ bonds. On the other hand, unlike most electrical insulators diamonds are good thermal conductors.

Graphite is another carbon allotrope, which consists of the sp^2 hybridized atoms. In each carbon atom, three of the four outer shell electrons are hybridized to sp^2 orbitals and form strong covalent σ bonds with the three neighboring carbon atoms [3]. The remaining valence electron in the π orbital provides the electron band network that is largely responsible for the charge transport in graphene [4]. This bonding structure forms a planar hexagonal network like a honeycomb as shown in Figure 2.2 (b). Monolayer is called a graphene sheet and layers are held together by van der Waals forces. The spacing between two graphene layers is 0.34 nm. Graphite conducts both electricity and heat due to its π bond electrons, which are free to move. Owing to its weak π bonds and the van der Waals interaction between the layers, graphite is a perfect lubricant hence the graphene sheets are able to glide away [5]. A spherical fullerene molecule, C_{60} , is demonstrated in Figure 2.2 (c). C_{60} molecules are composed of 20 hexagons and 12 pentagons forming a stable football like structure. The coordination at every carbon atom in fullerenes is not planar, they have curvatures with some sp^3 character present in the essentially sp^2 hybridized carbons [6]. They have novel properties and so far utilized in electronic, magnetic, optical, chemical, biological and medical applications.

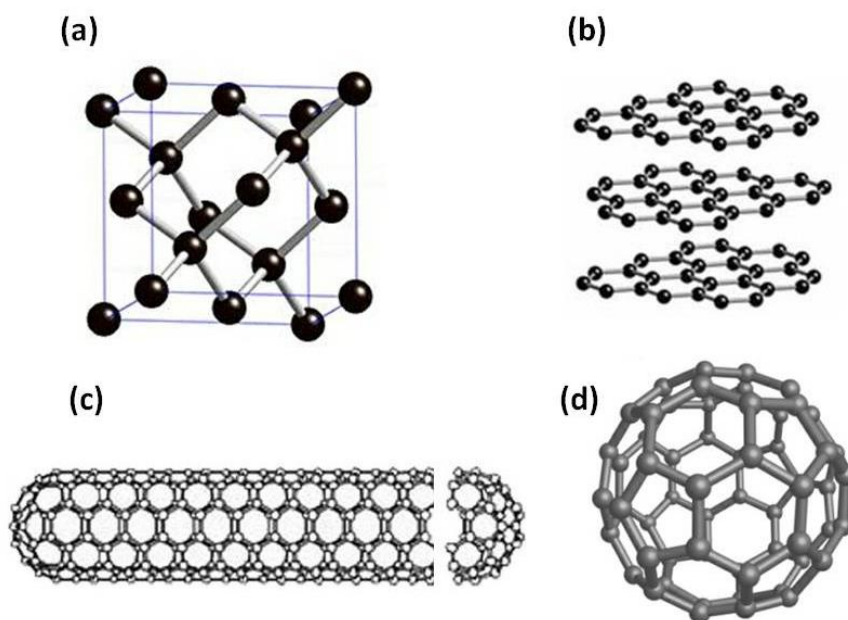


Figure 2.2 Models of carbon allotropes: (a) diamond, (b) graphite, (c) single walled carbon nanotube and (d) C_{60} fullerene [3].

CNTs are cylindrical microstructures and formed by rolling the graphene sheets. They can be open ended or their ends may be capped with bisected of fullerene as shown in Figure 2.2 (d). The sp^2 hybridization, which is the characteristic bonding of graphite, has a significant effect on the formation of the CNTs. Bonding in CNTs fundamentally depends on the sp^2 hybridization, which makes them stable; whereas, the hollow cylindrical part is more strong than the ends of the CNTs due to the presence of sp^3 bonding in the end caps [2].

2.1.2 Carbon Nanotubes

In 1991, CNTs were described as “helical microtubules of graphitic carbon” by S. Iijima [7] for the first time and then they became one the most important materials in nanotechnology. Over the last two decades, owing to their unique properties, CNTs have attracted a lot of interest from researchers over interdisciplinary fields. Two years after the discovery of multi walled carbon nanotubes (MWNTs), single walled carbon nanotubes (SWNTs) were also observed [8].

In addition to these two forms, double walled carbon nanotubes (DWNTs) are also observed as the third type with the properties of both MWNTs and SWNTs [9]. CNTs have the electrical and mechanical properties of graphene due to their bonding nature. The bonding structure of CNTs, as mentioned in 2.1.1, is generally composed of sp^2 bonds and they are found to have many extraordinary properties. CNTs have diameters within the nanometers range; but, they can be up to hundreds of micrometers long [2]. The difference gives them high aspect ratios, which could be as much as 1000:1.

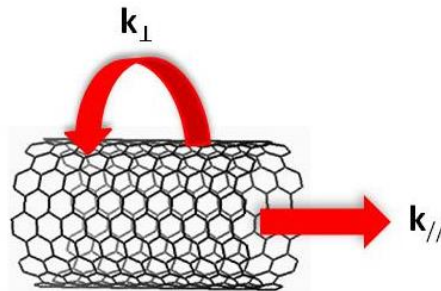


Figure 2.3 Quantized and the continuous electron wave vectors, k_{\perp} and k_{\parallel} adapted from [10].

Although CNTs are closely related to a two dimensional (2D) graphene sheet, the cylindrical symmetry that they have and the quantum confinement in the peripheral direction makes them different from the graphene sheets. Electron wave number k_{\perp} is quantized unlike the wave vector, which is parallel to the tube axis. Wave vectors around the nanotube are shown in Figure 2.3. Electrons propagate only along the tube axis and electron transport takes place on this axis because of the quantum confinement. Thus, the electronic properties of the CNTs are originated from their 1D nature [11].

2.1.2.1 Multiwalled Carbon Nanotubes (MWNTs)

CNTs are cylindrical forms that can be obtained from wrapping graphene layers. A MWNT can be regarded as a concentric assembly of these cylinders, one within another as shown in Figure 2.4 (a). The spacing between the cylinders and the separation between the graphite layers are approximately the same as can be expected and it is 0.34 nm. MWNTs can have external diameters that range from a few nanometers to tens of nanometers, as shown in Figure 2.4 (b), typically larger than SWNTs. The length of MWNTs can be several micrometers or even centimeters.

Electrical conductivity of the MWNTs could be comparable to that of graphite. They can conduct electrical current as good as metals. In graphite, electrical current is transmitted by the π orbitals within the graphene sheets. The external sheet conductance is higher than the internal sheets. Similar to graphite, MWNTs show smaller resistivity through their outer shells than the intershells due to overlapping of the π orbitals between the graphene sheets.

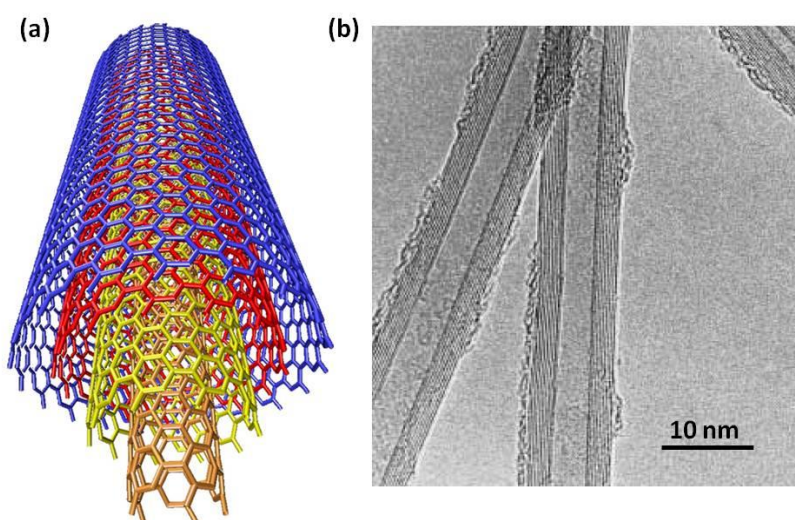


Figure 2.4 (a) Schematic of a MWNT, (b) a transmission electron microscopy (TEM) image of MWNTs [4, 12].

2.1.2.2 Single Walled Carbon Nanotubes (SWNTs)

The individual shells of a MWNT can be named as SWNTs. SWNTs have a single cylindrical wall, which was created by rolling a graphene sheet as shown in Figure 2.5 (a). A SWNT can be formed along different rolling directions. These different rolling directions, named chirality, impact their electronic properties and make SWNTs interesting electrical materials. SWNTs can be either semiconducting or metallic due to their chirality. A chiral vector along the circumference, C_h , can be used to determine the possible wrapping angles. There are two integers, n and m , which are used as indices to describe C_h .

The definition of C_h is given as,

$$\vec{C}_h = n\vec{a}_1 + m\vec{a}_2 \equiv (n, m) \quad (2.1)$$

where \mathbf{a}_1 and \mathbf{a}_2 are the graphene lattice vectors and C_h is a linear combination of these unit vectors as demonstrated in Figure 2.5 (b). n and m are making a positive set of integers, which satisfies that $n > m$. Basically, C_h makes a connection between two sites of the graphene sheet. Chiral angle, θ , is the angle between \mathbf{a}_1 and C_h . T is the translational vector along the tube axis. Chiral vectors of SWNT models are shown with the dark lines in Figure 2.5 (b). In a zigzag SWNT, m is zero because the chiral vector is parallel to \mathbf{a}_1 so the integer set will be always $(n, 0)$. On the other hand, the chiral vector of an armchair model is the sum of \mathbf{a}_1 and \mathbf{a}_2 that makes the integers equal ($n=m$) and the set will be like (n, n) .

Possible chiral vectors are given with their integer couples (n, m) and shown on a honeycomb graphene lattice in Figure 2.6 (a), which confirm the zigzag structure has the integer pairs as $(n, 0)$ and the armchair structure is formed by the specified (n, n) pairs. All other tubes (n, m) are classified as chiral. Atomic structures of zigzag, armchair and chiral SWNTs are shown in Figure 2.6 (b). (n, m) indices determine whether SWNTs are metallic or semiconducting, as well as their energy band gaps. If the difference between m and n is equal to the multiples of three, the nanotube is metallic [13]; otherwise the tube is semiconducting and has a band gap value of 0.4 - 0.7 eV [14].

SWNTs can be labeled by their diameters and chiral angles, too. Generally they have diameters on the order of nanometers and can take θ values between 0° to 30° . θ is defined by

$$\theta = \tan^{-1} \left[\frac{\sqrt{3}n}{(2m+n)} \right] \quad (2.2)$$

Since C_h defines the circumference of a SWNT, diameter of the tubes can be calculated from the equation below

$$d = C_h/\pi = a/\pi (m^2 + mn + n^2)^{1/2} \quad (2.3)$$

The lattice constant a is given by

$$a = \sqrt{3}a_{c-c} = \sqrt{3} \times 0.123 = 0.246 \text{ nm} \quad (2.4)$$

According to (d, θ) notation for zigzag nanotubes, θ equals to 0° and for armchair nanotubes θ equals to 30° .

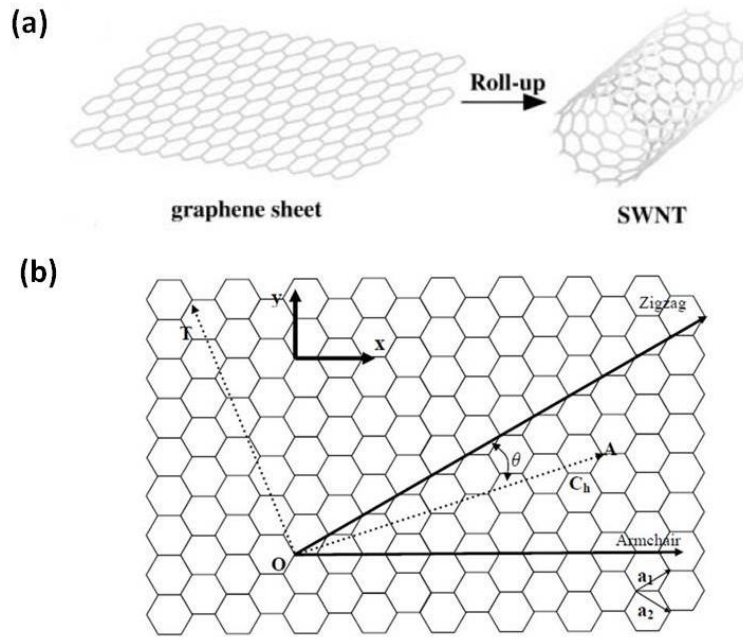


Figure 2.5 Schematic representations of a SWNT and a chiral vector: (a) Graphene sheet rolled into a seamless tube [2]. (b) Illustrating the vectors a_1 and a_2 , the chiral vector C_h shown as OA, the translation vector T is shown as OT which is perpendicular to C_h and the wrapping angle θ . Also possible zigzag and armchair patterns are demonstrated [10].

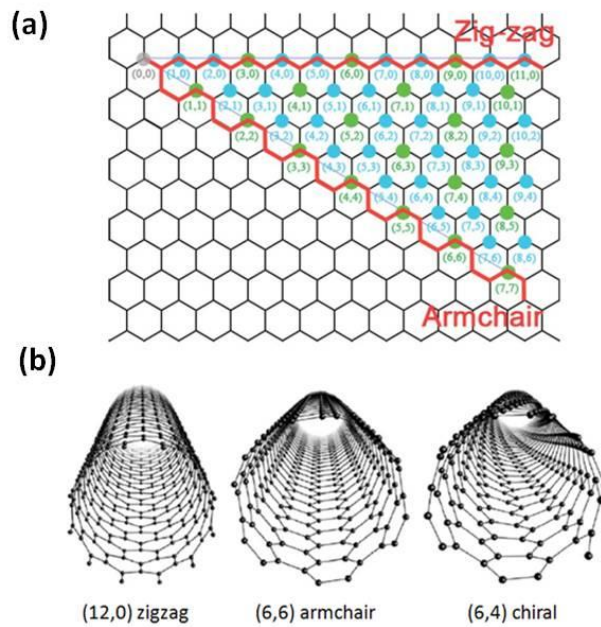


Figure 2.6 (a) Graphene network showing all the possible indices [15]. (b) Atomic structures of zigzag, armchair and chiral SWNTs. Taken from reference [16].

The resulting electron band structures for 3 different SWNTs are shown in Figure 2.7. Fermi energy can be defined as the energy of the highest state that an electron can occupy, at a temperature of absolute zero. The energy distribution curves show significant differences at the Fermi energy. Armchair SWNTs, which show metallic behavior, have energy distribution curves like the one in Figure 2.7 (a). In this case, a conduction band and a valence band intersect at the Fermi energy. On the other hand, there is a remarkable energy gap between the valence and the conduction bands in the zigzag SWNTs, which are semiconducting as shown in Figure 2.7 (b). Another energy distribution of a zigzag SWNT is given in Figure 2.7 (c) that is classified as metallic with an energy gap equal to zero. Such behaviors are possible in SWNTs and also depend on their diameters. The relationship between the energy gap (E_g) and the nanotube diameter is given by the equation: [17]

$$E_g \sim 1/d \quad (2.5)$$

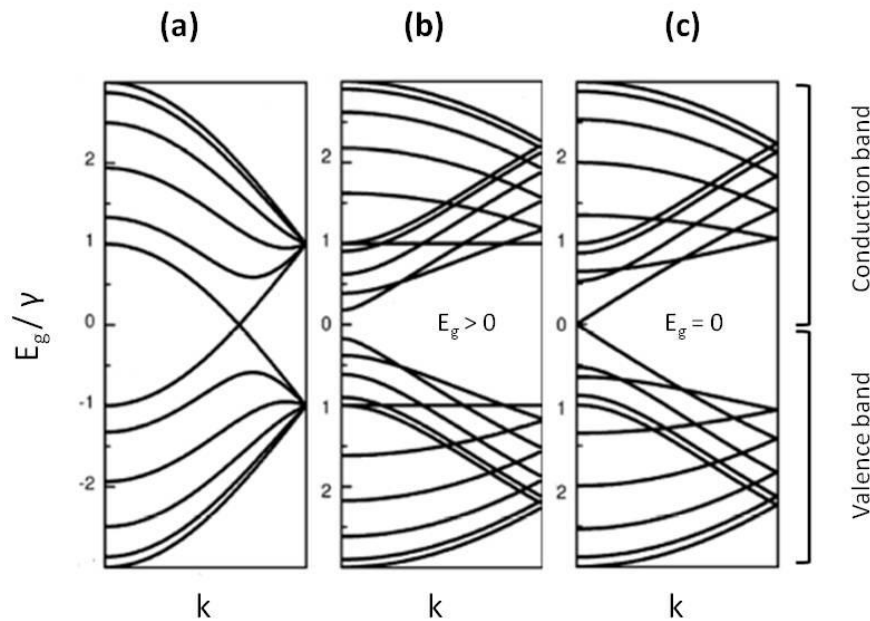


Figure 2.7 Band structures of SWNTs with indices of (a) (5, 5), (b) (10, 0) and (c) (9, 0) (derived by zone-folding of the band structure of the graphene sheet) [3].

As the CNT diameter increases, the band gap decreases. Larger nanotubes are more graphene like structures so the electronic transition increases [18].

2.1.3 SWNT Synthesis

Three basic methods are used to synthesize SWNTs. These are arc discharge [19], laser ablation [20] and chemical vapor deposition (CVD) [21]. The details of the SWNT synthesis methods are described below.

2.1.3.1 Arc Discharge

Arc discharge is the most common technique for the synthesis of high quality SWNTs. Both SWNTs and MWNTs can be synthesized by this method. Synthesis of SWNTs is done by applying a high direct current (dc) through the graphite rods, which are utilized as electrodes. Both of the electrodes are graphitic; but, the anode is a graphite-metal composite. Various elements have been used to prepare the composite mixture, including molybdenum (Mo), cobalt (Co), yttrium (Y), iron (Fe) or nickel (Ni). These catalysts facilitate the synthesis of SWNTs. A schematic representation of the process setup is shown in Figure 2.8.

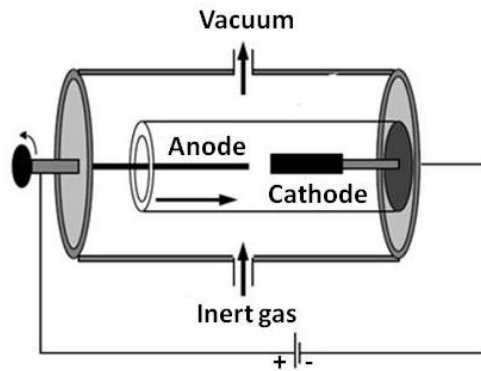


Figure 2.8 Schematic representation of an arc discharge set-up [19].

In anode, the metal catalysts and graphite evaporate due to the elevated temperatures generated by the arc discharge. SWNTs are deposited on the cathode.

Researchers have been using this method since 1993 [8] for the synthesis of SWNTs in large quantities. Quality of the SWNTs depend on the type of the utilized catalyst metal [19], inert gas [22, 23] and the gas pressure [24]. Preheating the catalyst [25] improves the yield. In this thesis, all the experiments were carried out with SWNTs that were synthesized through arc-discharge.

2.1.3.2 Laser Ablation

In 1995 Guo et al. found an alternative method for the synthesis of SWNTs [26]. Laser ablation is an expensive technique that requires large amounts of energy. Process involves the vaporization of a graphite target, which is consisting of 0.5 at % Ni and Co. The target

is placed inside a furnace that is maintained at 1200 °C, as shown in Figure 2.9 and an inert gas flows through the furnace during the process. The laser source vaporizes the target. Finally SWNTs develop, merge and condense. Laser ablation synthesis of SWNTs can be done at lower temperatures than the arc discharge method and the final product is very clean [20, 26].

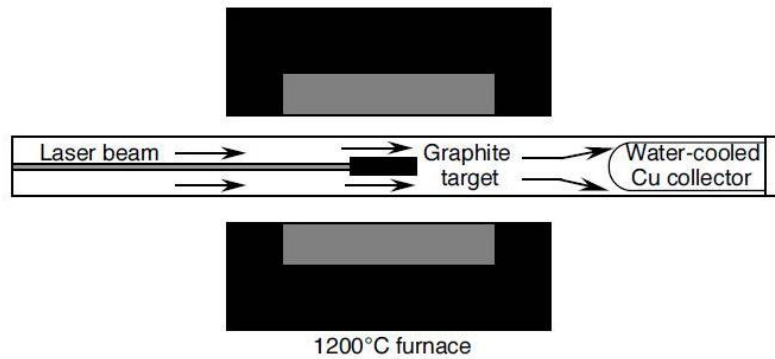


Figure 2.9 Schematic representation of a laser ablation set-up [20].

The properties and the quantities of SWNTs depend on the process parameters like source intensity and pulse width [27], target composition [28, 29], temperature [30], carrier gas type and pressure [20].

2.1.3.3 Chemical Vapor Deposition (CVD)

The CVD technique differs from the other two SWNT synthesis techniques. CVD method involves the degradation of hydrocarbons at temperatures between 750 and 1000 °C [3, 31]. Hydrocarbons including methane [31, 32, 33], carbon monoxide (CO) [33] and ethylene [31] can be used for CNT synthesis among others. The main parts of the CVD set-up are shown in Figure 2.10. Decomposition takes place in the furnace and the metal catalyst nanoparticles absorb the carbon. CNTs are formed subsequently [34]. The catalysts are generally Fe, Co or Ni.

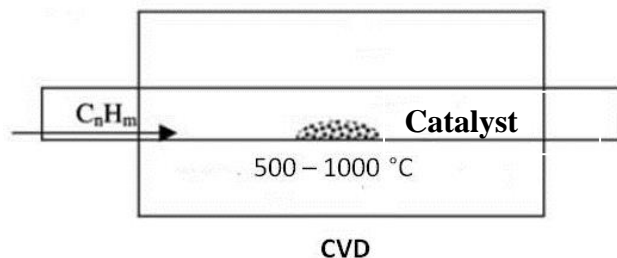


Figure 2.10 Schematic representation of the experimental set-up for CVD process [36].

Arc-discharge and laser ablation methods can synthesize SWNTs in the powder form. In contrast to these techniques most of the SWNTs synthesized by CVD are in the shape of individual ropes [35]. CVD method has some other advantages like diameter and alignment control. In addition, direct growth of SWNTs on various substrates can be achieved through the CVD method.

2.1.4 Potential Applications of SWNTs

Two decades ago, many enticing opportunities for CNT applications were predicted because of their novel structure, extraordinary topology and nanoscale dimensions. This valuable combination makes CNTs one of the most promising and exciting nanoscale materials in the field of nanotechnology. CNTs have found many application areas, such as electronic devices, conductive composites, sensors, energy storage devices and field emission displays. CNTs can be synthesized both in large quantities and good qualities. However, CNT applications have not achieved the predicted commercial success yet in the marketplace [15].

The discovery of the field emission properties of MWNTs showed the advantage of their high aspect ratio. For field emission measurements, a low voltage is applied between the emitting surface and the anode. The emitted current depends on the electric field at the emitting surface and MWNTs have high emission current densities due to their small diameters, which make them perfect field emission cold cathode materials. In polymer composites, MWNTs are used to impart conductivity and found that only very little addition allows percolation. MWNTs are more favorable than SWNTs due to their low cost [38, 39]. Another application of MWNTs is using them as atomic force microscope (AFM) cantilever tips [40, 41]. This application not only depends on their high aspect ratios; but, also on their high strength.

SWNTs can be either semiconducting or metallic depending on the wrapping angle. These different electronic abilities make SWNTs useful for various applications. Semiconducting SWNTs can be utilized in field effect transistors (FET) by making a connection with conductive electrodes [42, 43]. On the other hand, their metallic characteristics and the large current density conduction capabilities make them attractive for reducing the scale of electronic devices. It has been found that SWNTs can resist current densities up to 10^9 A/cm², surpassing Cu by a factor of 1000 [44], which make them functional in electronic circuits. SWNT network applications and thin film fabrication will be discussed in the following sections. The word ‘thin film’ will be used instead of ‘network’ for the remainder of this chapter.

2.1.5 Properties of SWNT Thin Films

CNTs have been widely investigated for their physical, chemical and mechanical properties since their discovery. Their device integration possibilities have also been studied and finally their network performances have drawn a lot of attention due to their new unique

properties and better reproducibility of the devices. This two dimensional network arrangement shows an average assembled behavior, which can be regarded as a new material for nanotechnology [45, 46, 47, 48, 49].

SWNTs can show either semiconducting or metallic properties due to the folding angle as discussed before. The random network of SWNT thin films is a collective mixture of this varying electronic structure and they may exhibit a metal-semiconductor transition depending on the density of the nanotubes in the thin films [50, 51]. SWNT thin films have important optoelectronic, mechanical and chemical properties. Their transport properties are also remarkable. Because of the large aspect ratio (1:1000) of SWNTs, percolation threshold is significantly low [52]. Crossing tubes in the network have different chiralities and only 1/3 of the SWNTs in the network are metallic, so that SWNT thin film consists of heterojunctions. These heterojunctions have significant effects on the electrical conductivities of the SWNT thin films [53]. SWNT thin films are thin scattered networks and they are optically transparent in the visible portion of the electromagnetic spectrum (400-700 nm) [15, 37, 54, 55].

SWNT thin films optical transmittance properties are comparable to other transparent and conductive thin films and coatings [56]. In addition, SWNT thin film transmittance is almost independent of the wavelength when compared to indium tin oxide (ITO) [15]. ITO is opaque to ultraviolet (UV) region, where SWNT thin films are still transparent. SWNT band gaps lie in between 0.4 - 0.7 eV for SWNTs with diameters of 1 - 1.5 nm [36] that is smaller than many semiconductor oxides, which have band gaps larger than 3 eV [57].

Figure 2.11 (a) shows the optical transmittance of SWNT thin films in the visible range. As the film thickness increases, optical transmittance of the film decreases. On the contrary, increasing film thickness increases the density within the network become denser so that the conductivity of the film increases. Figure 2.11 (b) shows the relation between the sheet resistance (R_s) and the film transmittance at a specific wavelength of 550 nm.

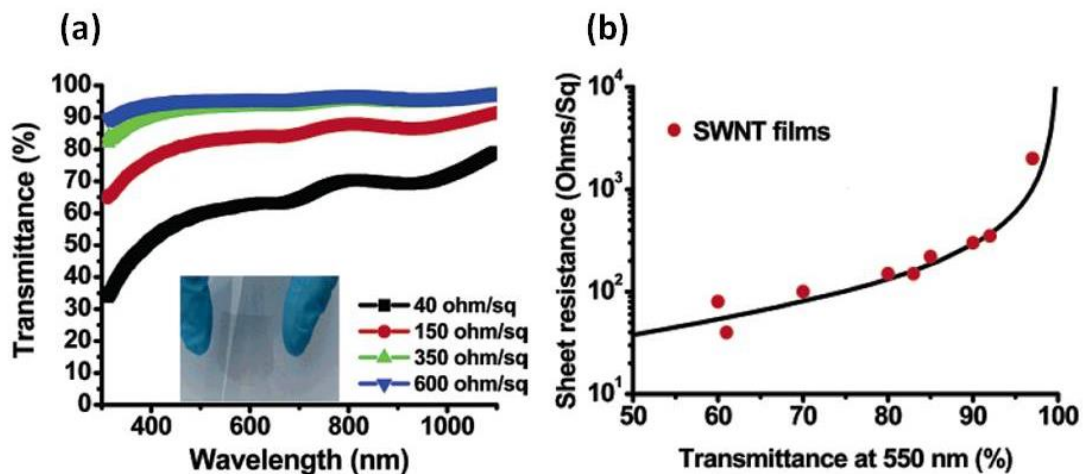


Figure 2.11 (a) Optical transmittance versus wavelength in the visible region. The inset shows a SWNT thin film on a flexible substrate. (b) Sheet resistance versus optical transmittance at 550 nm wavelength for different nanotube densities [37].

SWNTs have outstanding mechanical properties depending on their large aspect ratios and the strong bonding nature. Their flexibilities and the elastic properties under various loadings have been examined and reported by many researchers [58, 59]. SWNT thin films also show superior stretchability, flexibility and useful mechanical properties. For flexible transparent electronics such as flexible displays and solar cell electrodes, SWNT thin films are found to be very useful. SWNT thin films are bendable, while ITO on PET substrates fail to do so. Figure 2.12 (a) shows the comparison of the bending test results. Tensile testing of SWNT thin films have been studied by Luo et al. and it is found that the films have an elastic behavior up to 5 % tensile strains. After 5 % strain plastic deformation of the PET substrate starts. Figure 2.12 (b) shows that the ITO film fails nearly at 2 % tensile strain [61]. Furthermore, due to ITO's vacuum requirements for deposition, chemical instabilities and high cost, SWNT thin films became the strongest alternative to industrial standard ITO.

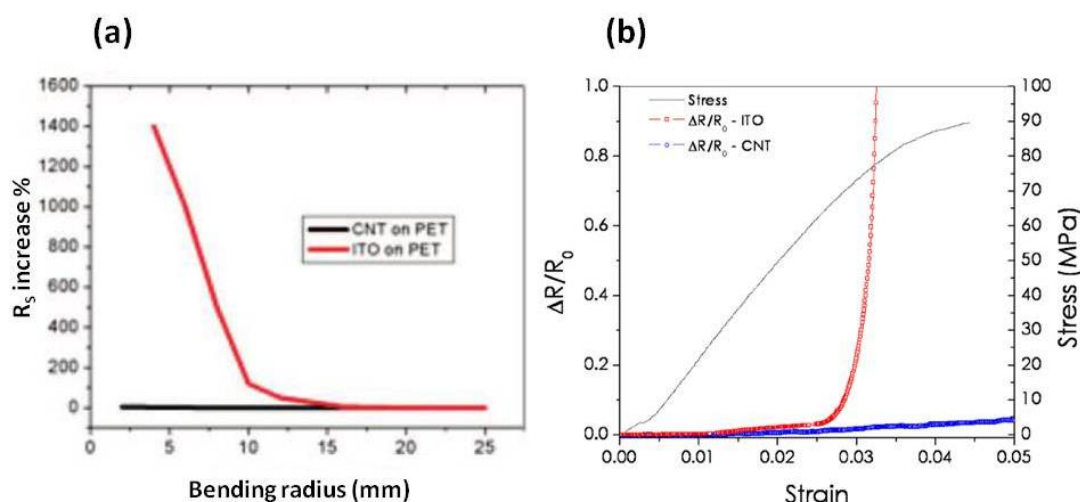


Figure 2.12 Bending (a) and tensile (b) test results comparing SWNT thin films and ITO on PET substrates [60].

Thin film stability is another important issue for their use in electronic devices. Thin films should be stable when exposed to chemicals during device fabrication. Optical transmittance of SWNT thin films was found to be insensitive to chemical exposure. In addition, sheet resistance of the SWNT thin films was found to be insensitive to common organic solvents used for device processing; however, solvents were found to tune the sheet resistance of the thin films [60].

SWNT thin films are one of the most promising candidates for the replacement of ITO. Their transparent conductive electrode characteristics show that SWNT thin films have many advantages over other transparent conductive coatings. Table 2.1 makes a clear comparison of various types of transparent electrodes and summarizes their overall properties. Although Ag nanowire (AgNW) networks have higher conductivities than SWNT thin films at the same optical transmittance, these materials have poor adhesion to underlying substrates [61] and high roughness values.

Table 2.1 The comparison between ITO and other alternative transparent conductors including CNT thin films [61].

| | ITO | CNT | Graphene | PEDOT:PSS | Silver grid | AgNWs film |
|--|------------------|----------------|----------------|----------------|-------------|-----------------------|
| Scalable Fabrication | PVD | Spray Printing | Spray Printing | Spray Printing | Printing | Spray Printing |
| Optoelectronic performance (highest value of σ_{DC}/σ_{Op}) | Excellent 330 | Median 35 | Median 11 | Median | Excellent | Excellent 450 |
| High NIR transparency | No | Yes | Yes | No | Yes | Yes |
| Flexibility | No | Yes | Yes | Yes | Yes | Yes |
| Abrasion resistance | Yes | Yes | Yes | No | Yes | Yes |
| Work Function (eV) | 4.7 | 4.7-5.1 | 4.6-4.7 | 5.0 | 4.26 | 4.26-5.1 ³ |
| Surface roughness | Excellent | Median | Excellent | Excellent | Poor | Excellent |
| Thermal stability | Excellent | Excellent | Excellent | Median | Excellent | Excellent |
| Chemical stability | Excellent | Excellent | Excellent | Median | Median | Median |

2.1.6 SWNT Thin Film Fabrication

Fabrication of SWNT thin films can be done by two major methods that are direct growth of CNTs on substrates and solution based deposition. SWNTs can be grown on substrates both in a random or aligned fashion by CVD method. Aligned growth of SWNT thin films have appreciable benefits to high mobility devices and electronics. However, it is easier to synthesize randomly distributed SWNT films.

Directly grown SWNT thin films can be produced nearly defectless and these films have higher conductivities. On the other hand, CVD method requires very high vacuum and temperature conditions unlike the solution based method.

Solution based deposition is a common practical method. It has significant advantages. First of all, it is a low temperature process. Generally, process occurs at temperatures below 100 °C. Secondly, in solution based deposition, no vacuum is needed and this property makes solution based deposition a low cost technique. Finally, this method can be applied on any substrate including PET unlike the CVD method. There are several deposition routes and each of them has their own advantages and disadvantages. The most preferred methods can be listed as, vacuum filtration, spray coating, spin coating and dip coating. To achieve the best available thin film quality, well purified CNTs are needed.

Another important factor that affects the thin film quality is the SWNT dispersion. Dispersion step and the deposition methods will be discussed in detail. This thesis focuses on SWNT thin films, which were fabricated by solution based depositions; namely by vacuum filtration and spray coating methods.

2.1.6.1 Dispersion

Dispersion of SWNTs has been investigated by many researchers since the separation of CNTs is of crucial importance for the thin film quality. SWNTs are dominated by van der Waals forces due to their large surface area. Van der Waals attractions cause SWNTs to stick together. This flocculation forms SWNT bundles, which could decrease the optical transmittance of the SWNT thin films. It is also important not to destroy SWNTs during their dispersion for the conservation of the electronic properties of the films. One has to be careful since, harsh conditions utilized during debundling of the SWNTs could deteriorate the electronic properties of the thin films.

There are three prominent categories for the preparation of SWNT dispersions namely: surfactant aided dispersions, polymer aided dispersions and dispersion of SWNTs directly in organic solvents. Anionic, cationic or nonionic surfactants can be used for surfactant assisted dispersion. This type of dispersion is commonly used for SWNT thin film fabrication. It is a favorable method for the fabrication process because of the noncovalent interactions between the surfactants and SWNTs. This interaction provides the functionalization of SWNTs without causing any change in the chemical bonding. The surfactants also prevent SWNTs from re-aggregation by creating an electrostatic repulsion around them. In addition, utilized surfactants can be easily rinsed off after the deposition process without altering optoelectronic properties of SWNT thin films.

Sodium dodecyl sulfate (SDS), sodium dodecylbenzene sulfonate (SDBS) and triton X-100 are the most widely used surfactants. Figure 2.13 (a) shows the adsorption of various surfactants on the surfaces of SWNTs.

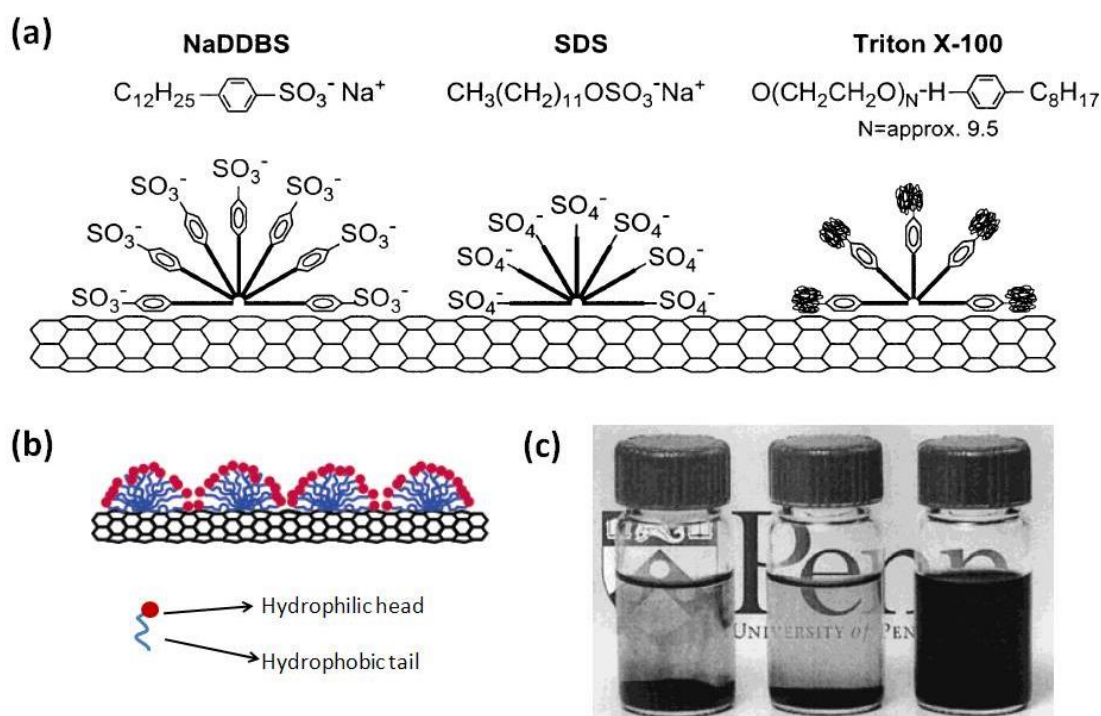


Figure 2.13 (a) Schematic representation of how surfactants may adsorb onto the SWNT surface [62]. (b) Hemispherical adsorption of surfactant micelles on energetically favorable positions on the SWNT. Additional schematic representation shows the hydrophilic and hydrophobic ends [66]. (c) Aqueous dispersions prepared by SDS, Triton X-100 and NaDDBS [62].

The hydrophilic heads of surfactants merge into the water and the hydrophobic tails attach onto the SWNT surfaces, as shown schematically in Figure 2.13 (b). It is revealed that the CNTs are stabilized by those hemispherical micelles, which are lying on the SWNT surface as a sheath [62, 66]. NaDDBS has shown the best performance among the other surfactants. Figure 2.13 (c) exhibits the SWNT dispersions in NaDDBS, SDS and Triton X-100 after 2 months and 5 days, respectively. It is obvious that the NaDDBS dispersed SWNT solution is homogeneous unlike the others. Dispersing capabilities of surfactants depends on the alkyl chain lengths and head group sizes. These properties affect the strength of their interactions with the CNT surfaces and this is the reason why Triton X-100 dispersed SWNT solutions have worse attainments than the others [62]. There are many studies on both SWNT and MWNT dispersion, which compare surfactant performances. Prior comparative test results have revealed and affirmed that Triton X-100 is the least dispersive surfactant [62, 63, 64, 65, 66, 67, 68].

In order to determine the most efficient SWNT concentration for dispersion, several SWNT solutions have been prepared. SWNTs have a tendency to agglomerate at higher concentrations. The optimized concentration of SWNTs in surfactant assisted dispersions is typically less than 1 mg/ml [72]. Another important parameter for improving the SWNT dispersion is sonication. Sonication is particularly necessary for the surfactant aided dispersions. High power sonication, such as tip sonication or ultrasonic bath sonication, can

easily disperse purified SWNTs into solvents for the following processing. Figure 2.14 shows schematics of the individualizing process including sonication and surfactant adsorption on the SWNTs. Estimating the sonication type, the sonication time and the sonication power is important to achieve a stable SWNT dispersion. Energy, which is imparted to the SWNT solution, has to be enough for breaking apart the SWNT bundles. Redundant energy may cause defect formation on SWNT walls so sonication has to be done without damaging or shortening SWNTs. Vichchulada et al. has prepared SDS dispersed SWNT solutions using a tip-sonicator and tried different sonication powers for obtaining high aspect ratio SWNTs [69]. Too high sonication power can also increase the temperature of the SWNT dispersion and affect the dynamics of the ultrasonic system. Longer sonication time can increase the individually dispersed SWNT concentration in the solution. However, SWNT solution may still have large bundles. De-bundling of the SWNTs has to be done without shortening or breaking them. Otherwise, percolation threshold can increase and the conductivities of the deposited films could decrease [70]. Following the ultrasonication, in most cases SWNT solutions are centrifuged to remove the remaining large SWNT bundles [71, 72].

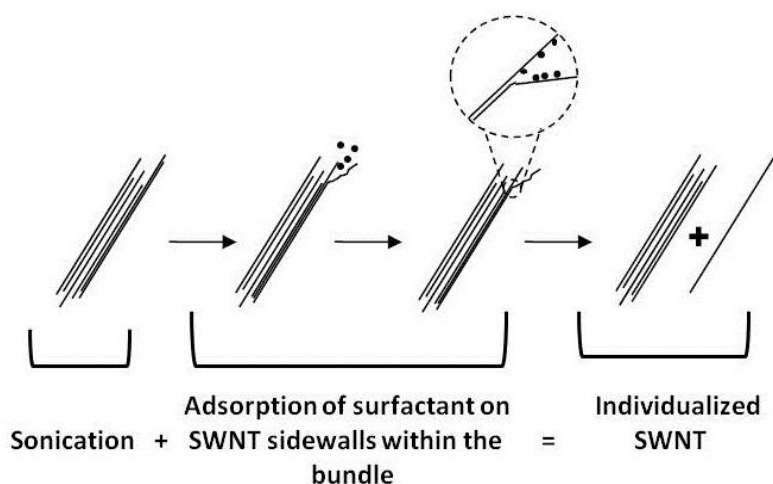


Figure 2.14 Schematic representation of the debundling process via sonication and surfactant adsorption. Adopted from reference [68].

SWNT dispersions can be also prepared by utilizing organic solvents such as N-dimethylformamide (DMF) [68, 73], N-methyl 2-pyrrolidone (NMP) [83] and dimethyl acetamide (DMAC) [68]. However, these solvents are not desired due to their high flammability and toxicity. Besides, they can lead to mechanical damage and electrical degradation of the SWNTs during sonication.

Polymer aided CNT dispersions are not commonly used for the deposition of thin films; because, it can be difficult to remove the insulating polymers after the deposition process. In other words, polymer assisted dispersions are not practical for SWNT thin film applications [74].

2.1.6.2 Deposition

A stabilized SWNT dispersion provides the basis for the fabrication of randomly distributed SWNT thin films. Solution based deposition of SWNTs onto various substrates can be achieved by several techniques such as dip coating [75], spin coating [76], spray coating [77], vacuum filtration [15], electrophoretic deposition [78], gel coating [79], transfer printing [48,49,80] and Langmuir-Blodgett [81]. Achieving a uniform network can be challenging and depends on many parameters like dispersion and SWNT solution- substrate interaction. Each of these methods has their own requirements that can be considered as an advantage or a disadvantage. The basic concepts of the deposition techniques above will be discussed in detail. In addition to this information, some major figures of merit, which are used to investigate SWNT thin films like optical transmittance and sheet resistance, will also be discussed.

2.1.6.2.1 Dip Coating

Dip coating method is a simple implementation of scaled SWNT coatings. It is a practical and cost effective technique. On the other hand, SWNT solution viscosity, SWNT ink-substrate interaction, coating speed and the drying conditions are important parameters that can easily affect the SWNT thin film quality. A schematic of the dip coating process is shown in Figure 2.15 (a). Dip coating method has been utilized to fabricate SWNT thin films on various substrates for different applications [75, 82]. Ng et al. used aminopropyltriethoxysilane (ATPS) to improve the adhesion between the SWNTs and the substrate [75]. After this pretreatment, substrates were dipped into SWNT solutions, which were prepared using different surfactants and solvents. Finally coated substrates were dried in ambient conditions. Optical image in Figure 2.15 (b) shows the SWNT films after several numbers of coatings. Since each dipping cycle increases the thickness of the film, optical transmittance values at a given wavelength decrease. In other words, each dipping cycle decreases the R_s of the film. Figure 2.15 (c) shows the change in their R_s values and their optical transmittance at 550 nm. Triton X-100 dispersed SWNT solution was compared to NMP based and SDS dispersed SWNT solutions. Samples that were immersed into a Triton X-100 solution have the lowest R_s at the highest transmittance. Thus, they have the highest yield [75]. Recently, other studies have been revealed that Triton X-100 is the best surfactant for fabricating uniform SWNT thin films by dip coating because of its higher viscosity [75, 82]. To sum up, dip coating is a simple and low cost method; but, it has a lot of stringent requirements and it is not suitable for large scale applications.

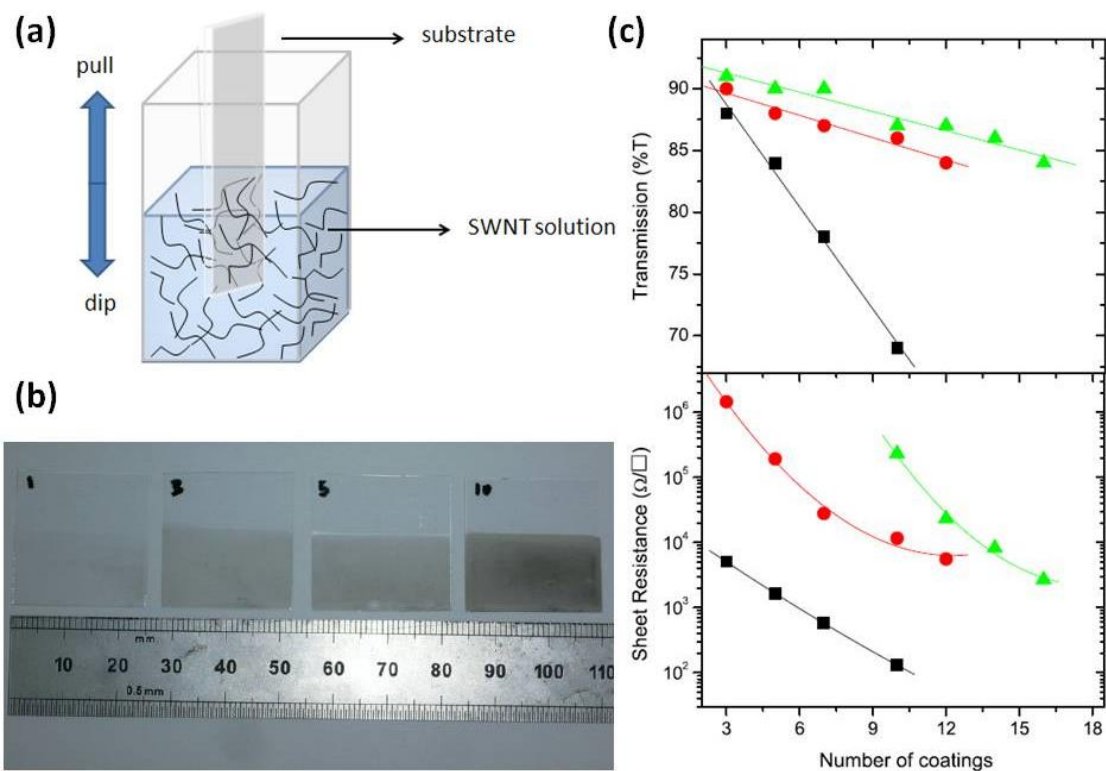


Figure 2.15 (a) Schematic illustration of the dip coating process. (b) Photograph of SWNT thin films after 1, 3, 5 and 10 dipping cycles. (c) Variation in optical transmittance and sheet resistance as a function of the number of coatings. Green line shows the results from NMP-SWNT solution, red line belongs to SDS aided SWNT dispersion and the black line represents the Triton X-100 dispersed SWNT solutions. Adopted from [75].

2.1.6.2.2 Spray Coating

Spray coating is another solution based deposition method for the fabrication of SWNT thin films. Unlike the high vacuum and time consuming processes, spray coating is a simple and low cost technique. In addition to these advantages, spray coating is the most suitable method for large area applications. Large, flexible substrates can be coated very quickly and SWNT thin film conductivity can easily be tuned by different coating steps. Spray coating procedure starts with the dispersion step. Following the preparation, SWNT dispersion is sprayed onto a substrate, which is usually fixed on a heated stage. The stage is heated to avoid the formation of large droplets. Spraying can be done using an air-brush pistol, which is illustrated in Figure 2.16 (a) or an atomizing nozzle. In both cases, a pumping or a steering unit is needed to carry the solution to the heated substrate with a constant flow rate. Through the utilization of a well dispersed SWNT solution and multiple coating steps a successful deposition can be achieved.

Many researchers have used spray coating for the deposition of SWNT networks [76, 77, 84, 85, 86, 87, 88, 89, 90]. Especially in fabricating large area flexible electronic devices, spray coating has obvious advantages over other techniques. Recently, it has been observed that spray coated SWNT thin films can have sheet resistances less than $400 \Omega/\square$ at a transmittance of 90 % [88]. Film thickness is directly proportional to the number of spraying cycles. Figure 2.16 (b) shows the tunable film thickness and optical transmittance (at 550 nm) of the SWNT networks [77]. At higher transmittance values, films thickness is much lower as can be expected. In contrast, the sheet resistance of the film decreases with increasing SWNT density. At a constant transmittance level, conductivities of the spray coated SWNT thin films are comparable to that of ITO. Figure 2.16 (c) shows the difference between various SWNT thin films and ITO coated plastic substrates on a resistivity versus transmittance plot. These comparisons clearly prove that the SWNT thin films are the best candidates to replace ITO as transparent conductive electrodes for many applications. Furthermore, it is possible to improve the conductivities of the films by various acid treatments.

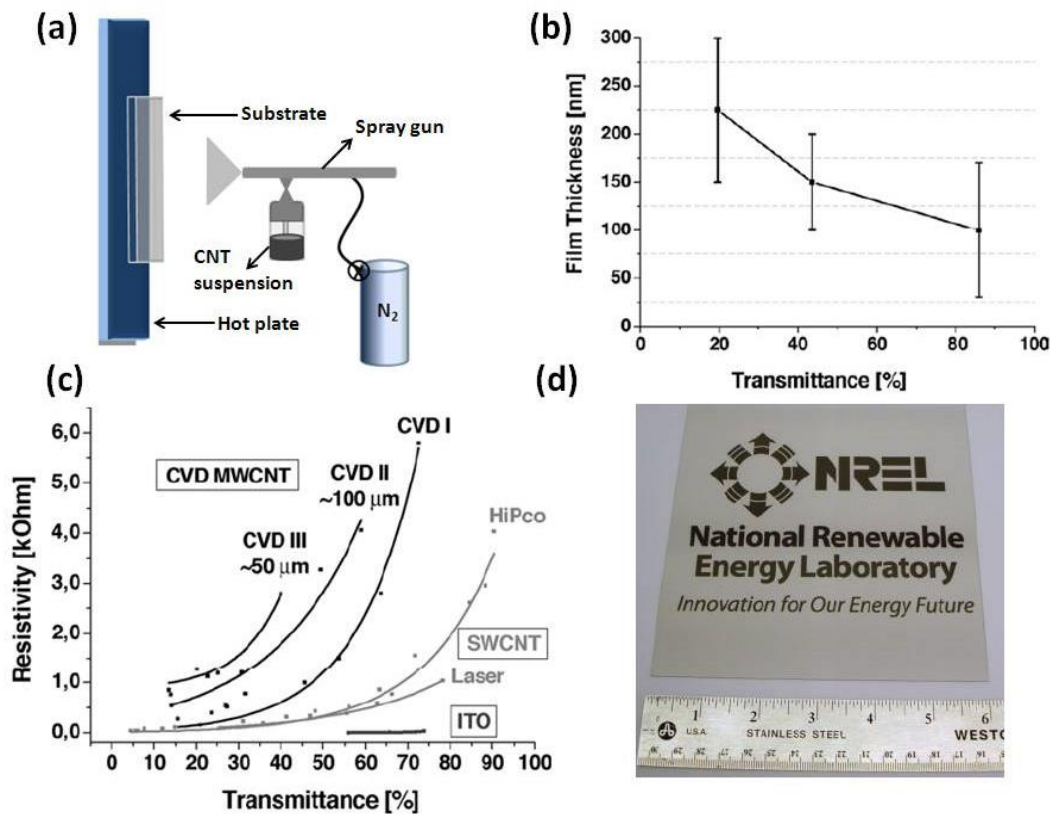


Figure 2.16 (a) Schematic illustration of the spray coating set-up. (b) Film thickness versus optical transmittance plot of spray coated SWNT networks [77]. (c) Resistivity versus optical transmittance plot for spray coated CNT networks and ITO [77]. (d) Spray coated SWNT thin film on glass substrate [77].

SWNT suspensions can be prepared by utilizing several surfactants. SDS and SDBS are commonly used surfactants for dispersing SWNTs; but, sodium carboxymethyl cellulose (CMC) can also be used for spray coating. It has been reported that extremely uniform SWNT thin films can be produced by spray coating using CMC dispersed SWNT solutions [90]. Figure 2.16 (d) shows a glass substrate spray coated from a CMC dispersed SWNT solution.

Spray coating technique has many advantages over other solution based deposition methods. However, the disadvantages arise from optimizing the set-up properties such as stage scan speed, substrate temperature and flow rate. Maintaining the film homogeneity is another challenge due to the apparent fine droplets so the spraying conditions and the SWNT dispersions should be well optimized before starting the spraying process.

2.1.6.2.3 Spin Coating

Spin coating is a widely used well known technique utilized to form monolayer films on flat substrates. Process starts with dropping a small amount of SWNT solution to the substrate. In order to avoid coating discontinuities, sufficient amounts of SWNT solution should be placed on the surface of the substrate. Deposition step subsequently continues with a high-speed rotating step, which spreads the solution homogeneously over the substrate. Following spinning the solution between 2000 and 8000 rpm centrifugal forces are removed and a thin layer occurs on the substrate. Finally, for obtaining the final thin film, remaining excessive solution is evaporated on a hot plate. Figure 2.17 schematically summarizes the spin coating process.

SWNT thin film thickness, conductivity and the optical transmittance values can be controlled by the number of coating cycles. A well dispersed SWNT solution is required for achieving a transparent SWNT thin film [91]. Dichloroethane (DCE) is preferred to prepare SWNT dispersions for spin coating due to its volatility [92]. Surfactant assisted SWNT dispersions can also be utilized in spin coating. However, during the spin coating process, methanol is added to surfactant-assisted dispersions to improve the surfactant removal [93].

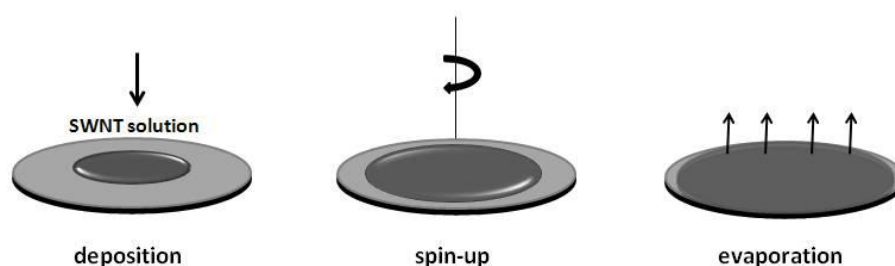


Figure 2.17 Schematic illustration of spin coating process.

Spin coating method is not suitable for many SWNT thin film applications. It requires multiple coating cycles to make a uniform film and it cannot be scaled-up.

2.1.6.2.4 Vacuum Filtration

Vacuum filtration, utilized for the fabrication of SWNT thin films first by Wu et al., is a simple deposition technique. It consists of a vacuum-induced flow of SWNT dispersion through the mixed cellulose ester filter membranes (MCE) [94]. Transparent and conducting SWNT thin films can then be transferred onto various substrates by a simple stamping method.

Vacuum filtration process starts with the preparation of SDS dispersed SWNT solution. After dispersing nanotubes, SWNT solution is filtered through a vacuum filtration apparatus (Millipore) that is shown in Figure 2.18 (a). SWNT solution directly filtered onto a MCE membrane, which has 220 nm pore size. As the dilute solution of SWNTs sifts through the MCE membrane, SWNTs start to form a network. Accumulation of the nanotubes on particular areas impedes the over flowing and blocks redundancy. Thus, less covered areas can be compensated easily by the permeation rate of the SWNT solution and get thicker. In other words, process consistency provides an improved uniformity and reproducibility. An illustration of the vacuum filtration process is shown in Figure 2.18 (b).

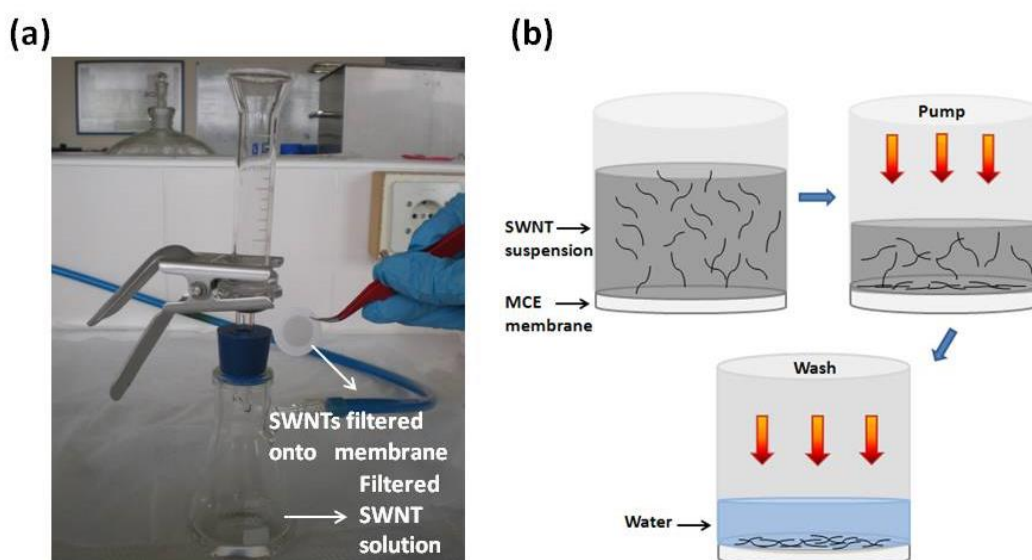


Figure 2.18 (a) Photograph of the filtration set-up utilized for the fabrication of SWNT thin films. (b) Schematic illustration of vacuum filtration process.

After filtering the SWNT suspension through the porous membrane, in order to remove the residual surfactant, the membrane can be washed with several milliliters of deionized (DI) water prior to the film transfer step. The rewashed porous membrane is placed on the substrate as shown in Figure 2.19 and then dried with the help of drying papers, under compressive loading on a hot plate. Transfer of the SWNT film onto various substrates is achieved through the dissolution of MCE membrane in acetone. For the removal of MCE membranes from the substrate surface, multiple acetone baths are applied. Finally, the remaining product forms the SWNT thin film on the substrate.

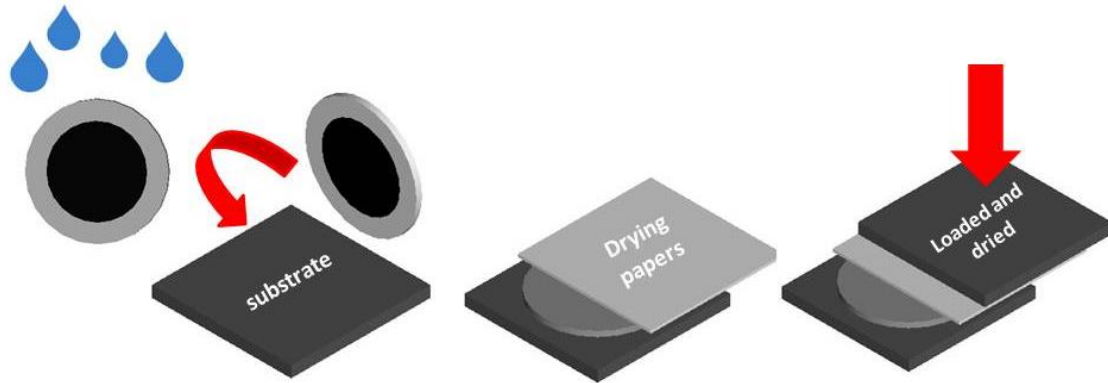


Figure 2.19 Illustration of the film transfer process.

Film thickness can be tuned by the volume of the filtered SWNT solution and thin film density ($\text{SWNT}/\mu\text{m}^2$) can easily be controlled by the SWNT concentration [15]. SEM images of the SWNT networks in Figure 2.20 prove the ability for controlling the film density by applying various SWNT solution concentrations and filtration volumes. R_s and the optical transmittance values of the films can also be controlled using vacuum filtration method. As the film density increases, both R_s and the optical transmittance decrease. SWNT thin films with R_s of $250 \Omega/\square$ and 80 % optical transmittance at 550 nm wavelength were carried out [95]; but, better results have been reported in many studies [96]. SWNT thin films with sheet resistance of $30 \Omega/\square$ and transmittance of greater than 70 % over the visible range were fabricated by Wu et al. and these films still have one of the best reported optoelectronic properties in the literature [94].

Vacuum filtration is a well controllable method to fabricate homogeneous SWNT thin films and it can also be applied over larger areas with larger filtration set-ups and MCE membranes. However, process needs an additional transfer step, which makes the technique not an ideal candidate for devices necessitating really large areas.

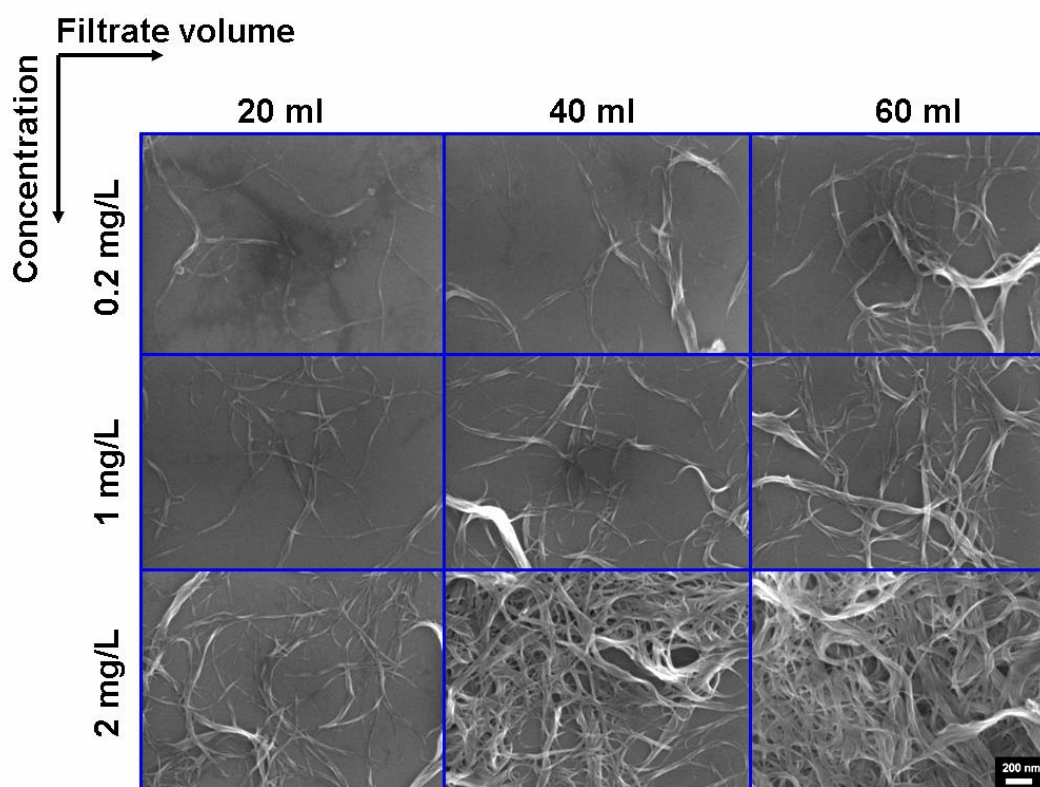


Figure 2.20 SEM images of the SWNT thin films deposited on silicon substrates utilizing various concentrations and filtration volumes [15].

2.1.7 Applications of SWNT Thin Films

SWNTs are unique one dimensional structures, which have shown fascinating capabilities of forming large area, transparent and conductive networks on various substrates. SWNT thin films are amenable for many applications due to their mechanical flexibility and uniformity. These remarkable properties make them good alternatives to brittle ITO in organic electronics. Since ITO is an oxide material, it suffers from instability. In other words, ITO film properties differ in different environmental conditions [97]. Furthermore, ITO films requires high cost processing, while SWNT thin films can be fabricated by low cost, solution based deposition methods that can be performed at room temperature.

SWNT films fabricated by CVD method have fewer defects than the solution deposited counterparts due to their longer nanotube lengths and individually grown patterns absence of a surfactant. These enhanced optoelectronic properties make them more suitable for small scale devices like thin film transistors [49, 93]. However, there is a necessity for cost effective large area SWNT thin films and thus, films deposited through solution processes are preferred in many electronic applications. SWNT thin films can be used in various applications as transparent electrodes in several devices such as organic light emitting diodes (OLEDs) [37], solar cells [98], electrochromic devices [101] and photodetectors [54,102] depending on their outstanding optoelectronic and chemical properties [37, 54].

SWNT thin films include both semiconducting and metallic nanotubes because of their nature. SWNT thin film transistors (TFTs) utilize semiconducting SWNT networks [42]. It has been studied that the transparent SWNT TFT performance is limited by the metallic SWNTs, even below their percolation threshold [99]. Solutions, which are enriched by semiconducting nanotubes, can lead to improved TFT performance [100].

Another important application area of SWNT thin films is their use as electrodes in energy storage devices such as supercapacitors and batteries. Their nanoporous structure makes them useful for supercapacitors. There are several studies on these flexible and transparent porous nanotube electrodes. SWNT thin film applications such as field emission displays and interconnects in microelectronics are also possible.

SWNTs offer numerous unique properties and networks are promising for a wide range of applications. In this thesis another particular application, the use of SWNT thin films for EMI shielding is investigated and will be discussed in detail.

2.2. EXPERIMENTAL DETAILS

2.2.1 SWNT Thin Film Fabrication

The methods utilized in this study for fabricating SWNT thin films are vacuum filtration and spray coating. Vacuum filtration method requires a subsequent film transfer step as mentioned earlier. Post-deposition acid treatments and centrifugation have also been applied to improve the film quality and optoelectronic properties. The details of these methods and processes are described and illustrated step by step in Figure 2.21.

2.2.1.1 Substrate Cleaning

Before starting the experiments, all glassware such as beakers, petridishes etc. were cleansed with water and a powder detergent (Alconox). After washing, they were immersed into an acidic solution prepared with nitric acid (HNO_3) and then put into pure water to remove this acidic solution from their surfaces. Finally a dilute basic solution prepared with sodium hydroxide (NaOH) was utilized and they were rinsed with pure water again to remove all the residuals. All the chemicals used in this study were purchased from Sigma-Aldrich and utilized without further purification. In addition, all glasses used as substrates were respectively sonicated in acetone (99.8 %), isopropanol (99.8 %) and deionized (DI) water (18.3 M Ω) for 5 minutes each. Flexible polyethylene terephthalate (PET) substrates were only subjected to isopropanol bath for 20 minutes.

2.2.1.2. Vacuum Filtration Method

2.2.1.2.1. Dispersion of SWNTs

In this work, a simple vacuum filtration method which was originally introduced by Wu et al. was used to form homogeneous SWNT thin films [94]. Process starts with the preparation of a stable SWNT dispersion. Arc-discharge synthesized and purified SWNTs (P2 and P3 types) were purchased from Carbon Solutions, Inc. and a sodium dodecyl sulfate (SDS) assisted SWNT dispersion was prepared in deionized water (DI, 18.3 M Ω). The concentrations of SWNTs were ideally 2 mg/L. SWNT solution was sonicated for 5 minutes using a 20 kHz tip-sonicator (Figure 2.21 (a)). The tip-sonicator (Sonopuls, HD 2070) was operated at 90 % for an approximate sonication power of 70 Watts. After sonication, the homogeneity of the SWNT dispersion can be seen from Figure 2.21 (b). Centrifuge step was used to enhance the dispersion by eliminating large SWNT bundles. As prepared SWNT solution was then centrifuged at 5500 rpm (Cence, TG16-VS) for 20 minutes and the supernatant solution was used for further process.

2.2.1.2.2. Deposition process

Following the dispersion step, different volumes of SWNT solution was filtered onto 200 nm mixed cellulose ester (MCE) membranes (Millipore) (Figure 2.21(c)). MCE membranes with 25, 47 and 90 mm diameters were used during the experiments. All membranes were washed with several milliliters of water to remove the surfactant residuals that were left on their surfaces. Afterwards, MCE membranes were transferred onto glass and PET substrates, dried at 80 °C for 2 hours on hot plate under 40 g/cm² load (Figure 2.21 (d)). Applied force contributes adhesion of SWNTs to the substrates. Finally, membranes were etched in consecutive acetone (99.8 %) and isopropyl alcohol (99.8 %) washings (Figure 2.21 (f)).

2.2.2. Post-deposition acid treatments

Following the deposition process, the functionalization treatments were carried out by dipping the SWNT films into a nitric acid (HNO₃, 69.7 %) bath for 3 hours. After they were completely dried with nitrogen flow, an additional treatment was subsequently done to improve their conductivities. SWNT thin films were immersed into a thionyl chloride (SOCl₂, 97 %) bath for 2 hours and dried with a gentle nitrogen flow. All the functionalization processes were performed at room temperature.

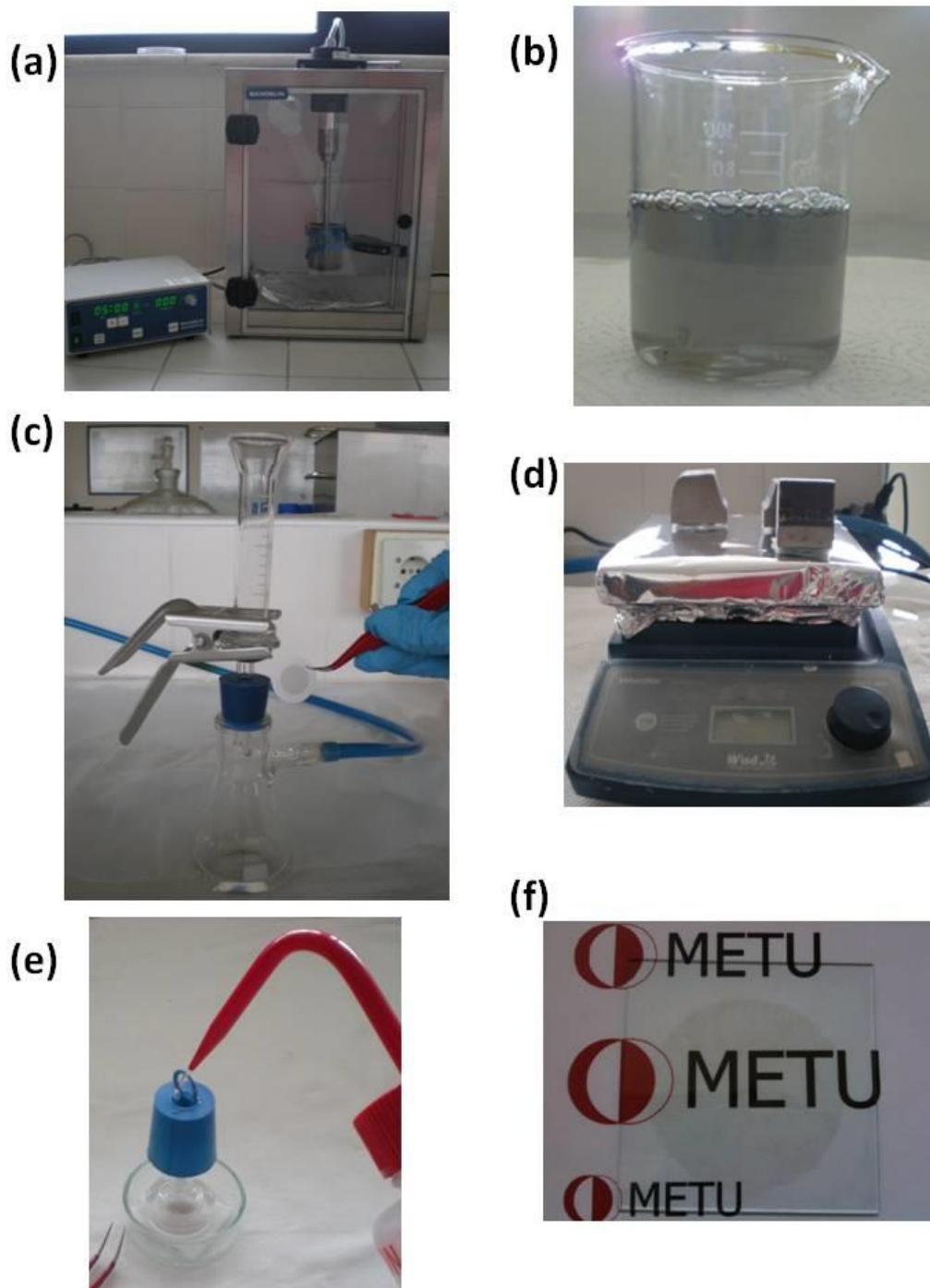


Figure 2.21 SWNT thin film fabrication process. (a) Sonication process. (b) SWNT solution after the dispersion step. (c) Vacuum filtration set-up and the SWNT network on MCE membrane. (d) Film transfer process. (e) Removal of the MCE membrane with acetone (f) SWNT thin film deposited on glass substrate.

2.2.3 Spray Coating Method

Spray coating was used as an alternative deposition technique in this study for large area applications. Spray coating process can be summarized in three steps. First step is the dispersion of SWNTs in aqueous solutions at a concentration of 10 mg/L with 1 wt % SDBS. After mixing, SWNT solution was sonicated for 5 minutes with tip-sonicator. Second step is the ultrasonic spray deposition. Substrates, that had been cleansed, were placed onto a stage capable of moving in two dimensions which was maintained at 200 °C to avoid fine droplets. SWNT thin films were spray coated onto 10 x 10 cm² glass substrates. Spraying conditions were optimized to reach the best film performance. The distance between the nozzle and the substrate was 8 cm and the stage scan speed was controlled with a software. Last step is the removal of surfactant. Spray coated samples were dipped into DI water for 3 h and then dried on a hot plate for 1 h at 80 °C.

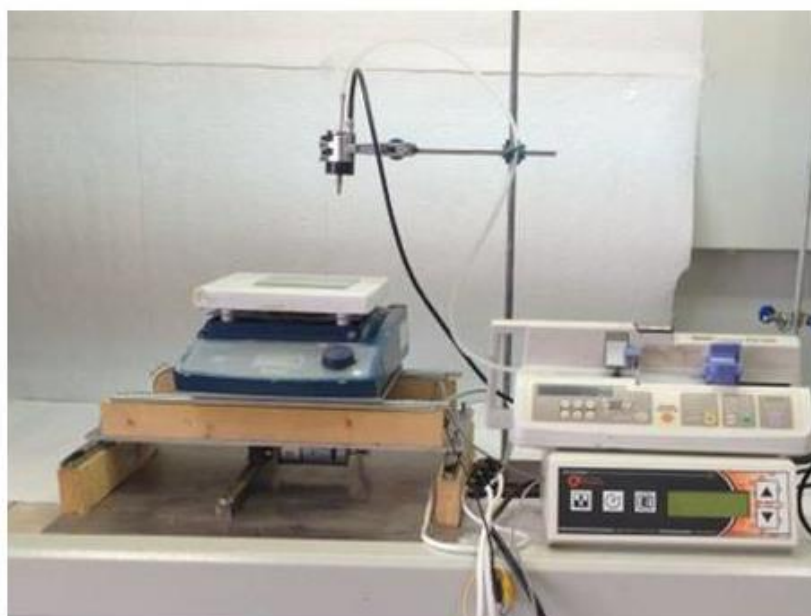


Figure 2.22 SWNT thin film spray coating process.

2.3. SWNT THIN FILM CHARACTERIZATION METHODS

2.3.1. Scanning Electron Microscope (SEM)

Homogeneity, density and morphology of the fabricated SWNT thin films were analyzed by field emission scanning electron microscopy (FE-SEM, Nova NanoSEM 430). The operating voltage was between 10 and 15 keV. Since the SWNT thin films were conductive, no further gold/carbon coating was utilized.

2.3.2. Optical Transmittance Measurements

Transmittance measurements of the SWNT thin films were all performed at room temperature using a UV-Vis spectrometer (Varian-Cary 100 Bio) within the range of 300-800 nm wavelengths. A clear bare glass slide was used for the baseline correction.

2.3.3. Sheet Resistance Measurements

Sheet resistance values of SWNT thin films were measured using a two probe measurement set-up, as shown in Figure 2.23 Gallium-indium (GaIn) alloy (99.99 %, SigmaAldrich) is utilized as contacts for the sheet resistance measurements. Keithley 2400 sourcemeter was used as the voltage source. Contact diameters (D) were 1.5 mm and the distance (L) between them was equal to 3 mm. The given formula was used to calculate the sheet resistance (Ω/\square) and the measured value from Keithley was put in the equation as resistance (R).

$$R \times \frac{L}{D} = r \quad (2.6)$$

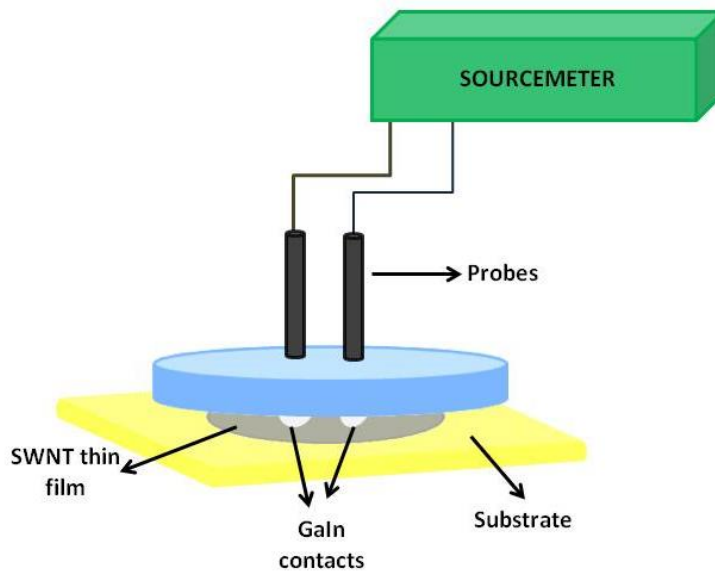


Figure 2.23 Schematic of the two probe sheet resistance measurement set up.

2.4 RESULTS

2.4.1. Effect of Sonication

Sonication process is an important parameter for obtaining stable SWNT dispersions due to the agglomeration tendency of the SWNTs into large bundles. Ultrasonic bath and tip sonicators were utilized during the dispersion processes. Both sonication types were examined and the final SWNT solutions were compared. There was a significant difference between the solutions. Figure 2.24 shows photographs of those two different SWNT solutions prepared at the same concentration. SWNT solution which was bath sonicated for 3 hours is shown in Figure 2.24 (a). It can be clearly seen that the dispersion of SWNTs is still poor even after 3 hours of sonication. Agglomerated SWNTs were found to float in the suspension. On the other hand, Figure 2.24 (b) shows a homogeneous SWNT solution, which was sonicated using a tip sonicator for 5 minutes. Only after 5 minutes, a homogeneous and stable SWNT dispersion was obtained. In addition, the dispersion remained completely aggregation free for a week. Sonication times utilized in this thesis varied from 5 minutes to 15 minutes for tip sonication and 3 hours to 24 hours for ultrasonic bath sonication.

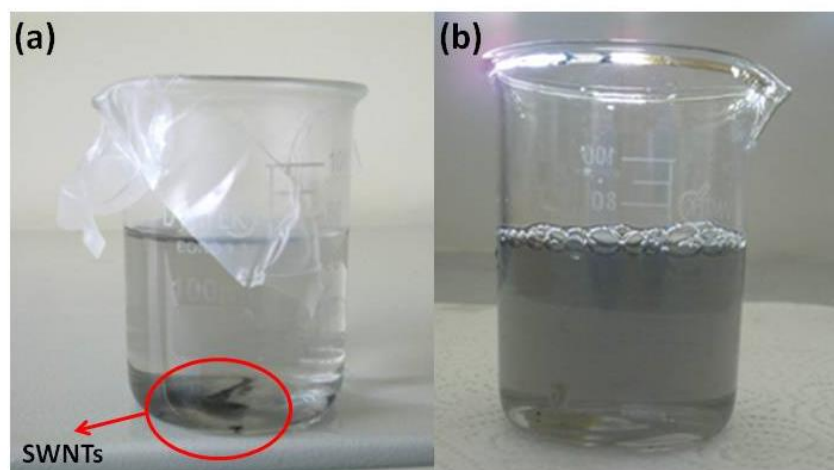


Figure 2.24 Photographs of the SWNT solutions after (a) 3 hours of ultrasonic bath sonication and (b) 5 minutes of tip-sonication. Red circle on (a) indicates the aggregates formed by SWNT bundles.

Tip sonicator has enough energy to break apart the SWNT bundles without shortening them. Hence, utilizing a tip sonicator increase the concentration of the unbundled SWNTs in the solution and the dispersion quality. In addition, the time required for the dispersion process significantly decreases through the use of a tip sonicator.

2.4.2. Effect of SWNT Type

Two different types of SWNTs (P2 and P3) were purchased in powder form. Both types were arc-discharge. The average diameter and lengths of the SWNTs were 1.4 nm and 1 μm , respectively. The metal catalyst impurity contents of both P2 and P3 SWNT powders are reported as 5-8 wt % by the vendor. The carbonaceous purity of the SWNT powders, in other words, the SWNT ratio as a percent of all carbonaceous materials were higher than 90 %.

SWNT thin films were fabricated utilizing both P2 and P3 SWNTs. In order to evaluate the effect of the SWNT type on the film performance and to compare their optoelectronic properties, two different sets of samples were prepared using vacuum filtration method. Figure 2.25 summarizes the film performances with a sheet resistance vs. optical transmittance (at 550 nm) plot. The data points of each set correspond to SWNT thin films with different densities. P3 type SWNT thin films have shown a better performance compared to P2 type. Measured optical transmittance values were similar; however, their sheet resistance values were found to be different.

P3 SWNTs were functionalized, which were purified with HNO_3 . On the other hand, P2 SWNTs were purified by air oxidation so they were resembling the pristine state with low functionality and chemical doping. P3 SWNTs contained 1 - 3 atomic % of carboxylic acid groups. These carboxylic acid groups were attached to SWNT surfaces and created a negative charge on them. Therefore, those negatively charged SWNTs were hydrophilic. The high percentages of the functional groups in P3 SWNTs reduced the interaction between the SWNT side walls and overcome bundling. As a result, higher conductivity values were obtained from the thin films fabricated using P3 SWNTs.

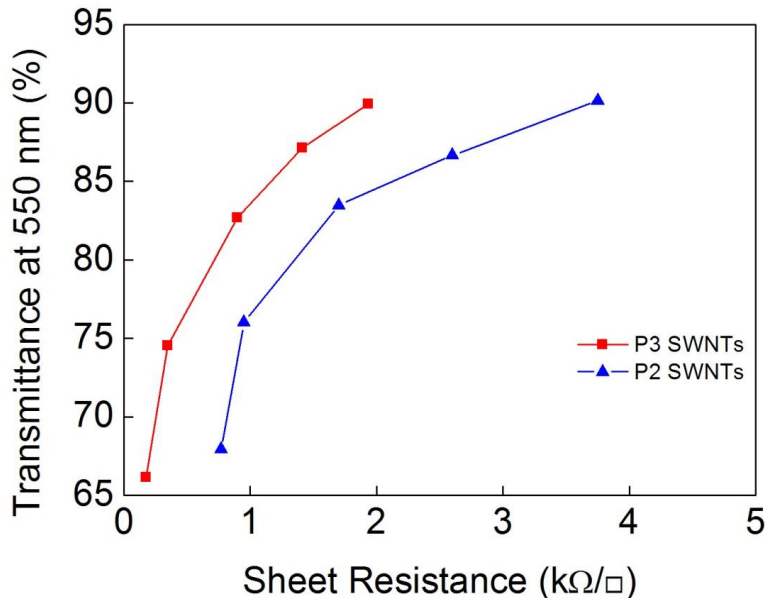


Figure 2.25 Sheet resistance vs. optical transmittance plot for P2 and P3 SWNT thin films. Lines are for visual aid.

2.4.3. Effect of Density

Optoelectronic properties of the thin films deposited on glass substrates using vacuum filtration method at a SWNT solution concentration of 2 mg/L and different filtration volumes (2.5 – 12.5 ml) were investigated. Figure 2.26 shows a photograph of SWNT thin films with different densities. METU logo behind the thin films was evident even for the highest filtration volume, clearly showing the transparency of the films. SWNT thin film densities were calculated using a simple relation. SWNT amount in every filtered volume is directly proportional to the solution concentration so that the amount per film area was calculated. SWNT thin film densities are 1.24×10^{-4} mg/mm², 9.95×10^{-5} mg/mm², 7.46×10^{-5} mg/mm², 4.97×10^{-5} mg/mm² and 2.48×10^{-5} mg/mm² for the filtration volumes of 12.5, 10, 7.5, 5 and 2.5 ml, respectively.

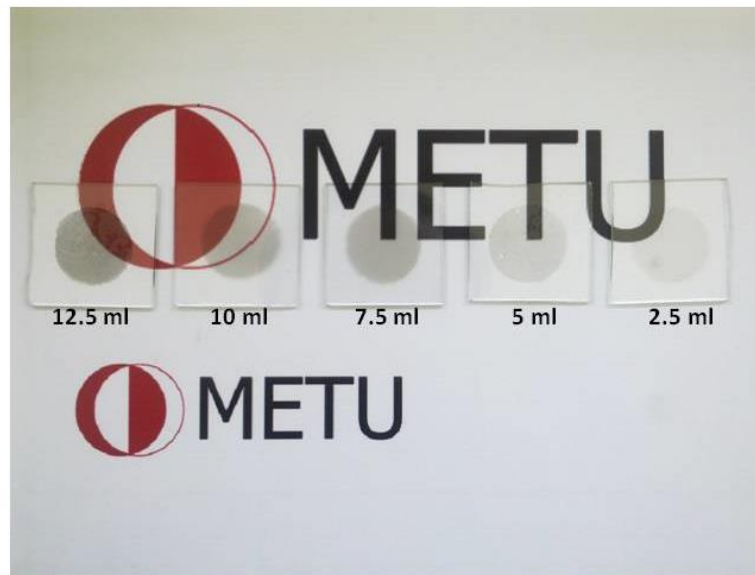


Figure 2.26 Photograph of SWNT thin films deposited on glass substrates by vacuum filtration method at the same concentration and five different filtration volumes.

Figure 2.27 (a) and (b) shows the SEM images of SWNT thin films prepared with filtration volumes of 2.5 and 12.5 ml, respectively. Individual SWNTs and the underlying glass substrate is evident for the SWNT thin film prepared with a filtration volume of 2.5 ml.

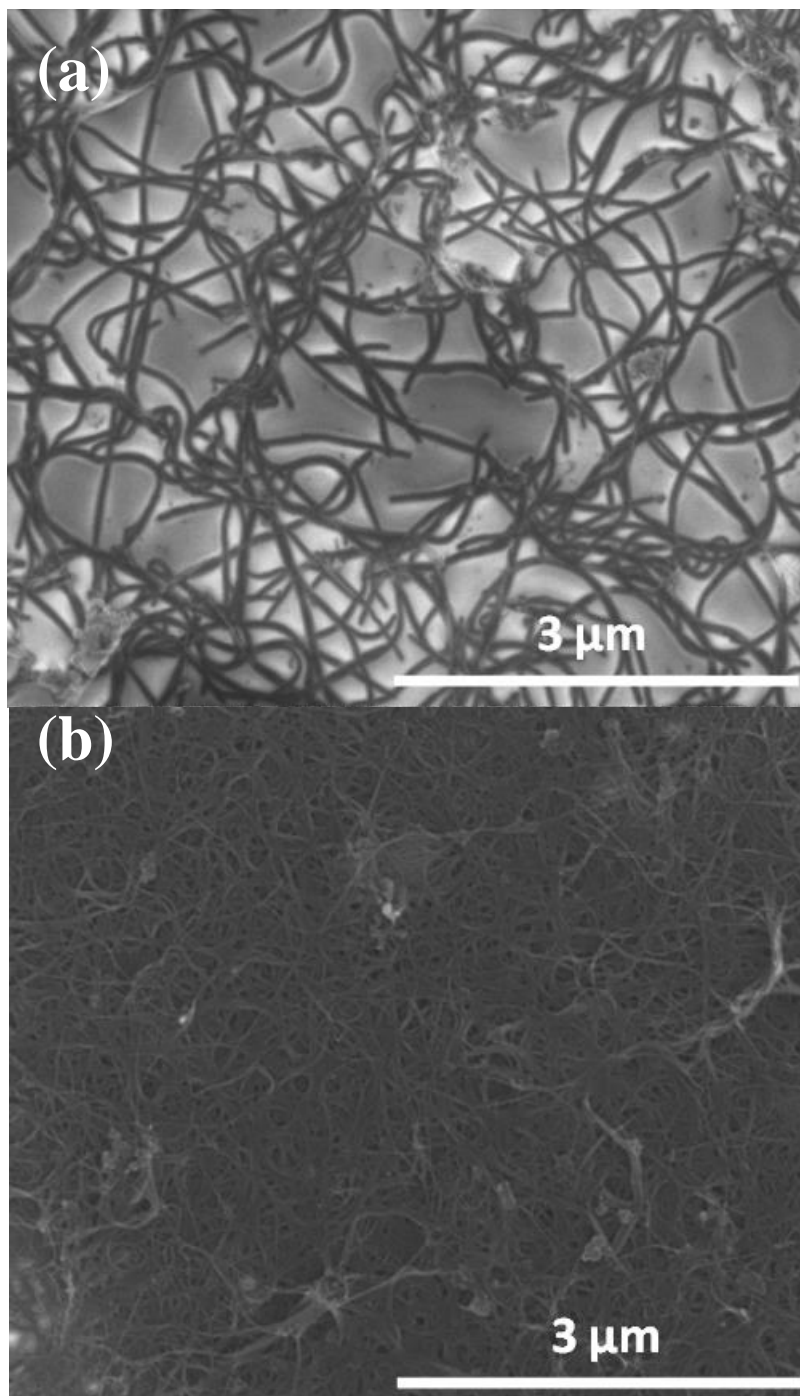


Figure 2.27 SEM images of the SWNT thin films prepared from filtration volumes of (a) 2.5 ml and (b) 12.5 ml.

Figure 2.28 (a) shows the optical transmittance versus wavelength data for the films prepared with different filtration volumes. The plot proves the influence of film density on the film transmittance and as expected, optical transmittance decreases with the film density.

Figure 2.28 (b) shows the correlation between the sheet resistance and transmittance of SWNT films at a wavelength of 550 nm. Transmittance decreases with the film density.

However, increasing SWNT density decreases the sheet resistance of SWNT thin films due to an increase in the number of conducting pathways along the network.

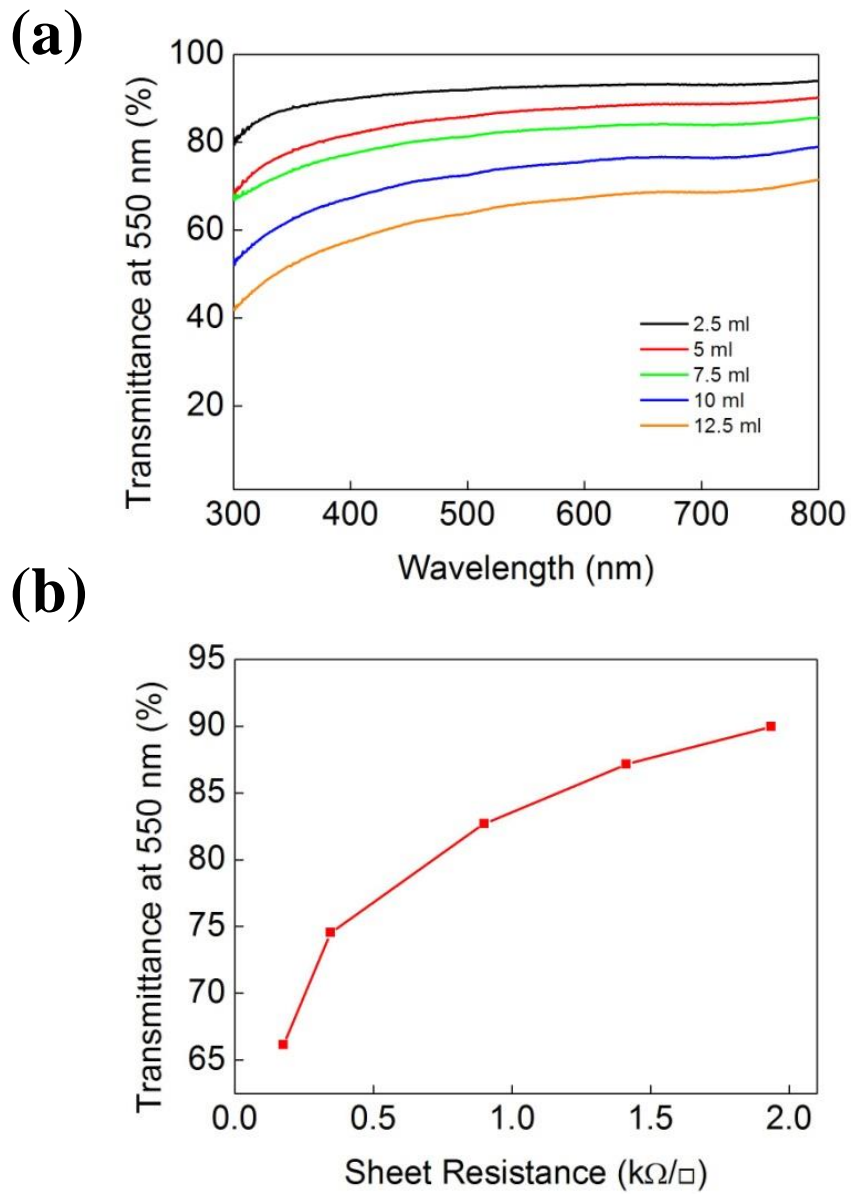


Figure 2.28 (a) Transmittance of the SWNT films prepared with different filtration volumes. (b) Sheet resistance vs. optical transmittance plot for SWNT thin films. Lines are for visual aid.

2.4.4. Effect of Surfactant

SWNT dispersions with three different surfactant types were prepared and compared. All solutions were sonicated using a tip sonicator for 5 minutes. Figure 2.29 shows a photograph of the vials containing (left to the right) SDBS, SDS and Triton X-100 assisted SWNT dispersions at the same concentration. It can be seen that the SDS dispersed SWNT solution is homogeneous; whereas the SDBS and the Triton X-100 dispersed SWNT solutions contain SWNT bundles following the sonication process. Aggregation free SWNT solutions were obtained at longer sonication times for SDBS and Triton X-100 assisted dispersions.



Figure 2.29 Photograph of vials (10 ml) containing SDBS, SDS and Triton X-100 assisted SWNT dispersions taken 5 minutes after sonication.

Vacuum filtration method was utilized for the deposition of the SWNT thin films and their optoelectronic properties have been investigated. Figure 2.30 shows the sheet resistance versus optical transmittance plot for SWNT thin films prepared from dispersions of SWNTs with different surfactants. It is found that the films fabricated from SDS dispersed SWNT solutions show the best optoelectronic performance. SDS provides the best dispersion due to the strong electrostatic attraction of its own molecules with the nanotube surfaces. As a result they have lower sheet resistance values under similar transmittance values.

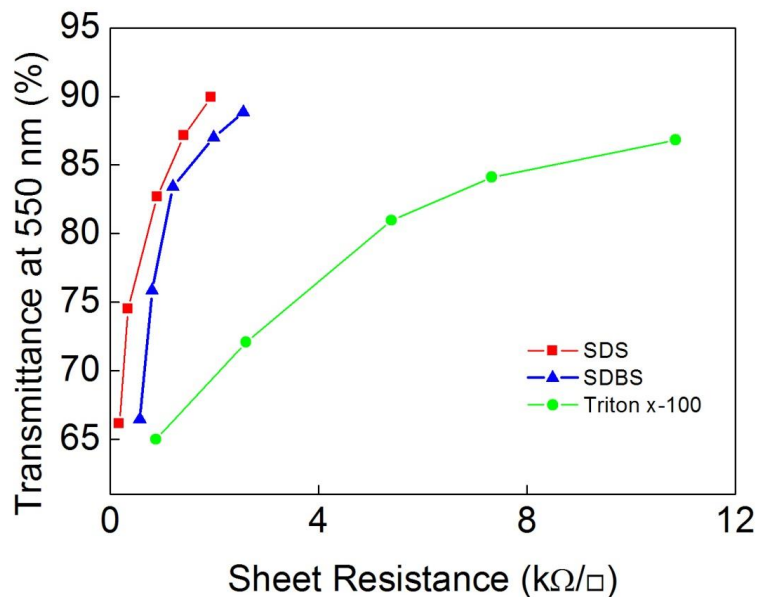


Figure 2.30 Sheet resistance vs. optical transmittance plot for the SWNT thin films prepared with different surfactants. Lines are for visual aid.

2.4.5. Effect of Post Deposition Treatments

In order to improve the conductivity, SWNT thin films were immersed in an acid bath followed by thionyl chloride (SOCl_2) immersion. It is found that sheet resistance of the SWNT thin films can be decreased by a factor of 5 after these treatments. It can be seen from Figure 2.31 that the sheet resistance decreases by a factor of 3 after the initial 3 h nitric acid (HNO_3) treatment. An additional 3 h SOCl_2 bath provides a further decrease in the sheet resistance of thin films. Optical transmittance values of the films were not affected by those treatments. These results were in agreement with the literature [98].

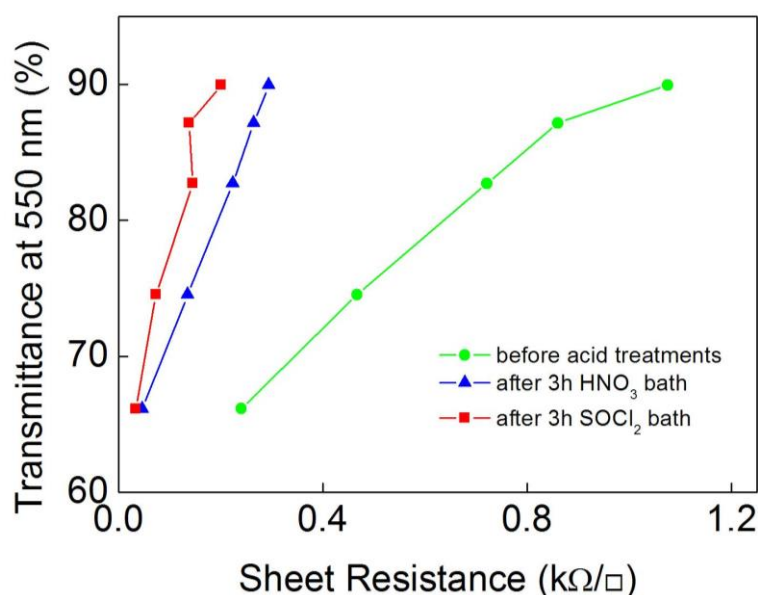


Figure 2.31 Sheet resistance vs. optical transmittance plot for post deposition treated acid functionalized SWNT thin films. Lines are for visual aid.

Following post deposition treatments, SWNT thin films exhibited improved optoelectronic properties. Lower sheet resistance values were achieved at high transmittance levels. All SWNT thin films, even the untreated ones obtained in this work, are comparable to the reported ones in literature. Thin films with a sheet resistance of $180 \Omega/\square$ was obtained at a transmittance of 91%. In the densest films, which were prepared using a filtration volume of 12.5 ml, sheet resistance values were lower than $40 \Omega/\square$.

The enhancement in electrical conductivity of the films depends on two factors. One of them is the removal of the insulating residual surfactant. Residual SDS on the SWNTs sidewalls cannot be washed away completely during the vacuum filtration process and limit the interaction between nanotubes. The other factor is the increased charge carriers due the p-type doping effect. P3 SWNTs with 1-3 % of carboxylic acid groups were utilized during the experiments. After immersing the films into a SOCl_2 bath those carboxylic acid groups were substituted with acyl chloride groups. These groups contribute holes to the SWNTs and improve the overall conductivity of the films.

2.4.6. Effect of Centrifugation

Experimental results revealed that an additional centrifuge step following the sonication process was effective in enhancing the performance of SWNT thin films. Removing large SWNT bundles from the dispersion increase the transmittance of the SWNT thin films by increasing the void fraction of the films. Figure 2.32 shows the transmittance versus wavelength plot for SWNT films deposited using centrifuged solutions. Four different filtration volumes were examined.

Centrifugation forces eliminate the undispersed and heavy SWNT bundles including the remaining residual impurities in the SWNT solution. As a result, sheet resistance values of the SWNT films show a significant decrease. This means that, higher filtration volumes should be utilized for the deposition of SWNT thin films with low sheet resistance values. Figure 2.33 shows a clear comparison in optoelectronic properties of SWNT thin films deposited using regular and centrifuged solutions. For comparison, data for post deposition functionalized SWNT thin films were also provided on the same plot. SWNT thin films deposited using centrifuged solutions exhibited the best performance.

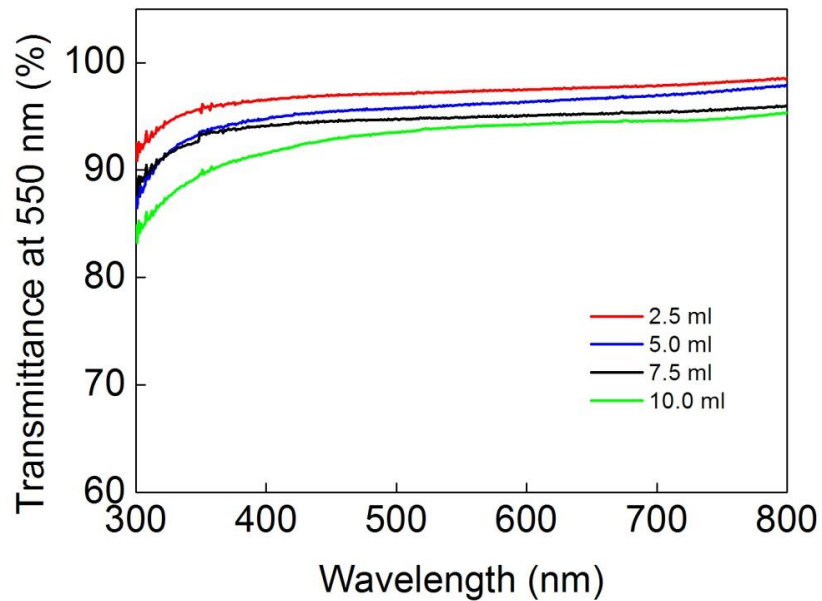


Figure 2.32 Improved optical transmittance data of the SWNT films deposited after centrifugation for four different filtration volumes.

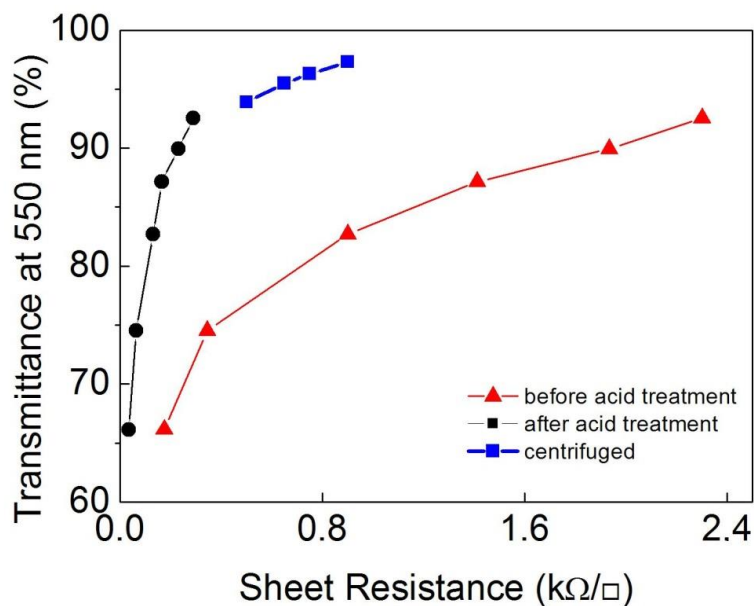


Figure 2.33 Sheet resistance vs. optical transmittance plot for various SWNT thin films. Lines are for visual aid.

SEM images in Figure 2.34 reveal the difference between SWNT thin films deposited using regular and centrifuged solutions. SEM images in Figure 2.33 (a) and (b) belongs to the thin films prepared with regular and centrifuged solutions, respectively. A filtration volume of 10 ml has been used for the deposition of both films. Individual SWNTs that are free of bundles are evident for the thin film deposited using centrifuged solution.

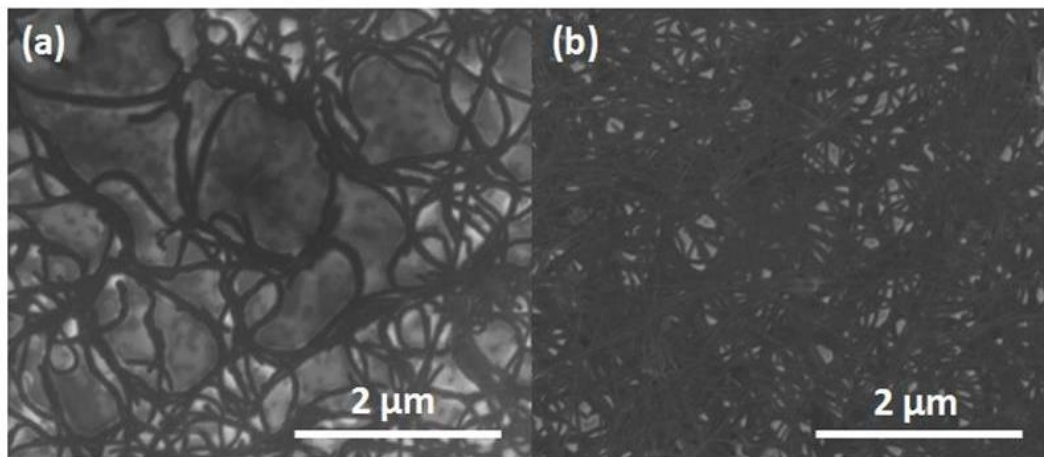


Figure 2.34 SEM images of the SWNT thin films deposited by vacuum filtration on glass from (a) centrifuged SWNT solution and (b) regular SWNT solution.

2.4.7. Large Area Applications

Vacuum filtration method can be scaled-up and used for large area applications. Figure 2.35 (a) and (b) shows photographs of the large area, transparent and conducting SWNT films on glass and PET substrates, respectively. These films were fabricated using larger filtration set-ups and 90 mm MCE membranes. Similar to the thin films fabricated so far, high quality and uniform SWNT thin films were deposited over large areas. A low sheet resistance value of $150 \Omega/\square$ with 83 % transmittance (at 550 nm) was measured for the films deposited over large areas.

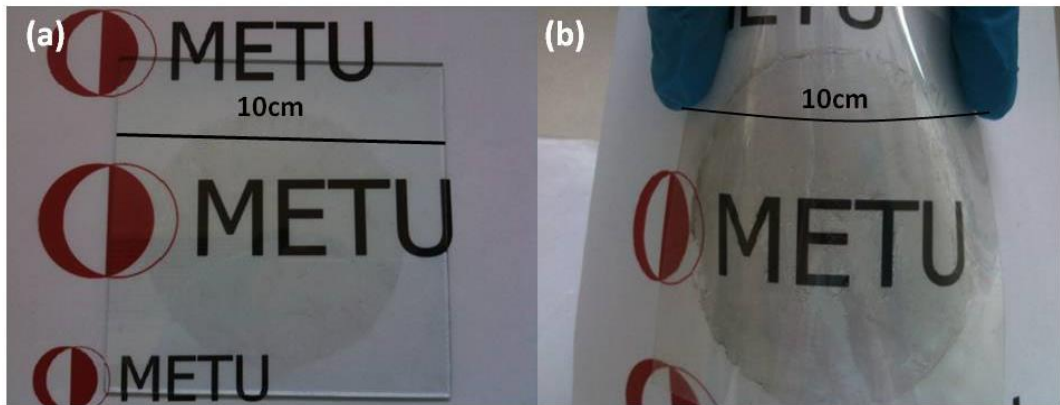


Figure 2.35 Photographs of SWNT thin films deposited on 10 cm x 10 cm (a) glass and (b) PET substrates using vacuum filtration method.

Spray coating method was also utilized, for the fabrication of SWNT thin films. Figure 2.36 shows photographs of the SWNT thin films that were spray coated on 10 x10 cm glass substrates at a SWNT solution concentration of 10 mg/L and different volumes (20 – 70 ml). Transmittance decreases with the film density. Minimum sheet resistance value for the spray deposited SWNT thin film was measured as 1 k Ω / \square .

Since spray coating is a fast and easily scalable technique, it is preferred for large area applications. However, optoelectronic properties of the spray deposited SWNT films did not show the same performance with the films deposited using vacuum filtration method. Spray coating parameters such as stage scan speed, ultrasonic nozzle frequency and substrate temperature should all be individually controlled to prevent droplet formation on the film surface. Therefore, the film uniformity could not be easily maintained like in vacuum filtration process.

Spray coated SWNT thin films were found to flake-off easily from the substrates. In addition, removal of the surfactants was also a problem. Following spray coating, SWNT thin films were only dipped into DI water in order to remove the residual surfactant. Nevertheless, DI water was not effective as acetone or isopropyl alcohol and surfactant could be removed from the SWNT thin films. Due to residual surfactant, sheet resistance of the spray deposited SWNT thin films were higher than the ones deposited through vacuum filtration method on glass substrates.

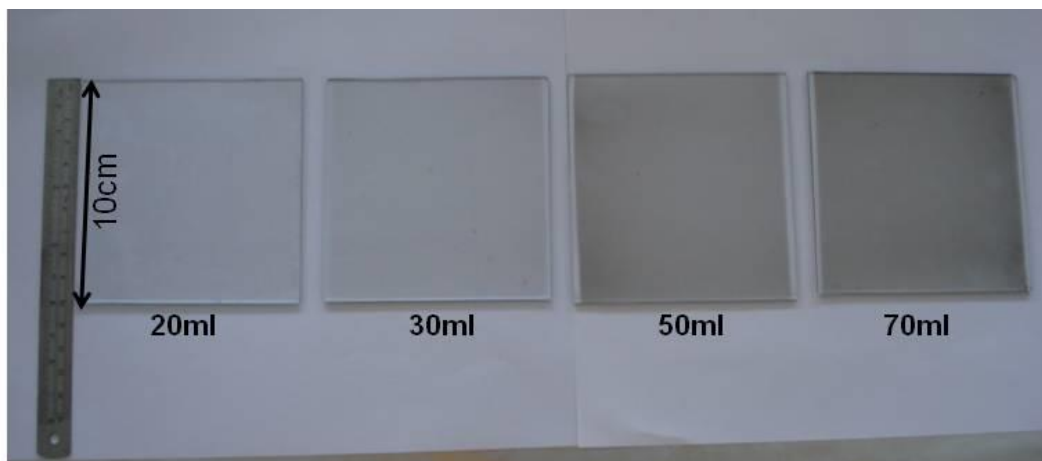


Figure 2.36 Photographs of SWNT thin films deposited on 10 x 10 cm glass substrates using spray coating method.

2.4.8. Mechanical stability of SWNT thin films

Unlike ITO thin films, SWNT thin films are well suited for flexible electronic applications. SWNT thin films have excellent mechanical properties. In order to evaluate their mechanical stability, electrical measurements were conducted while the SWNT films deposited on flexible PET substrates were bent to different radius of curvatures. Results are shown in Figure 2.37 (a) As-deposited and post-deposition functionalized SWNT thin films were used for these measurements. Data for ITO thin films deposited onto PET substrates, obtained from literature was also plotted on the same figure for comparison. Up to a bending radius of 10 mm neither SWNT films nor the ITO shows a significant change in sheet resistance. However, after a bending radius of 10 mm, ITO fails due to crack propagation, while the sheet resistance of SWNT thin films were unaffected.

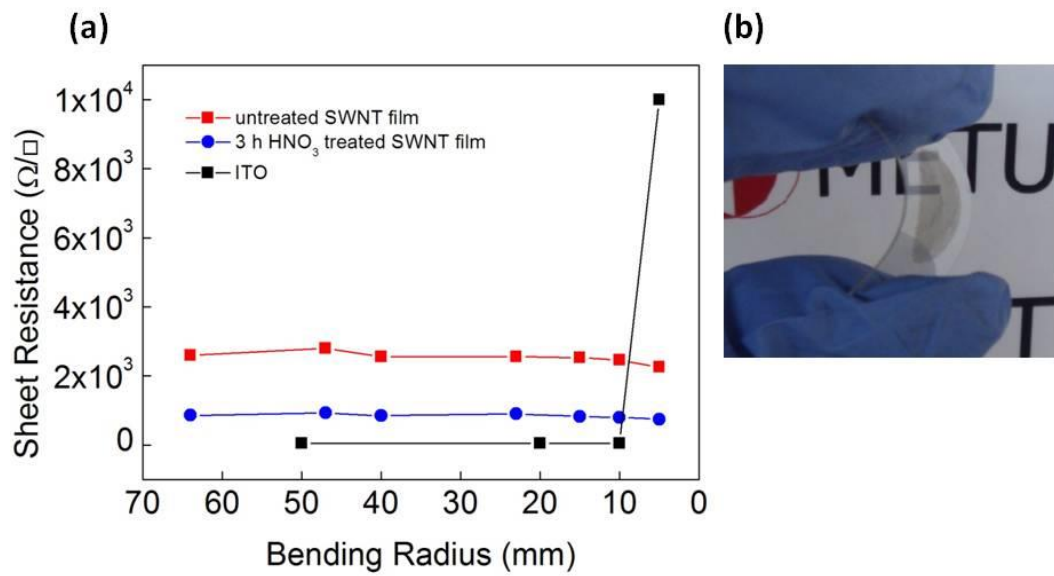


Figure 2.37 Mechanical stability of SWNT films on PET substrates. (a) Sheet resistance vs. bending radius plot. ITO data was obtained from [103]. (b) Photograph of a flexed SWNT thin film deposited on PET substrate.

CHAPTER 3

CHARACTERIZATION OF ELECTROMAGNETIC PROPERTIES OF SINGLE WALLED CARBON NANOTUBE THIN FILM COATED GLASS FIBER WOVEN FABRICS

3.1. INTRODUCTION

3.1.1. Electromagnetic Waves

Electromagnetic theory was first presented by James Clerk Maxwell and a set of equations named as Maxwell's equations were used to describe the electromagnetic (EM) phenomena by relating both electric field and magnetic field. From Maxwell's equations, it is deduced that an oscillating electric field can generate an oscillating magnetic field and in the same manner a magnetic field with an altering magnitude can generate an alternating electric field. Following generation, as shown in Figure 3.1 (a), EM waves propagate in the form of closed loops at the near field of an AC source. Contrary to this, EM wave propagation becomes planar as shown in Figure 3.1 (b) at the far field. Directions of the electric and magnetic fields are perpendicular to each other and they are also perpendicular to the direction in which the waves propagate. Figure 3.1 (c) shows both the oscillating electric and magnetic field components of an EM wave, which is travelling outwards from the source [104].

EM waves can travel on self-propagation through the space at the speed of light (3×10^8 m/s). The equation 3.1, shows the relation between the speed of light (c), wave frequency (f) and wavelength (λ).

$$c = \lambda f \quad (3.1)$$

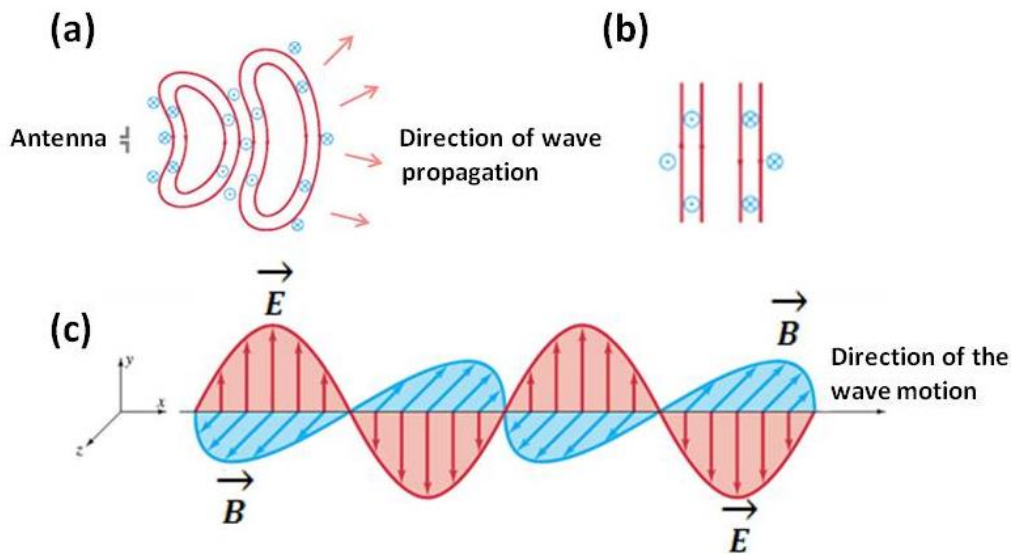


Figure 3.1 Propagation of an EM wave at (a) near field and (b) far field. (c) Representation of transverse oscillating EM wave with the electric and magnetic field components [104].

An electromagnetic spectrum is constituted to exhibit and elaborate the relation between frequency and wavelength as shown in Figure 3.2.

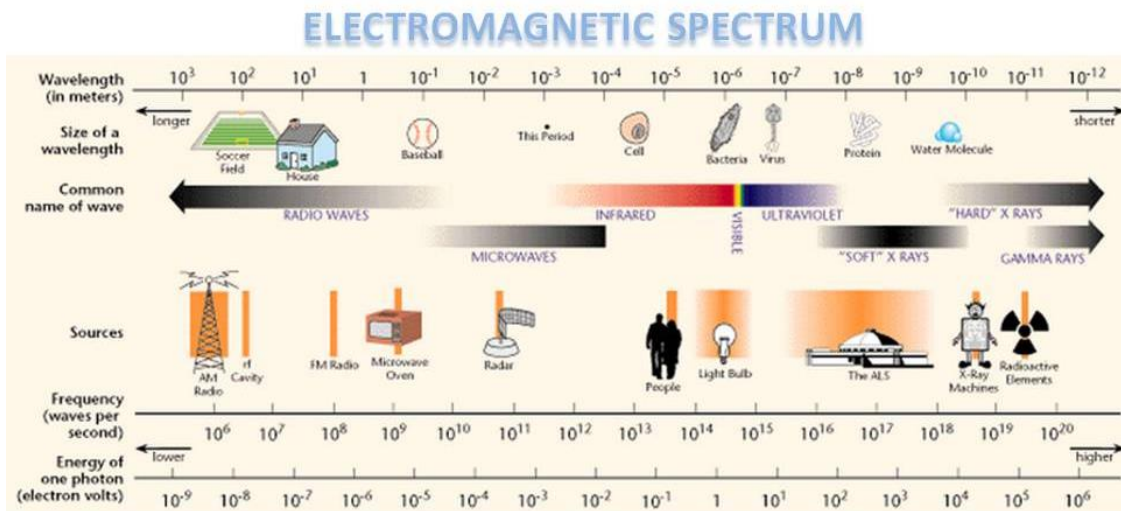


Figure 3.2 Electromagnetic spectrum [105].

According to the spectrum, it is obvious that, as the frequency increases, wavelengths of the EM waves decrease. In other words, there is an inverse proportion between them as shown in equation 3.2. In addition to that proportion, higher frequencies increase the energy of EM

waves. All of these parameters are important in determination of the utilization of EM waves in engineering applications.

$$E = hf = \frac{hc}{\lambda} \quad (3.2)$$

EM waves interact with objects as they interact with each other. For the first case, EM wave interaction with materials is being used to detect objects through a large scale by several methods. The latter case is about another distinctive characteristic of EM waves. EM waves can interact with each other and depending on the conditions, superpositions, intensifications or cancellations can occur. Those constructive and destructive interferences of EM waves are utilized in several areas such as wireless communications and broadcasting [107]. In atmospheric circumstances, progressive EM waves can also interact with the constituents, which are naturally found in the atmosphere. Figure 3.3 shows a plot of the opacity of atmospheric media to a broad-spectrum of various wavelengths of EM waves [106]. According to Figure 3.3, gamma rays, X-rays, Ultraviolet (UV) and infrared wavelengths are absorbed by the atmosphere, while visible light and radio waves are observable.

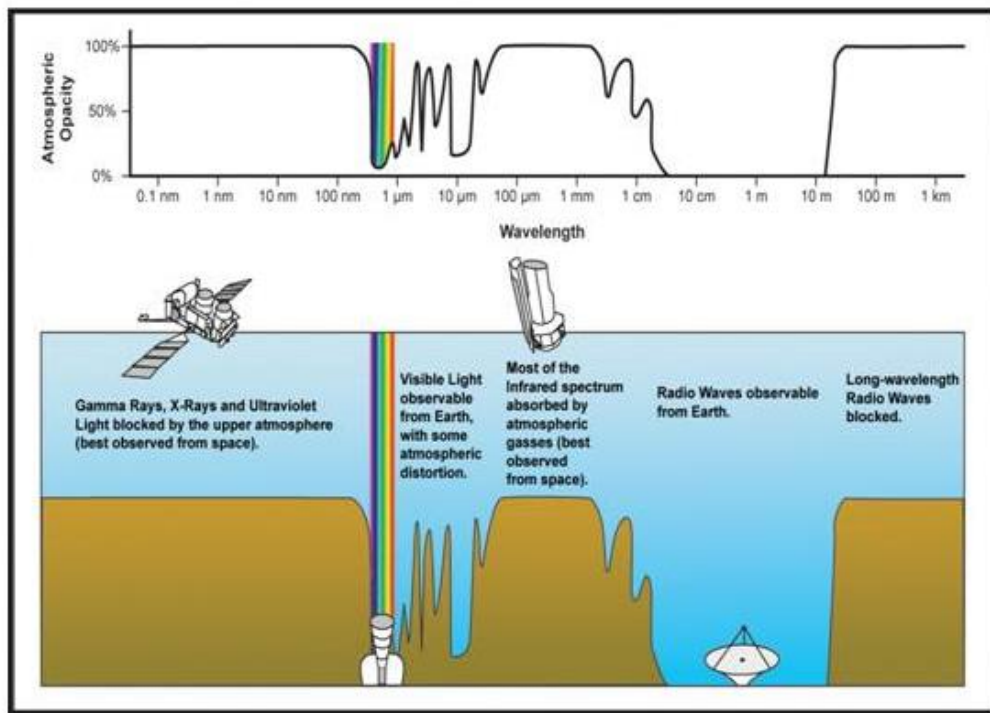


Figure 3.3 Atmospheric window [106].

In the recent years, electronic systems and devices have gone under rapid and also consistent development. Thus, with increased usage of devices in commercial, industrial or defense sectors, EM radiation has become a potential danger for human health and created some functional problems. In addition, EM wave interactions can also cause misinterpretations of the data and quality losses. In many cases, electromagnetic interference (EMI) leads to loss of time, money or life [108].

In the view of such information on EM wave interactions, electromagnetic interference (EMI) is an inevitable, undesired problem for many applications in engineering. Therefore, EMI shielding materials, composites and EM wave absorbing structures are being used to avoid health problems or the information loss due to EM wave interactions. In order to provide a sufficient, feasible and also cost effective shielding, shielding material should either have charge carriers or dipoles that are interacting with both electric and magnetic field components of the EM wave.

3.1.1.1. Microwave Band Applications

Microwave radiation occupies a position which lies between infrared and radio waves; corresponding to wavelengths from 1 mm to 1 m. In other words, microwave band covers the frequencies from 300 MHz to 300 GHz, throughout the EM spectrum. There are a lot of applications that can be operated at frequencies within the 1 to 40 GHz range in engineering. Table 3.1 shows a brief summary of the radar bands and their general application areas. Microwave radiation offers distinct advantages in various application areas, such as communication, navigation, cooking, medical diagnostics, defense applications etc. Microwaves travel without bending by the ionosphere, so they provide higher capacities in communication when compared to low frequency techniques. In medical diagnostics, their insensitivity to high impedance makes their penetration profile deeper. Moreover, in defense applications, detection of physical objects with low radar cross-section can be done by radars that are operating at higher frequencies. However, besides their advantages, for the applications requiring short wavelengths, manufacturing and designing microwave components can have some disadvantages due to their small sizes [109].

Table 3.1 Radar bands and their application fields [109].

| Radar Frequency Bands and General Usages | | |
|---|------------------------|---|
| Band Designation | Frequency Range | General Usage |
| VHF | 50 - 300 MHz | Very Long-Range Surveillance |
| UHF | 300 - 1000 MHz | Very Long-Range Surveillance |
| L | 1 - 2 GHz | Long Range Surveillance, Enroute Traffic Control |
| S | 2 - 4 GHz | Moderate Range Surveillance, Terminal Traffic Control, Long Range Weather |
| C | 4 - 8 GHz | Long Range Tracking, Airborne Weather Detection |
| X | 8 - 12 GHz | Short Range Tracking, Missile Guidance, Mapping, Marine Radar, Airborne Intercept |
| Ku | 12 - 18 GHz | High Resolution Mapping, Satellite Altimetry |
| K | 18 - 27 GHz | Little Used (Water Vapor Absorption) |
| Ka | 27 - 40 GHz | Very High Resolution Mapping, Airport Surveillance |
| Millimeter | 40+ GHz | Experimental |

According to Table 3.1 microwaves can be separated into multiple bands some of which are very common in daily life. Systems operating at high frequencies bring along problems in EMI. In order to sort out this problem and satisfy the needs, development of EMI shielding materials is essential. In this chapter, EMI shielding properties and characterization of SWNT thin films will be discussed for frequencies within 18 - 40 GHz.

3.1.2. Electromagnetic Wave– Matter Interactions

EM waves primarily travel through an atmospheric media after they emitted from an electronic source as mentioned in Section 3.1.1. As they go further from the source, power of the EM waves weakens. EM wave interactions with materials also accelerate the degree of this power attenuation. When EM waves encounter materials along their pathway, EM energy transfer takes place.

Loss of EM energy depends on the electromagnetic characteristics of the matter and the environment. EM energy can be reflected, scattered in different directions, transmitted through the material or absorbed by the material as represented in Figure 3.4. The sum of all the reflected (P_R / P_0), transmitted (P_T / P_0) and absorbed (P_A / P_0) power fractions must be equal to 1 as shown in the formula below, according to energy conservation principle, where P_0 represents the power of the incident wave emitted from the source ignoring scattering.

$$1 = \frac{P_R}{P_0} + \frac{P_T}{P_0} + \frac{P_A}{P_0} \quad (3.3)$$

Depending on a direct proportion, maximizing the reflection and absorption, minimizes other power losses caused by transmission.

3.1.2.1. Shielding Theory

EMI can be shielded by a material that is capable of reflecting and absorbing EM radiation. In other words, EMI shielding material should provide a barrier for reducing the EM radiation across the bulk material. Shielding effectiveness and EMI attenuation depends on many parameters, such as the distance between the EM source and the shielding material, the frequency, the thickness of the shielding material and the intrinsic impedance matching between the media and the material.

Shielding effectiveness (SE) is expressed in decibels (dB). It represents the total loss as a function of logarithm of the intensity ratios of the initial and final electric and magnetic fields as given by the equations 3.4 and 3.5 [110,111]:

$$SE(\text{dB}) = 20\log(E_0/E_1) \quad (3.4)$$

$$SE(\text{dB}) = 20\log(H_0/H_1) \quad (3.5)$$

There are three main mechanisms that are contributing to the SE. As shown in Figure 3.4, reflection of the incident beam (R_{Loss}), absorbed part of the incident beam by the shielding material (A_{Loss}) and the second reflection comes from the rear surface of the shielding material could affect SE depending on the phase difference between the incident EM wave and the reflected or absorbed EM waves. Therefore, SE of the material can be expressed as the sum of the reflection and absorption factors.

$$SE(\text{dB}) = R + A + b \quad (3.6)$$

If the absorption loss is less than 10 dB, the correction factor that represents the multiple reflections at several surfaces or interfaces within the shielding material, b , can be counted and contributed to the total loss. Otherwise, b can be neglected. Figure 3.4 represents the shielding mechanism in detail.

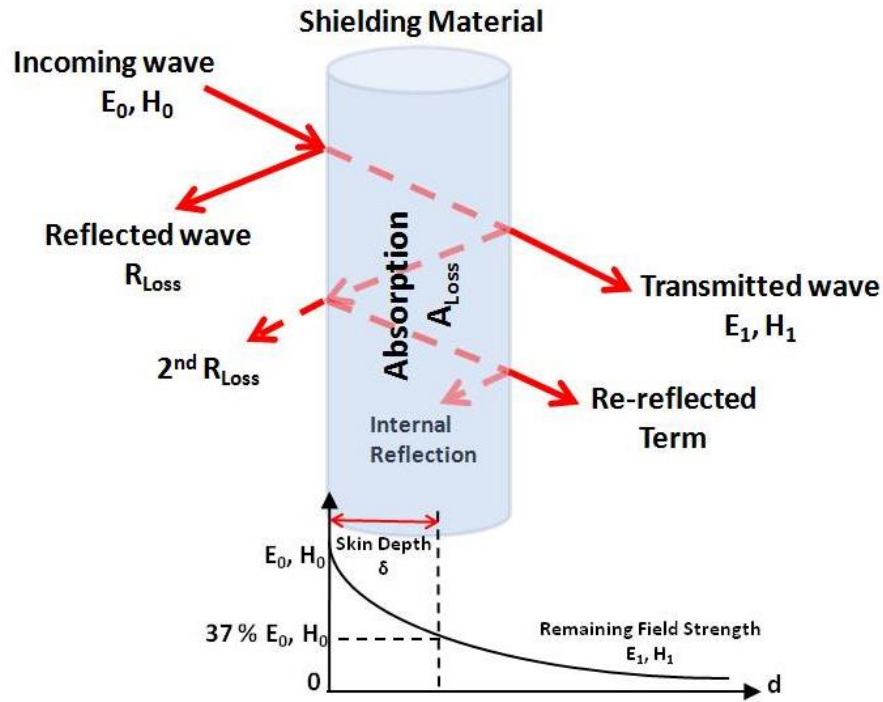


Figure 3.4 Interaction of electromagnetic radiation with the shielding material. Adopted from [112].

3.1.2.2. Electromagnetic Loss Mechanisms

There are 2 main mechanisms for EMI shielding. First one is the reflection mechanism. Shielding materials reflect the incoming EM wave via their mobile charge carriers, such as electrons and holes that interact with the EM radiation. The secondary mechanism is absorption which transfers the incident EM wave energy to the material. EM wave absorbing materials are capable of storing substantial amount of energy that is carried by the EM waves. Hence alternating magnetic and electric fields are related to each other, one causes the other and vice versa. In order to maintain a significant absorption, the absorbing material should simultaneously suppress both the electric and magnetic field components of the incident EM wave [104, 107].

Atomic structure, electron-hole pairs, dipoles and bonding characteristics of the material affect the absorbed and reflected amounts of the EM radiation. EM loss mechanisms are also expressed in dB similar to SE.

3.1.2.2.1. Dielectric Loss

Insulating materials that are capable of polarization in the presence of an applied electric field are defined as dielectric materials [113]. Electric charges do not flow freely within such poor conductors (less than $10^{-10} \Omega^{-1}\text{m}^{-1}$) named as dielectric materials.

However, when they are placed in an electric field, positive and negative charges are displaced slightly from their initial positions under a polarization vector. Separation of equal but opposite charges can be considered as dipoles. Due to the dielectric polarization, positive charges shift toward the applied electric field, while the negative charges migrate in the opposite direction as shown in Figure 3.5.

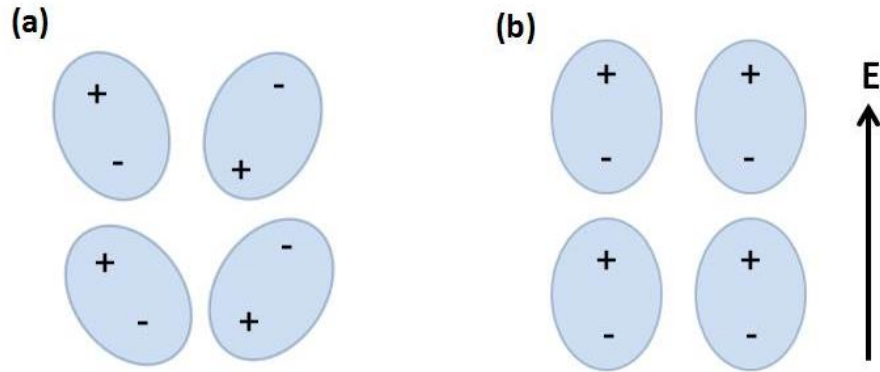


Figure 3.5 (a) Polar dipoles and (b) their polarization in the presence of an electric field.

Redistribution of the charges creates an internal electric field, leading to an overall electric field change within the dielectric material. Depending on the dielectric constant, reaction of the dielectric materials differs. This constant is related to the polarizability. Polarization takes place, due to the ability of the dipole to align with an alternating electric field. This is called as dipole rotation. Weakly bonded molecules become polarized, which is the alignment of their symmetry axis by reorientation. Moreover, ionization and thermal changes can also affect polarization.

Permittivity (ϵ) is a measure of the encountered resistance that occurs during the formation of an electric field within a dielectric medium. It can be shown as a constant of proportionality and can be written as [114]:

$$D = \epsilon E \quad (3.7)$$

where, D is the electric displacement field, which is about the dipole reorientation and charge migration caused by an electric field E and it is related to the polarization density. Permittivity increases with electric polarization. The ratio of total dielectric permittivity (ϵ) to the permittivity that is in vacuum or free space ($\epsilon_0 = 8.854 \times 10^{-12} \text{farads/meter}$) gives relative permittivity, (ϵ_r) :

$$\epsilon_r = \frac{\epsilon}{\epsilon_0} \quad (3.8)$$

Frequency dependent relaxation takes place, in the presence of an alternating electric field. Dipole reorientation and rotation due to polarization, affect the degree of relaxation in homogeneous dielectric materials [115]. Frequency dependent permittivity is shown in Figure 3.6.

$$\epsilon = \epsilon' - j\epsilon'' = \epsilon_0(\epsilon'_r - j\epsilon''_r) \quad (3.9)$$

The equation above consists of a real part, the dielectric constant and a complex part. Complex permittivity is utilized to express the dielectric loss. The ratio between those real and complex parts gives the power loss tangent:

$$\tan\delta_\epsilon = \frac{\epsilon''}{\epsilon'} \quad (3.10)$$

Alternating current (AC) frequency limits the relaxation time (τ) and if the oscillation rate of electric field is faster than the relaxation time τ , the polarization cannot catch up with the AC frequency. As a result, energy absorption occurs and dielectric material dissipates the energy as heat.

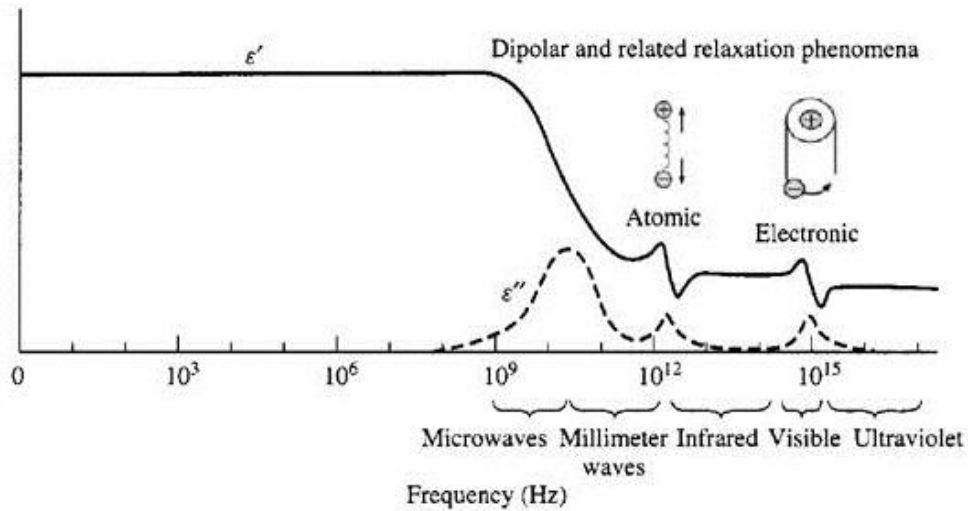


Figure 3.6 Dielectric constant and loss dispersion of dielectric materials with respect to frequency [116].

Dielectric loss can be summarized as the energy dissipation due to the dipole movement in an alternating EM field as polarization switches in direction. All of the parameters mentioned above can change dielectric loss. Nevertheless, it can be controlled and managed by resonance loss, conductance loss and dielectric relaxation loss [107].

Relaxation and resonance frequencies increase the dielectric loss depending on the polarization lagging. When the incident EM wave frequency and the oscillation frequency of the atoms in the material becomes the same, resonance loss appears. Resonance loss is also emitted as heat similar to dielectric loss.

Dielectric relaxation loss depends on the relaxation time, thus, increasing frequency limits relaxation loss. An energy transfer occurs between the EM energy and the mechanical energy, while dipoles are reorienting. Therefore, polarization mechanism cannot keep up with the alternating electric field [107, 117].

Free electrons and charges that flow through the matter in conductive materials can gain the electric field component of the EM wave. Conductive materials absorb the energy, which is occurred by heating. However, the energy of the incident EM radiation is mostly reflected by conductive materials, only a little part of the energy is absorbed [118]. In this thesis study, conductive SWNT thin films were coated onto glass fiber woven fabrics. As the thickness of SWNT thin film layer or the applied surface area increases, conductance loss increases due to resistance decrease.

3.1.2.2. Magnetic Loss

As detailed in section 3.1.1, EM waves have both electrical and magnetic field components. Dielectric or conductance loss is caused by the interaction between electrical field component of the incident EM wave and the materials. On the contrary, magnetic loss originates from the interaction between magnetic field component of the EM wave and the magnetic materials. Magnetic dipoles in paramagnetic materials can be aligned in the same direction of the applied magnetic field whereas diamagnetic materials repel the magnetic field [113, 117]. Figure 3.7 represents the initial and the final states of both paramagnetic and diamagnetic materials in the presence of an applied magnetic field.

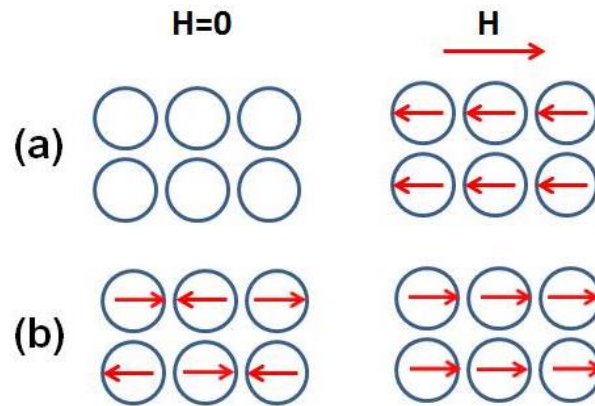


Figure 3.7 Dipole configurations in the existence of an external magnetic field (H) for (a) diamagnetic and (b) paramagnetic materials.

Magnetic field strength (H) represents the magnetic field produced by the electric current flow. When a magnetic material encounters an external magnetic field, it gives a response. Permeability is a measure of that response. Magnetic permeability (μ) is defined as the ratio of magnetic flux (B), which is the actual magnetic field within the material per unit cross sectional area, to H .

$$B = \mu H \quad (3.11)$$

Relative permeability (μ_r) is the ratio of total magnetic permeability μ to the permeability that is in free space conditions ($\mu_0 = 4\pi \times 10^{-7}$ henrys/meter).

$$\mu_r = \frac{\mu}{\mu_0} \quad (3.12)$$

Permeability can be defined by complex numbers under alternating magnetic field strengths, just like frequency dependent permittivity. In the equation below, power loss is represented by the imaginary part, while stored energy is shown by the real part [119].

$$\mu = \mu' - j\mu'' = \mu_0(\mu_r' - j\mu_r'') \quad (3.13)$$

Unlike diamagnetic materials, ferromagnetic materials have magnetic domains that give them unique permanent magnetic properties. Under an applied magnetic field, ferromagnetic materials can be permanently magnetized. Thus, they can store energy. These magnetic properties make ferromagnetic materials useful in EMI shielding [120]. Eddy-current loss and magnetic hysteresis loss can also contribute to magnetic loss.

Electrical currents which are induced within conductive materials by changing the magnetic field are called Eddy-currents. This electron flow and current circulation leads to loss of electromagnetic energy. Conductive materials can easily be induced through the application of alternating magnetic fields; thus, power loss occurs. Strength of the field, electrical conductivity of the material and the rate of change within the magnetic field affect the Eddy-current loss [119]. Magnetic domain movements and magnetic dipole rotations can also cause magnetic hysteresis loss [117].

3.1.2.2.3. Reflection Loss and Absorption Loss

EM waves can be refracted, diffracted or reflected when they interact with physical objects during their travel. According to these interactions and the intrinsic impedance of the medium in which they travel, some power loss occurs. Homogeneous materials can be characterized by intrinsic impedance. The symbol η is utilized to express the intrinsic impedance and it is denoted in units of ohms (Ω), where ω is angular frequency and σ is the electrical conductivity of the material.

$$\eta = \sqrt{\frac{j\omega\mu}{\sigma + j\omega\epsilon}} \quad (3.14)$$

Intrinsic impedance can be defined as the ratio of permeability (μ) to permittivity (ϵ) for dielectric materials [121, 122]. For an EM wave that is travelling through the free space, wave impedance equals to the intrinsic impedance of the free space ($\eta_0 \approx 120\pi\Omega \approx 377\Omega$) [42].

$$\eta = \sqrt{\frac{\mu}{\epsilon}} \quad (3.15)$$

Incident EM wave changes within a medium that has different intrinsic impedance. In other words, depending on the encountered material and the refractive index of the medium (n), EM waves can change their direction. Refractive index of the medium is represented as in the equation below and varies with relative permeability (μ_r) and relative permittivity as (ϵ_r).

$$n = \sqrt{\mu_r\epsilon_r} \quad (3.16)$$

Refraction brings out reflection. Some of the EM wave power is reflected and the remaining EM wave power is absorbed or transmitted. Low reflection loss can be achieved by obtaining high EM power absorption. The reflection loss is proportional to the relative impedance mismatch between the shielding material surface and incoming wave. Reflectivity coefficient (Γ) can be calculated from the characteristic impedance of the obstacle ($z = \sqrt{\mu_r/\epsilon_r}$) as given below;

$$\Gamma = \frac{z-1}{z+1} \quad (3.17)$$

In order to maximize the absorption, reflectivity coefficient should be minimized. From the equation given above, characteristic impedance, z , should be equal to 1 to obtain zero reflectivity coefficient. In other words, intrinsic impedance values of the material and the free space should be similar. Magnetic materials that have appropriate electrical properties can be good candidates for efficient EM wave absorption, due to their high ϵ_r and low μ_r [125,126]. High conductivity and high μ_r is required for achieving sufficient absorption.

Skin depth is another important parameter for EM wave-material interactions as shown in the shielding theory (in Figure 3.4). It represents the penetration depth of the EM radiation into the material. The depth from the surface of the material where the amplitude of the EM wave attenuates to 37 % of its initial value is named as the skin depth. Equation below shows the skin depth (δ) and the related parameters such as angular frequency ($\omega = 2\pi f$), electrical conductivity (σ) [109,122].

$$\delta_s = \sqrt{\frac{2}{\omega\mu\sigma}} \quad (3.18)$$

Increasing σ reduces the δ ; hence conductive materials behave reflective to EM radiation. Conductive surface modifications and coatings provide the same effect. If the thickness of the shielding material is much less than δ , reflection loss is the main source of the attenuation. Attenuation due to absorption can be negligible. On the contrary, especially at higher frequencies, if the thickness of the shielding material is more than δ , attenuations can be caused by both absorption and reflection [129]. In this study, SWNT thin films were utilized as conductive surface modifications and their effects on EM wave shielding properties of the glass fiber woven fabric layers were investigated.

3.1.3. Characterization Methods for the EMI Shielding Effectiveness

EMI shielding effectiveness and EM wave absorption properties of the materials can be analyzed and investigated through several characterization methods. The most appropriate method is determined by the physical structures and characteristic features of the materials.

Waveguide method, coaxial air line method and free-space method are the most common techniques for the investigation of the shielding properties of the materials. In this study, free-space method was utilized for the analysis of EM reflection and EM transmission properties of the samples.

EM characterization of SWNT thin film coated glass fiber woven fabrics should be characterized by a non-destructive, contact free technique [107, 116, 127].

Therefore, free-space method is the most suitable and effective method. In order to analyze the complex EM behavior of the samples by free-space measurements, a set-up which is similar to the one schematized in Figure 3.8 was utilized.

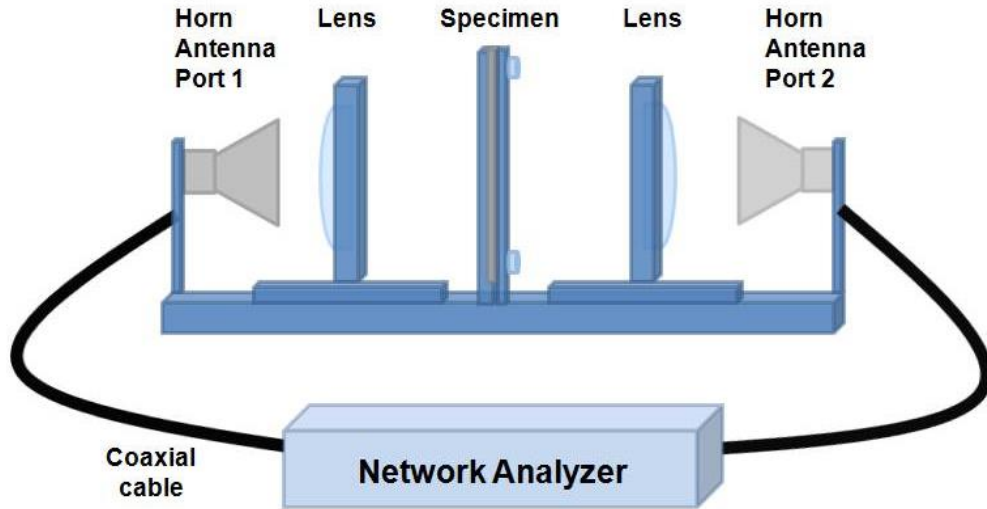


Figure 3.8 Schematic free-space method set-up.

Free-space measurement set-up depends on a basic condensing lens system including two antennas that are fixed and aligned on a stage. Network analyzer generates the power and transfers it via coaxial cables. EM waves that are emitted through the antennas, focused on the specimen surface by condensing lenses. Condensing lenses, specimen and the antennas are all aligned in the same axis. Evaluation of the transmitted and reflected EM power is done by a network analyzer depending on an EM circuit theory.

Free-space measurement technique can be regarded as a suitable method for many samples including inhomogeneous composite materials. However, there are some environmental requirements and regular calibration methods that provide accurate measurements [128]. In order to obtain stable and accurate results, losses originated from electronic devices, characteristic impedances and coaxial junction cables should be decimated by the calibration methods, which are explained below.

3.1.2.1. SOLT (Short – Open – Load - Thru) Calibration

The aim of the SOLT calibration is to define a reference point for the measurements and the calibrations that will be done afterwards. SOLT calibration introduces the apertures to the network analyzer before measurements. This calibration technique is composed of two resistances and an open circuit. Calibration depends on short, open, load and thru standards and has to be done using the network analyzer.

3.1.2.2. Thru - Reflect - Line (TRL) Calibration

TRL calibration method is the general name of calibrations involving two transmission and one reflection references. This calibration is done following SOLT calibration in order to

provide the reference values for the measurement setup. TRM (Thru – Reflect – Match), LRM (Line-Reflect-Match) and LRL (Line-Reflect-Line) calibrations can all be included in TRL calibration.

TRL calibration utilizes the zero-length thru (test ports are directly connected together), reflection and line standards. However, when non-zero length thru (short length of transmission line between the ports) is used instead of zero length thru, the calibration becomes LRL. Moreover, calibration technique which uses the zero length thru, reflection and match standards is named as TRM. In the case of using non-zero length thru, the case is called LRM. TRM and LRM calibrations are more suitable for low frequencies. TRL and LRL calibrations are capable of determining the phase difference caused by the changes in wavelength. Thus TRL or LRL calibrations are more suitable for composite or multilayered specimen analysis. Furthermore, these calibration techniques are more applicable in non-coaxial areas like free-space when compared with other calibration methods.

As it is shown in Figure 3.9, focal length is the distance between a lens and the specimen holder (focal plane). The thru standard is applied by maintaining the distance between two horns equal to twice of the focal distance. The reflect standard is obtained by putting a metal plate at the focal plane and the line standard is achieved by placing the focal plane at a quarter of the wavelength of the free-space.

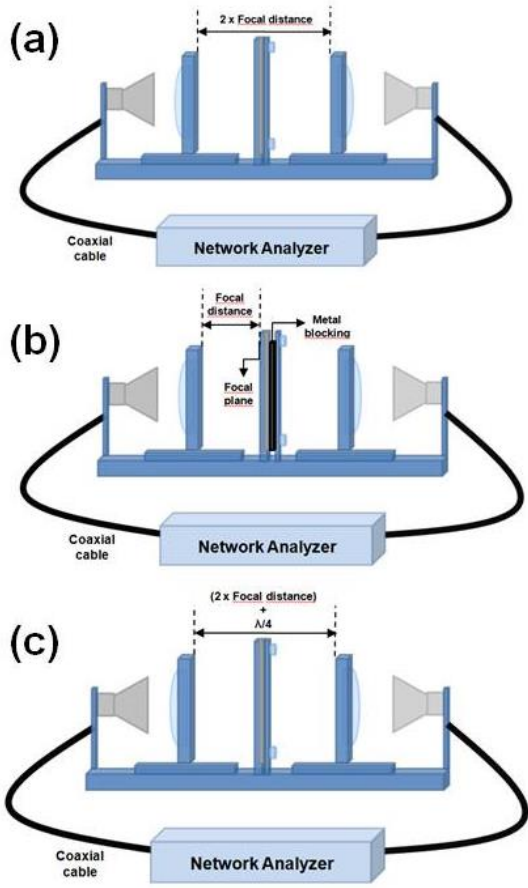


Figure 3.9 TRL calibration method (a) thru, (b) reflect and (c) line standards adopted from [130].

3.1.4. EMI Shielding Materials

Recently, widespread use of electronic devices and the rapid growth of the industry have led to EMI problems. All of the electronic equipment in the industry emits EM radiation in various energy levels and frequencies [131]. To give an example, EM radiation especially at microwave frequency range that effused from mobile phones provides EMI with electronic devices and as a result undesired electronic problems occur. Awareness of the EMI problem has made the manufacturers of many sectors including communication, medicine and military sources to comply with the shielding requirements [91].

The reflection mechanism is the most basic one for EMI shielding. Sheet metals, metal screens or grids are the most common materials that are being used for reflection. Shielding material should not have any holes larger than the EM wave's wavelength. A continuous, enduring conductive layer can increase the shielding effectiveness. Shielding material design, modifications and novel composites have caught the attention of researchers. In the recent years, shielding materials, which are effective and also flexible and light-weight become quite popular. Conductive polymer coatings [91], composites with conductive fillers, textile based composite materials [91, 130], carbon-based materials such as graphite or carbon fibers [91] are some of the good EMI shielding materials.

Among all the shielding materials, CNTs appear to be one of the most promising candidates. Both MWNTs and SWNTs were utilized in several shielding applications in literature. Efficiency of a composite material can be improved with high intrinsic conductivity, high aspect ratio or high mechanical strength. All of these properties make CNTs excellent for EMI shielding [131]. Polymer matrices filled with MWNTs investigated in a frequency range of 8.12 – 12.4 GHz and provide 20 dB of SE with 7 % nanotube loading [132,133]. In addition highly conductive SWNT - polymer composite was achieved a 49 dB SE at 10 MHz for 15 % loading [133].

SWNT films have been widely used and studied by many researchers as transparent electrodes due to their high conductivities and transmittance at visible and infrared wavelengths [134]. Especially for transparent EMI shielding material designs, SWNT thin films can be regarded as an ideal option. SWNT films with 80 % optical transmittance has shown 33 dB SE at 10 GHz and 46 dB at 10 MHz, which satisfy the requirements of an efficient shielding for commercial applications such as mobile phones. Furthermore, 80 % transparent, another frequently used shielding material ITO, has 30 dB SE at 1 GHz, while SWNT thin film was 36 dB at the same frequency [135]. In this study, SE properties of SWNT film coated glass fiber woven fabrics were investigated between the frequency range of 18 – 40 GHz.

3.1.5. EM Wave Absorbing Materials

EM wave absorbing materials have been widely used in many areas. EMI problems led to, false imaging, insufficient performance, unwanted noise and increased clutter on radar systems. Especially microwave absorbing materials help to eliminate or reduce these problems. Development and enhancement of EM wave absorbing materials have attracted researchers' attention and increased their utilization areas.

Many industries including military and civilian purposes are designing materials or coatings to improve the absorbing efficiency. An EM wave absorbing material should have altered electrical and magnetic properties providing broadband frequency absorbance. These materials reduce the reflected and transmitted EM radiation and provide an increase in the absorption. EM energy transfers into internal energy within the material.

Recently, development of both certain frequency and broadband radar systems become very popular. Multi-frequency absorbing systems require novel material designs that could avoid extra weight due to increased thickness [119]. Therefore, intrinsic properties of the EM absorbing materials should be simultaneously modified and improved.

According to the utilized loss mechanism, EM wave absorbing materials can be classified into a few groups [115]. Salisbury Screen absorbers are one of the most common products in this era which works with a principle of quarter wavelength (λ) resonance. System consists of a resistive sheet/film that is placed $\lambda/4$ away from a metal block/surface as represented schematically in Figure 3.10 (a). Incident EM wave is partially reflected from the thin resistive sheet and partially transmitted through the metal sheet. Transmitted EM wave that remains in between the resistive sheet and the metal sheet is reflected back from the metal surface. Internally reflected EM wave and EM wave reflected from the resistive sheet have equal amplitudes and $\lambda/2$ phase difference resulting in a destructive interference. Therefore, zero reflection and transmission takes place due to the metal sheet, while absorption quality is enhanced. Figure 3.10 (b) illustrates the whole system. Dallenbach layers that are shown in Figure 3.10 (c), are very similar to Salisbury screens, where the only difference between them is the dielectric filling. Space between the resistive film and metallic plate is filled with a homogeneous lossy media. They are favorable for composite materials in the sandwich structure. Salisbury screens and Dallenbach layers are the most basic and common types of EM wave absorbing systems. However, they are inconvenient in broadband applications [109, 119].

Jaumann absorbers are developed in order to obtain the minimum reflection loss for optimum bandwidth. They are basically composed of multi-layered Salisbury sheets and dielectric fillers. As the number of layers increase, reflection loss decreases at a range of frequency values rather than at an individual frequency as shown in Figure 3.10 (d). They have many advantages; but, adding layers increases their thickness and weight consecutively [6].

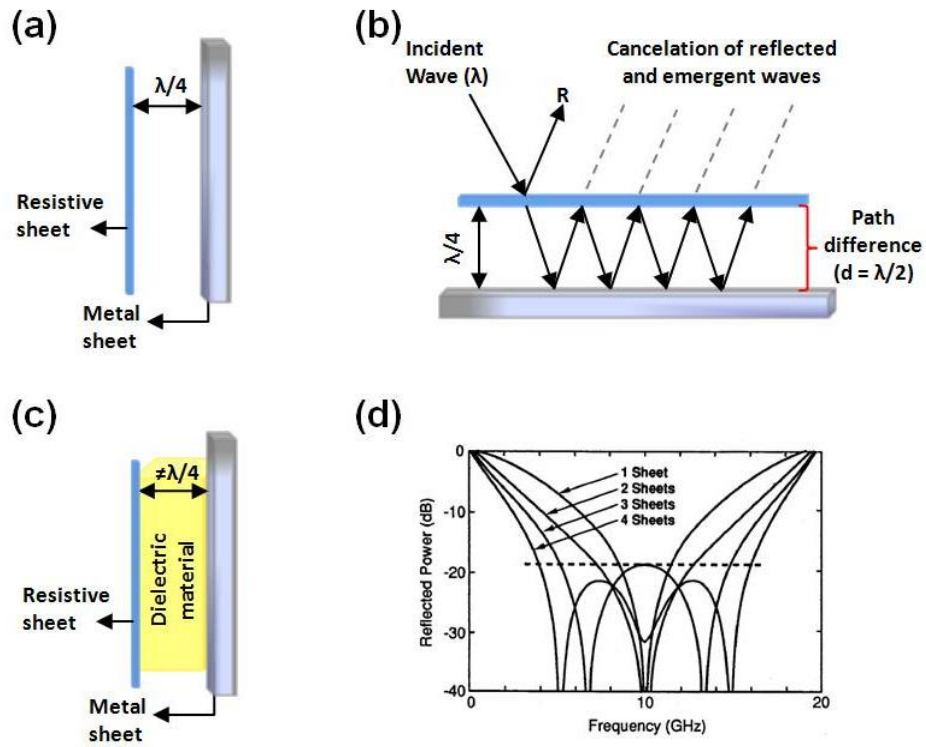


Figure 3.10 Schematic of electromagnetic wave absorbing materials (a) Salisbury screens, (b) Dallenbach layer, (c) Jaumann absorbers and (d) performance of multi-layered Jaumann absorbers Adopted from [119].

Utilization of magnetic absorbers, especially magnetic ceramics is another common technique for EM wave absorption. Ferrite layers in polymer composites, ferrite grids [115], cobalt (Co), nickel (Ni) or iron (Fe) ferromagnetic particles [139] can be used in EM absorption. Various metallic geometries and textures such as grids, loops and crosses can be utilized as a filter for certain frequencies [109].

EM wave absorbing polymeric materials, on the other hand, are light-weight and are widely used in automotive, marine industry, consumer goods, civil or aerospace applications including others. Glass fiber reinforced plastics (GFRP) are composite materials that can effectively satisfy many absorption requirements. They are cost effective insulating materials with superior mechanical properties [139].

GFRPs can be produced in two main forms as chopped-strand glass fibers and glass fiber woven fabrics [140]. Weaving textures of the glass fiber woven fabrics, as shown in Figure 3.11, can change the ductility and load carrying capacity of the GFRP composites due to their anisotropic mechanical properties.

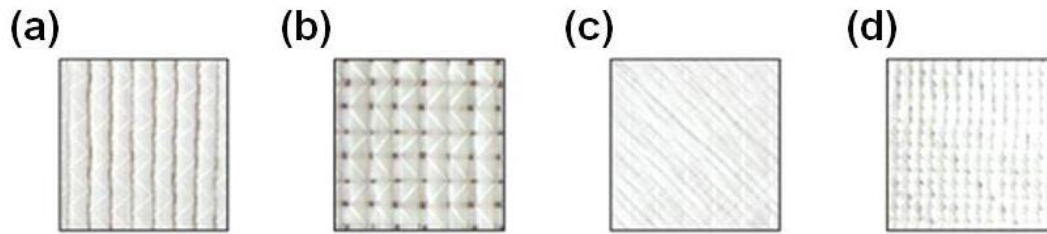


Figure 3.11 (a) Uniaxial, (b) ± 90 biaxial, (c) ± 45 biaxial and (d) quadraxial weaving textures in glass fiber woven fabrics [107].

EM wave absorbing properties of GFRP composites were investigated in recent years. EM particle filled matrices, heat treatments, surface modifications like thin film coatings are some of the applications examined on GFRPs [117, 130, 127]. Surface modified glass fiber reinforced multi-layered structures are also providing efficient EM wave absorption [117].

3.2. EXPERIMENTAL DETAILS

3.2.1. General Procedure

All the glass fiber woven fabrics utilized as a substrate in this study were purchased from METYX Telateks Textile Products Co. Ltd. Glass fibers were woven in quadraxial geometry with $0^\circ / \pm 45^\circ / 90^\circ$ reinforcement angles in order to provide a robust mesh. Schematic view of quadraxial glass fiber woven fabric is given in Figure 3.12. The areal density of the glass fiber woven fabrics is 625 gr /m^2 , the thickness of a woven sheet is about $0.40 \text{ }\mu\text{m}$ and the tensile strength of a glass fiber woven fabric is given as 208 MPa [141]. Fiber diameter and the tensile strength value have an inverse proportion, where decreasing fiber diameter provides increased strength values. Figure 3.12 illustrates the woven glass fiber bundles and the geometry.

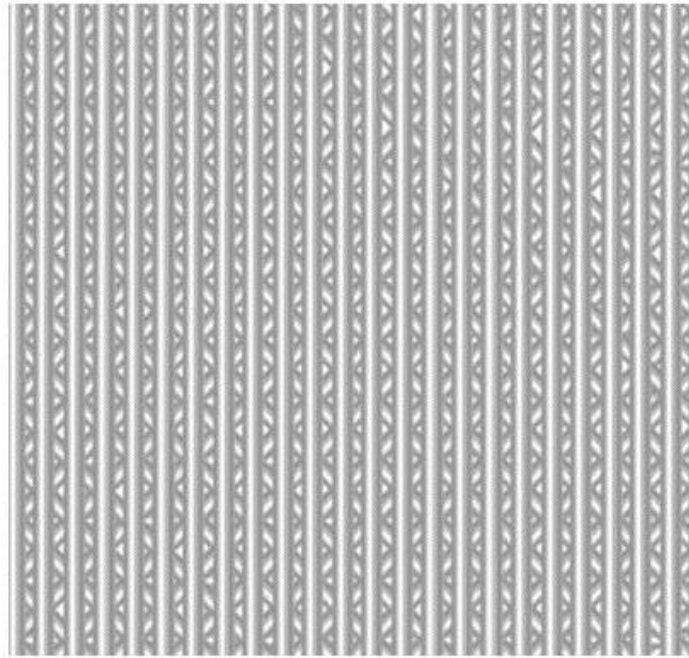


Figure 3.12 Schematic view of quadriaxial glass fiber woven fabric.

In order to investigate the EMI shielding properties, glass fiber woven fabrics and conductive SWNT networks were used. Inherently Q625 type woven glass fibers transmit EM radiation. Therefore, in order to supply an increased EM loss, glass fiber woven fabric surfaces were modified through the deposition of SWNT networks at different densities. Spray coating method was preferred to prepare large area, homogeneous SWNT films. All samples had a size of 10 x 10 cm. EMI shielding properties of the SWNT network coated glass fiber woven fabrics were characterized by free-space method with a network analyzer. Analyses were done through 18 – 40 GHz frequency range.

3.2.2. Spray coating of SWNT films

Before starting the experiments to prepare SWNT coatings, all glass ware (petridishes, beakers etc.) were cleansed as written in Section 2.2.1.1. In order to fabricate large area SWNT films on a rough surface like glass fiber woven fabrics, spray coating method was utilized.

Spray coating process can be summarized within two steps. First step is the dispersion of SWNTs in a suspension. Arc-discharge synthesized and purified P3 type SWNTs were purchased from Carbon Solutions, Inc. in powder form. Dispersions of SWNTs were prepared in N-methyl-2-pyrrolidone (NMP) (Sigma-Aldrich) at a nanotube concentration of 0.1 mg/ml. SWNT suspensions were sonicated for 10 minutes using a 20 kHz ultrasonic tip-sonicator. The ultrasonic tip-sonicator (Sonopuls, HD 2070) was operated at 80 % for an approximate sonication power of 70 Watts. All suspensions were subsequently sonicated in a low power ultrasonic bath for 10 minutes. After sonication, SWNT dispersions or inks were kept at rest for a while to let the SWNT bundles precipitate.

Second step is the spray deposition of SWNT inks. Glass fiber woven fabric substrates were placed onto a hot-plate and maintained at 230 °C. An air-brush was utilized for the spray coating of SWNT inks onto the glass fiber woven fabric surfaces.

3.2.3. Characterization Methods

3.2.3.1. Scanning Electron Microscope (SEM)

SWNT film coated glass fiber woven fabrics were analyzed by field emission scanning electron microscope (FE-SEM, Nova NanoSEM 430) that is operated at an accelerating voltage of 10 kV. Despite the presence of conductive SWNT film coatings; in order to prevent charging top surfaces of the fabrics were coated with gold.

3.2.3.2. Free-Space Technique

EMI shielding characterization method for the SWNT film coated glass fiber woven fabrics was free-space technique. Free-space technique is the most suitable and applicable method on anisotropic and inhomogeneous samples. The system utilized for the analysis is shown in Figure 3.13. As mentioned in Section 3.1.3 free-space system consists of two antennas, two lenses and a specimen holder. All the analyses were done by the network analyzer (Anritsu 37269E) within 18- 40 GHz frequency range. Before the measurements, TRL calibration was done.



Figure 3.13 Free-space measurement set-up and the network analyzer.

Free-space set-up can evaluate both reflected and transmitted waves. Transmission and reflection losses were collected and recorded through the frequency range of interest for several samples. Network analyzer shows the reflection loss S_{11} , caused by the EM wave which is emitted from horn antenna 1 and reflected back to horn antenna 1. S_{11} is basically the return loss and can be described as the ratio of the reflected wave power (P_R) to the initial wave power (P_0). S_{21} represents the EM waves which are emitted from horn antenna 1 and transmit through the sample finally reaching to horn antenna 2. In other words S_{21} is the transmission loss that is the ratio of transmitted power (P_T) to the initial power. S_{22} and S_{12} are the expressions of the reflection and transmission losses from the second port in a symmetrical sense.

Reflection (S_{11}) and transmission losses (S_{21}) are given as:

$$S_{11} = 10 \log \frac{|P_R|}{|P_0|} \quad (3.19)$$

$$S_{21} = 10 \log \frac{|P_T|}{|P_0|} \quad (3.20)$$

Reflection and transmission loss values were utilized in the equation below to calculate the EM wave absorption percentage (% EM Wave Absorption) based on the conservation of energy.

$$\% \text{ EM Wave Absorption} = (1 - 10^{S_{11}/10} - 10^{S_{21}/10}) \times 100 \quad (3.21)$$

3.3. RESULTS

Free-space method was utilized for the characterization of the samples, and the effect of the SWNT film density on the EMI shielding characteristic of the glass fiber woven fabrics was investigated.

The films were coated on Q625 woven fabrics, using the air-brush spraying method at a stable SWNT dispersion concentration of 0.1 mg/ml. Various dispersion quantities (25 – 100 ml) were sprayed and analyzed. Figure 3.14 shows a photograph of SWNT films coated on glass fiber woven fabrics with three different dispersion volumes corresponding to varying SWNT areal densities. 2.5×10^{-5} mg/mm², 5.0×10^{-5} mg/mm², 7.5×10^{-5} mg/mm² and 10×10^{-5} mg/mm² are the areal density values corresponding to sprayed dispersion volumes of 25, 50, 75 and 100 ml, respectively.

SEM images given in Figure 3.15 also show the areal density difference and the morphologies of the SWNT films on glass fiber woven fabrics at two different sprayed dispersion volumes of (a) 25 and (b) 100 ml. SWNT film morphologies observed in the SEM images provide information about the correlation between the electrical conductivity

and the areal density of the SWNT film. A SWNT film should provide a homogeneous conductive layer. Otherwise, the inhomogeneous SWNT network cannot overcome the degradation due to charging. 25 ml SWNT dispersion sprayed glass fiber woven fabric is less conductive than the sample coated with 100 ml spraying volume. High surface roughness and large level differences within the sample surfaces cause an inhomogeneous SWNT distribution. Therefore, sheet resistance values of the SWNT films on the glass fiber woven fabric surfaces could not be measured precisely using the sheet resistance measurement set-up. Sheet resistance values of the SWNT thin films on glass substrates that have the same SWNT dispersion concentrations were measured in order to analyze the effect of varying areal density. Sheet resistance values of the SWNT films on glass substrates change within 1 – 10 $k\Omega/\square$ range.

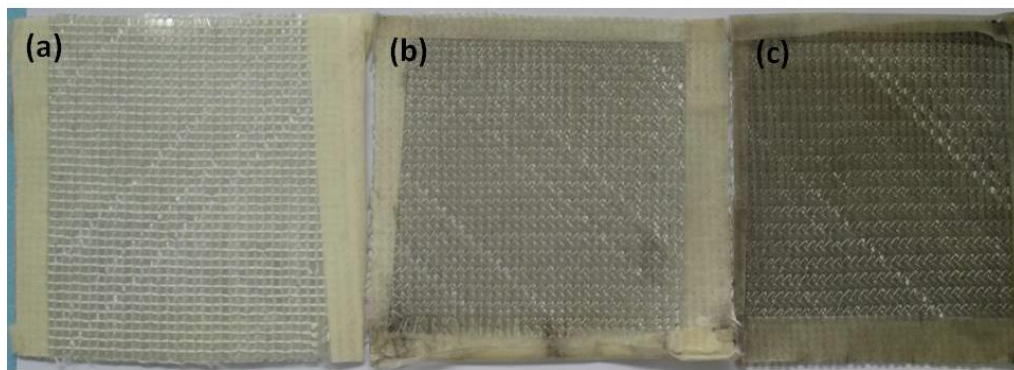


Figure 3.14 Photograph of spray coated SWNT films on glass fiber woven fabrics for (a) 25 ml, (b) 50 ml and (c) 100 ml sprayed dispersion volumes.

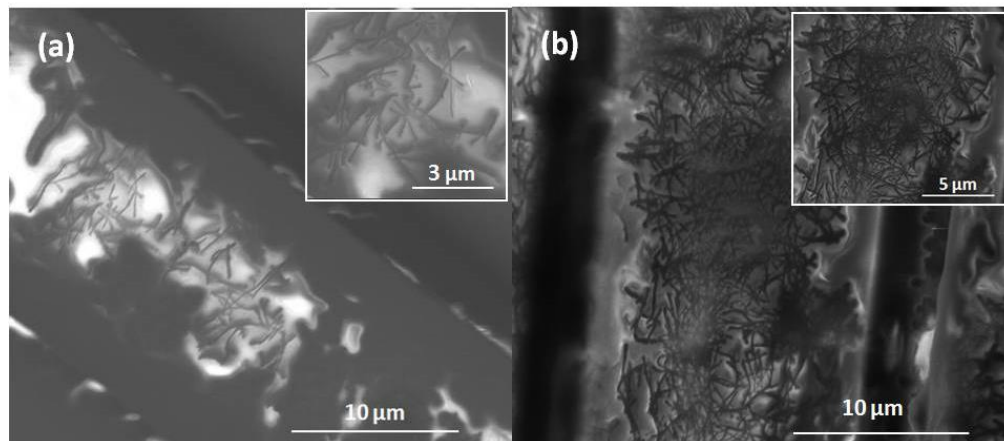


Figure 3.15 SEM images of spray coated SWNT films on glass fiber woven fabrics for (a) 25 ml and (b) 100 ml sprayed dispersion volumes.

Q625 type glass fiber woven fabrics are insulators and they do not possess any magnetic properties. Thus, transmission loss can be expected to be more dominant over reflection loss. Glass fiber woven fabrics show dielectric characteristics due to 57% glass content. This amount provides mainly a dielectric loss and the resulting interaction with the incident EM wave can be seen in Figure 3.16, on the reflection loss curve for the bare glass fiber woven. In this graph lower reflection loss (R) values in terms of dB correspond to weaker reflection from the material surface. Therefore, the uncoated bare glass fiber woven fabric seems to be the least reflective against the EM radiation.

Due to the surface conductivity achieved, SWNT film coated glass fiber woven fabrics become more reflective. Reflection loss curves show the direct proportionality between the SWNT amount and the reflection loss. As the SWNT film areal densities increase, the surface conductivity of the spray coated glass fiber woven fabrics increases. Therefore, maximum reflection loss was achieved at the maximum SWNT film density at a 100 ml sprayed dispersion volume. Even though reflection loss values of 25, 50, 75 and 100 ml SWNT dispersion coated Q625 type woven fabrics show slight variation, it is evident that reflection loss increases with increasing SWNT film areal density, and hence surface conductivity. Reflection loss amount can be controlled by changing SWNT film areal density. There is not a significant reflection loss fluctuation through the 18 – 40 GHz frequency range. However, it was found that reflection loss slightly increases with frequency.

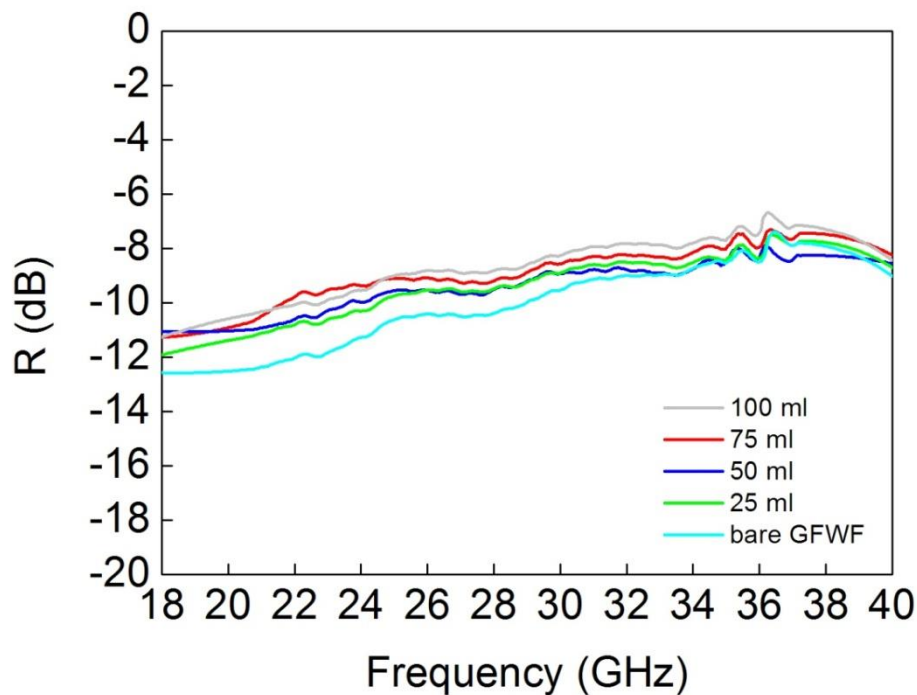


Figure 3.16 Reflection loss versus frequency plot for the SWNT film coated glass fiber woven fabrics with different spraying volumes.

In Figure 3.17, transmission loss curves for the same samples are given. Transmission characteristic difference between SWNT film coated and bare Q625 type glass fiber woven fabrics is remarkable. Q625 type woven fabrics are insulators mainly composed of glass, silane as the polymeric sizing and air trapped in the woven structure [4]. Thus, they behave transparent to EM waves, where bare glass fiber woven fabric shows the maximum transmission loss, as expected. Conductive SWNT film coating for 100 ml sprayed dispersion volume reduces the transmission loss by about 50 % at 30 GHz. Transmission loss decreases with increasing SWNT film areal density.

SWNT film coated glass fiber woven fabrics both reflect and transmit EM waves within the 18 – 40 GHz frequency range. 100 ml sprayed dispersion volume provides an average reflection loss of -9 dB and an average transmission loss of -1.2dB. This sample providing the highest surface conductivity shows 11.5 % EM wave absorption according to Equation 3.21.

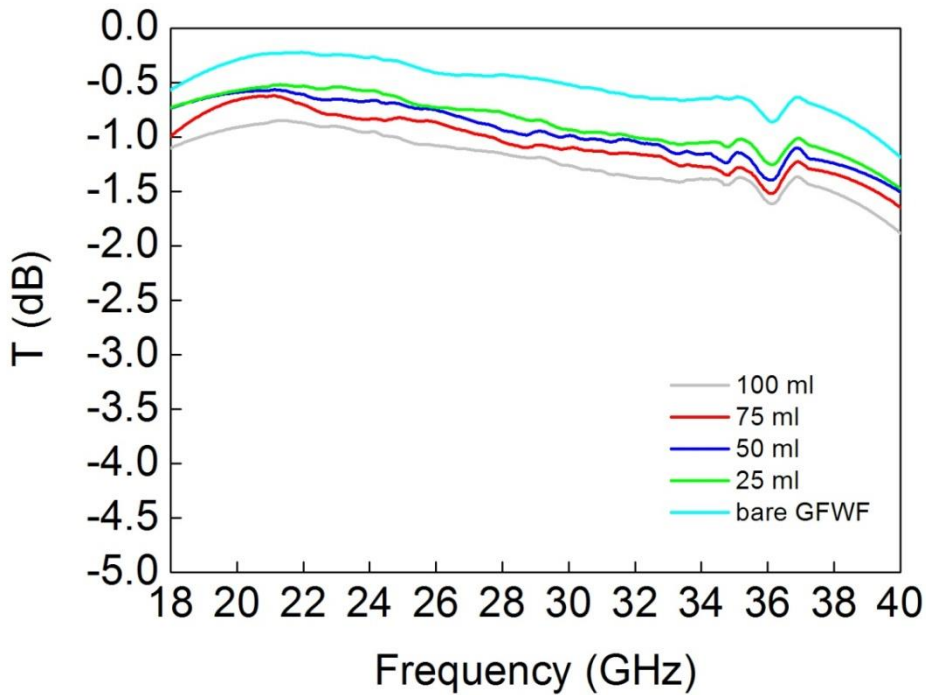


Figure 3.17 Transmission loss versus frequency plot for the SWNT film coated glass fiber woven fabrics with different spraying volumes.

EM wave absorption percentages were calculated using Equation 3.21 based on the reflection and transmission loss values. % EM wave absorption versus frequency plot is shown in Figure 3.18. Approximately a maximum of 15 % EM wave absorption can be achieved by SWNT film coated Q625 type glass fiber woven fabrics. Although absorption values of 25, 50, 75 and 100 ml SWNT dispersion coated Q625 type woven fabrics show

slight variation, it is evident that absorption increases with SWNT film areal density, and hence surface conductivity.

Despite the electrical conductivities they provide, SWNT film coated glass fiber woven fabrics did not show the expected EMI shielding performance improvement, especially in terms of reflection loss. This is probably caused by the inhomogeneous and discontinuous film coverage on the rough glass fiber woven fabric surfaces. This problem may have resulted from insufficient SWNT dispersion, inevitable droplet formation during the spray coating, NMP – glass fiber woven fabric interaction or the porous structure of the Q625 type fabrics.

An improved SWNT dispersion prepared in a different solvent with a different surfactant can change the results. It can be seen obviously from the plots that increasing surface conductivity increases the reflection loss, and consequently EM wave absorption percentages also show certain increase. In addition to this, cascading SWNT film coated glass fiber woven fabrics to form a multilayer structure, in which the surface conductivities are increasing from the outermost fabric to the interior may result in more absorbing characteristics where, such multilayer structures can potentially be used as reinforcements in polymer matrix EM wave absorbing composites.

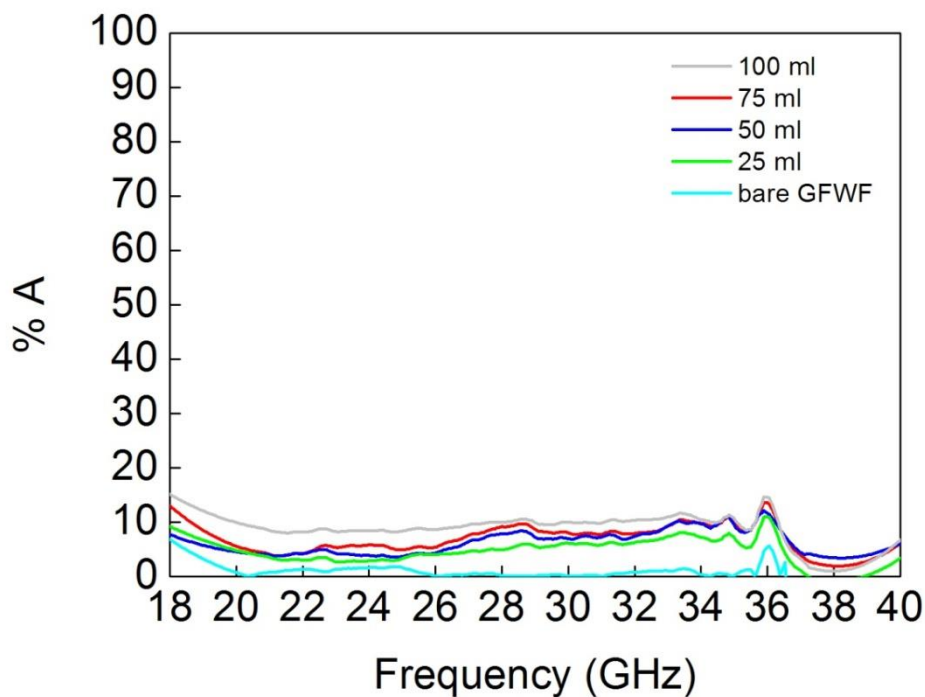


Figure 3.18 % EM wave absorption versus frequency plot for the SWNT film coated glass fiber woven fabrics with different spraying volumes.

CHAPTER 4

CONCLUSIONS AND FUTURE RECOMMENDATIONS

4.1. Conclusions

In this thesis, SWNT thin film fabrication processes and EMI shielding characteristic of the SWNT thin films were investigated.

In the first part, SWNT thin films were fabricated utilizing two different cost-effective deposition techniques. Vacuum filtration and spray coating methods were used to fabricate SWNT thin films at different densities. At the first stage of the fabrication, SWNT dispersions were prepared. Effect of surfactants, SWNT types, sonication type and also sonication time were examined and a stable SWNT dispersion was optimized. It is found that; SDS assisted P3 type SWNT dispersions provide the most stable and homogeneous solutions when compared to different surfactant - SWNT combinations. At the second stage, utilizing that stabilized SWNT dispersion, deposition of the SWNT thin films were done using vacuum filtration method at different filtration volumes on glass and PET substrates. Transmittance of the fabricated SWNT thin films was found to be varying between 50 % - 91 % (at 550 nm) and sheet resistance values were within the 500 Ω/\square -2 k Ω/\square range, respectively. SWNT thin films that were deposited at different filtration volumes were immersed in HNO₃ and SOCl₂ baths, in order to enhance their optoelectronic properties. Optoelectronic measurements of the fabricated SWNT thin films revealed that lower sheet resistance values can be achieved at higher transmittance, following acid functionalization. Thin films with a sheet resistance of 180 Ω/\square was obtained at a transmittance of 91%. Centrifugation of SWNT dispersions and the effect of centrifugation on SWNT thin films was further investigated and it is found that, 200 Ω/\square sheet resistance can be achieved at an optical transmittance of 90 % (at 550 nm) without any acid treatment. Mechanical stability of the SWNT thin films on PET substrates was also evaluated and compared with the ITO. Electrical measurements revealed that sheet resistance of SWNT thin films were unaffected, while ITO failed due to crack propagation. SWNT thin films were coated on 10 x 10 cm glass substrates for large area applications using both vacuum filtration and spray coating methods. Vacuum filtration technique needs larger filtration setups for large area applications, thus spray coating method is more suitable for SWNT thin film deposition over larger areas. However, sheet resistance values of the SWNT thin films were not homogeneous as in vacuum filtered SWNT thin films.

In the second part, EMI shielding properties of the SWNT thin films were investigated within a frequency range of 18 – 40 GHz. SWNT thin films were spray coated on glass fiber woven fabrics and EM wave reflection and transmission properties were analyzed using a network analyzer and free-space method. Moreover EM wave absorption properties were calculated utilizing reflection and transmission data. The results revealed that SWNT

film coated glass fiber woven fabrics were more reflective and the reflection loss amount can be controlled by changing SWNT film areal density. As the SWNT film density increase, surface conductivity of the spray coated glass fiber woven fabrics increase. Maximum reflection loss was achieved at the maximum film density. In contrast, maximum transmission was achieved at the minimum film density. However, SWNT film coated glass fiber woven fabrics did not show the expected performance despite the electrical conductivities they provide. The densest SWNT film showed approximately a maximum of 15 % EM wave absorption and 7 dB reflection loss at 36 GHz.

4.2. Future Recommendations

In this thesis, NMP dispersed SWNT solutions were used for spray coating in the second part. An air-brush technique was preferred for SWNT film deposition due to the practical usage for large area applications. Another solvent or surfactant assisted SWNT can be utilized to improve the stability of the SWNT dispersion and spray coating can be done using ultrasonic atomizer as mentioned in Section 2.2.3 in order to make a more homogeneous SWNT film. Spraying parameters can also be changed depending on the new SWNT dispersion. Different SWNT dispersion concentrations can be examined with less destructive solvents unlike NMP in order to have a continuous SWNT network.

On the other hand, EM wave properties of SWNT thin films electrical conductivity can be improved; thus, the EMI shielding efficiency can be further increased by the increasing reflection loss. Moreover, SWNT thin film coated glass fiber woven fabrics can be investigated within lower frequency ranges in order to compare with the literature.

Magnetic nanoparticles can be attached onto the SWNT thin films and their reflection properties can be investigated.

Multilayered specimen analysis can be done as a further investigation following the SWNT dispersion and deposition improvements.

REFERENCES

- [1] M. S. Dresselhaus, G. Dresselhaus, K. Sugihara, I. L. Spain, H. A. Goldberg, 1988, "Graphite Fibers and Filaments," Springer Ser. Mater. Sci., 5, pp. 12, 16, 17.
- [2] M. S. Dresselhaus, M. Endo, 2001, "Relation of Carbon Nanotubes to Other Carbon Materials," Appl. Phys., 80, pp. 11-28.
- [3] V. N. Popov, 2004, "Carbon Nanotubes: Properties and Applications," Materials Science & Engineering R-Reports," 43, pp. 61-102.
- [4] P. J. F. Harris, 1999, "Carbon Nanotubes and Related Structures," Cambridge University Press. pp. 3-5.
- [5] M. Meyyappan, 2005, "Carbon Nanotubes: Science and Applications," pp.2
- [6] A. Govindaraj, 2005, "Nanotubes and Nanowires," RSC Publications, pp.1
- [7] S. Iijima, 1991, "Helical Microtubules of Graphitic Carbon," Nature, 354, pp. 56-58.
- [8] S. Iijima, T. Ichihashi, 1993, Nature, 363, 603-605
- [9] S. Bandow, M. Takizawa, K. Hirahara, M. Yudasaka, S. Iijima, 2001, Chem. Phys. Lett., 337, 48-54
- [10] X. Zhou, 2008, "Carbon Nanotube Transistors, Sensors and Beyond," PhD. Thesis Cornell University, pp. 28.
- [11] T. Yamabe, 1995, Synthetic Metals, 70, 1511-1518
- [12] University of Surrey, <http://www.umi.surrey.ac.uk/people/profiles/postgrads>, (Last Visited on: 17.07.2012).
- [13] M. Ouyang, J. L. Huang, C.L. Cheung, C.M. Lieber, 2001, Science, 292, 702-705
- [14] M. S. Dresselhaus, G. Dresselhaus, R. Saito, 1992, Phys. Rev. B., 45, 6234-6242
- [15] H. E. Unalan, 2006, "Single Walled Carbon Nanotube Thin Films: Properties and Applications," PhD. Thesis, Rutgers University, pp.12, 157.
- [16] J. C. Charlier, X. Blase, S. Roche, 2007, "Electronic and Transport Properties of Nanotubes," Reviews of Modern Physics, 79, pp. 677-732.
- [17] M. S. Dresselhaus, P. C. Eklund, 2000, "Phonons in Carbon Nanotubes," Advances in Physics, 49, pp. 705-814.
- [18] H. Katura, Y. Kumazawa, Y. Maniwa, I. Umezumi, S. Suzuki, Y. Ohtsuka, Y. Achiba, 1999, "Optical Properties of Single-Wall Carbon Nanotubes," Synthetic Metals, 103, pp. 2555-2558.

- [19] C. Journet, W. K. Maser, P. Bernier, A. Loiseau, M. Lamyde la Chapelle, S. Lefrant, P. Deniard, R. Leek, J. E. Fischerk, 1997, "Large-scale production of single-walled carbon nanotubes by the electric-arc technique," *Nature*, 388, pp.756-758.
- [20] C. Journet, P. Bernier, 1998, "Production of Carbon Nanotubes," *Appl. Phys. A*, 67, pp. 1-9.
- [21] D. Kondo, S. Sato, Y. Awano, 2006, "Low-temperature Synthesis of Single-Walled Carbon Nanotubes with a Narrow Diameter Distribution Using Size-Classified Catalyst Nanoparticles," *Chemical Physics Letters*, 422, pp. 481–487.
- [22] F. Du, Y. Ma, X. Lv, Y. Huang, F. Li, Y. Chen, 2006, "The Synthesis of Single-Walled Carbon Nanotubes with Controlled Length and Bundle Size Using the Electric Arc Method," *Carbon*, 44, pp. 1298–1352.
- [23] Y. Su, Z. Yang, H. Wei, E. S. Kong, Y. Zhang, 2011, "Synthesis of Single-Walled Carbon Nanotubes with Selective Diameter Distributions Using DC Arc Discharge Under CO Mixed Atmosphere," *Applied Surface Science*, 257, pp. 3123–3127.
- [24] Y. Saito, Y. Tani, 2000, "Diameters of Single-Wall Carbon Nanotubes Depending on Helium Gas Pressure in an Arc Discharge," *J. Phys. Chem. B*, 104, pp. 2495-2499.
- [25] Z. Li, P. liu, B. Zhao, H. Wang, Y. Zhang, 2008, "Improving the Synthesis of Single-Walled Carbon Nanotubes by Pulsed Arc Discharge in Air by Preheating the Catalysts," *Carbon*, 46, pp. 1792-1828.
- [26] T. Guo, P. Nikolaev, A. Thess, D.T. Colbert, R. E. Smalley, 1995, "Catalytic Growth of Single Walled Nanotubes by Laser Vaporization, *Chem. Phys. Lett.*, 243, pp. 49-54.
- [27] A.A. Puzos, D.J. Styers-Barnett, C.M. Rouleau, H. Hu, B. Zhao, I.N. Ivanov, D.B. Geohegan, 2008, "Cumulative and Continuous Laser Vaporization Synthesis of Single Wall Carbon Nanotubes and Nanohorns," *Appl Phys A*, 93, pp. 849–855.
- [28] X. Lin, M. H. Rummeli, T. Gemming, T. Pichler, D. Valentin, G. Ruani, C. Taliani, 2007, "Single-Wall Carbon Nanotubes Prepared with Different Kinds of Ni–Co Catalysts: Raman and Optical Spectrum Analysis," *Carbon*, 45, pp. 196-207.
- [29] M. H. Rummeli, E. Borowiak-Palen, T. Gemming, T. Pichler, M. Knupfer, M. Kalbac, L. Dunsch, O. Jost, S. Ravi P. Silva, W. Pompe, B. Buchner, 2005, "Novel Catalysts, Room Temperature and the Importance of Oxygen for the Synthesis of Single-Walled Carbon Nanotubes," *Nano Lett.*, 5, pp. 1209-1215.
- [30] P. Nikolaev, W. Holmes, E. Sosa, P. Boul, S. Arepalli, L. Yowell, 2006, "Effect of Vaporization Temperature on the Diameter and Chiral Angle Distributions of Single-Walled Carbon Nanotubes", *Journal of Nanoscience and Nanotechnology*, 10, pp. 3780-3789.
- [31] G. Che, B. B. Lakshmi, C. R. Martin, E. R. Fisher, R. S. Ruoff, 1998, "Chemical Vapor Deposition Based Synthesis of Carbon Nanotubes and Nanofibers Using a Template Method," *Chemistry of Materials*, 10, pp. 260-267.

- [32] J. Kong, H. T. Soh, A. M. Cassell, C. F. Quate, H. J. Dai, 1998, "Synthesis of Individual Single-Walled Carbon Nanotubes on Patterned Silicon Wafers," *Nature*, 395, pp. 878-881.
- [33] J. H. Hafner, M. J. Bronikowski, B. R. Azamian, P. Nikolaev, A. G. Rinzler, D. T. Colbert, K. A. Smith, R. E. Smalley, 1998, "Catalytic Growth of Single-Wall Carbon Nanotubes from Metal Particles," *Chemical Physics Letters*, 296, pp. 195-202.
- [34] C. E. Baddour, C. Briens, 2005, "Carbon Nanotube Synthesis: A Review," *International Journal of Chemical Reactor Engineering*, 3.
- [35] M. E. Itkis, S. Niyogi, M. E. Meng, M. A. Hamon, H. Hu, R. C. Haddon, 2002, "Spectroscopic Study of the Fermi Level Electronic Structure of Single-Walled Carbon Nanotubes," *Nano Letters*, 2, pp. 155-159.
- [36] M. S. Dresselhaus, G. Dresselhaus, Ph. Avouris, 2001, "Carbon Nanotubes," *Topics Appl. Phys.* 80, 11–28 Springer-Verlag Berlin Heidelberg.
- [37] J. Li, L. Hu, L. Wang, Y. Zhou, G. Gruner, T. J. Marks, 2006, "Organic Light-Emitting Diodes Having Carbon Nanotube Anodes" *Nano Letters*, 6, pp. 2472-2477.
- [38] W.A.de Heer, A. Chatelain, D. Ugarte, 1995, "A Carbon Nanotube Field-Emission Electron Source," *Science*, 270, 1179-1181.
- [39] P. Calvert, 1999, "Nanotube composites: A recipe for strength," *Nature*, 399, 210-211.
- [40] H.J. Dai, A.G. Rinzler, D.T. Colbert, R.E. Smalley, 1996, "Nanotubes as Nanoprobes in Scanning Probe Microscopy," *Nature*, 394, 147-149.
- [41] H. Nishijima, S. Kamo, S. Akita, Y. Nakayama, K.I. Hohmura, S.H. Yoshimura, K. Takeyasu, 1999, "Carbon Nanotube Tips for Scanning Probe Microscopy: Preparation by a Controlled Process and Observation of Deoxyribonucleic Acid," *Appl. Phys. Lett.*, 74, 4061-4063.
- [42] R. Martel, T. Schmidt, H.R. Shea, T. Hertel, Ph. Avouris, 1998, "Single- and Multi-Wall Carbon Nanotube Field-Effect Transistors," *Appl. Phys. Lett.*, 73, 2447-2449.
- [43] A. Bachtold, P. Hadley, T. Nakanishi, C. Dekker, 2001, "Logic Circuits with Carbon Nanotube Transistors," *Science*, 294, 1317-1320.
- [44] Z. Yao, C. L. Kane, C. Dekker, 2000, "High-Field Electrical Transport in Single-Wall Carbon Nanotubes," *Phys. Rev. Lett.*, 84, 2941-2944.
- [45] E. S. Snow, J.P. Novak, P. M. Campbell, D. Park, 2003, "Random Networks of Carbon Nanotubes as an Electronic Material," *Appl. Phys. Lett.*, 82, 2145-2147.
- [46] E. Artukovic, M. Kaempgen, D.S. Hecht, S. Roth, G. Gruner, 2005, "Transparent and Flexible Carbon Nanotube Transistors," *Nano Lett.*, 5, 757-760.
- [47] K. Bradley, J.P. Gabriel, G. Gruner, 2003, "Flexible Nanotube Electronics," *Nano Lett.*, 3, 1353-1355.

- [48] S. H. Hur, O. Ok. Park, J. A. Rogers, 2005, "Extreme Bendability of Single-Walled Carbon Nanotube Networks Transferred from High-Temperature Growth Substrates to Plastic and Their Use in Thin-Film Transistors," *Appl. Phys. Lett.*, 86, 243502.
- [49] Q. Cao, S. H. Hur, Z. T. Tao, Y. Sun, C. Wang, M. A. Meitl, M. Shim, J. A. Rogers, 2006, "Highly Bendable, Transparent Thin-Film Transistors That Use Carbon-Nanotube-Based Conductors and Semiconductors with Elastomeric Dielectrics," *Adv. Mater.*, 18, pp. 304-309.
- [50] T. Ohta, A. Bostwick, T. Seyller, K. Horn, E. Rotenberg, 2006," Controlling the Electronic Structure of Bilayer Graphene," *Science*, 313, pp. 951.
- [51] E. Bekyarova, M. E. Itkis, N. Cabrera, B. Zhao, A.P. Yu, J. B. Gao, R. C. Haddon, 2005, "Electronic Properties of Single-Walled Carbon Nanotube Networks," *J. Am. Chem. Soc.*, 127, pp. 5990.
- [52] L. Hu, D. S. Hecht, G. Gruner, 2004, "Percolation in Transparent and Conducting Carbon Nanotube Networks," *Nano Lett.*, 4, pp. 2513
- [53] Z. Yao, H.W.C. Postma, L. Balents, C. Dekker, 1999, "Carbon Nanotube Intramolecular Junctions," *Nature*, 402, pp. 273.
- [54] D. H. Zhang, K. Ryu, X. L. Liu, E. Polikarpov, L. Ly, M. E. Tompson, C. W. Zhou, 2006, "Transparent, Conductive, and Flexible Carbon Nanotube Films and Their Application in Organic Light-Emitting Diodes," *Nano Lett.*, 6, pp. 1880.
- [55] B. Dan, G. C. Irvin, M. Pasquali, 2009, "Continuous and Scalable Fabrication of Transparent Conducting Carbon Nanotube Films," *ACS Nano*, 3, pp. 835.
- [56] K. Nomura, H. Ohta, K. Ueda, T. Kamiya, M. Hirano, H. Hosono, 2003, "Thin-Film Transistor Fabricated in Single-Crystalline Transparent Oxide Semiconductor," *Science*, 300, pp. 1269-1272.
- [57] G. Thomas, 1997, "Materials Science: Invisible Circuits," *Nature*, 389, pp. 907-908.
- [58] B. I. Yakobson, C. J. Brabec, J. Bernholc, 1996, "Nanomechanics of Carbon Tubes: Instabilities beyond Linear Response," *Phys. Rev. Lett.*, 76, pp. 2511.
- [59] S. Iijima, C. Brabec, A. Maiti, J. Bernholc, 1996, "Structural Flexibility of Carbon Nanotubes," *J. Chem. Phys.*, 104, pp. 2089.
- [60] C. M. Trottier, P. Glatkowski, P. Wallis, J. Luo, 2005, "Properties and Characterization of Carbon-Nanotube-Based Transparent Conductive Coating," *J. Soc. Inf. Disp.*, 13, pp. 759.
- [61] X. Zeng , Q. Zhang , R. Yu , C. Lu, 2010, "A New Transparent Conductor: Silver Nanowire Film Buried at the Surface of a Transparent Polymer," *Adv. Mater.*, 22, pp. 4484–4488.

- [62] M. F. Islam,* E. Rojas, D. M. Bergey, A. T. Johnson, and A. G. Yodh, 2003, "High Weight Fraction Surfactant Solubilization of Single-Wall Carbon Nanotubes in Water," *Nano Letters*, 3, pp. 269-273.
- [63] V. C. Moore, M. S. Strano, E. H. Haroz, R. H. Hauge, R. E. Smalley, 2003, "Individually Suspended Single-Walled Carbon Nanotubes in Various Surfactants," *Nano Letters*, 3, pp. 1379-1382.
- [64] R. Rastogi, R. Kaushal, S.K. Tripathi, A. L. Sharma, I. Kaur, L. M. Bharadwaj, 2008, "Comparative study of carbon nanotube dispersion using surfactants," *Journal of Colloid and Interface Science*, 328, pp. 421-428.
- [65] O. Matarredona, H. Rhoads, Z. Li, J. H. Harwell, L. Balzano, D. E. Resasco, 2003, "Dispersion of Single-Walled Carbon Nanotubes in Aqueous Solutions of the Anionic Surfactant NaDDBS," *J. Phys. Chem.*, 107, pp. 13357-13367.
- [66] K. Yurekli, C. A. Mitchell, R. Krishnamoorti, 2004, "Small-Angle Neutron Scattering from Surfactant-Assisted Aqueous Dispersions of Carbon Nanotubes," *J. AM. CHEM. SOC.*, 126, pp. 9902-9903.
- [67] H. Wang, 2009, "Dispersing Carbon Nanotubes Using Surfactants," *Current Opinion in Colloid & Interface Science*, 14, pp. 364-371.
- [68] L. Vaisman, H. D. Wagner, G. Marom, 2006, "The role of surfactants in dispersion of carbon nanotubes," *Advances in Colloid and Interface Science*, 128-130, pp. 37-46.
- [69] P. Vichchulada, M. A. Cauble, E. A. Abdi, E. I. Obi, Q. Zhang, M. D. Lay, 2010, "Sonication Power for Length Control of Single-Walled Carbon Nanotubes in Aqueous Suspensions Used for 2-Dimensional Network Formation," *J. Phys. Chem. C*, 114, pp. 12490-12495.
- [70] S. N. Barman, M. C. LeMieux, J. Baek, R. Rivera, Z. Bao, 2010, "Effects of Dispersion Conditions of Single-Walled Carbon Nanotubes on the Electrical Characteristics of Thin Film Network Transistors," *App. Mat. & Int.*, 2, pp. 2672-2678.
- [71] J. Wang, W. J. Blau, 2008, "Solvent Effect on Optical Limiting Properties of Single-Walled Carbon Nanotube Dispersions," *J. Phys. Chem. C*, 112, pp. 2298-2303.
- [72] S. Giordani, S. D. Bergin, V. Nicolosi, S. Lebedkin, M. M. Kappes, W. J. Blau, J. N. Coleman, 2006, "Debundling of Single-Walled Nanotubes by Dilution: Observation of Large Populations of Individual Nanotubes in Amide Solvent Dispersions," *J. Phys. Chem. B*, 110, pp. 15708-15718.
- [73] G. W. Lee, S. Kumar, 2005, "Dispersion of nitric acid-treated SWNTs in organic solvents and solvent mixtures," *Journal of Physical Chemistry B*, 109, pp. 17128-17133.
- [74] J. Y. Hwang, A. Nish, J. Doig, S. Douven, C. W. Chen, L. C. Chen, R. J. Nicholas, 2008, "Polymer Structure and Solvent Effects on the Selective Dispersion of Single-Walled Carbon Nanotubes," *J. Am. Chem. Soc.*, 130, pp. 3543.

- [75] M. H. A. Ng, L. T. Hartadi, H. Tan, C. H. P. Poa, 2008, "Efficient Coating of Transparent and Conductive Carbon Nanotube Thin Films on Plastic Substrates," *Nanotechnology*, 19, pp. 205703.
- [76] S. Kim, J. Yim, X. Wang, D. D. C. Bradley, S. Lee, J. C. deMello, 2010, "Spin- and Spray-Deposited Single-Walled Carbon-Nanotube Electrodes for Organic Solar Cells," *Adv. Funct. Mater.*, 20, pp. 2310–2316.
- [77] M. Kaempgen, G.S. Duesberg, S. Roth, 2005, "Transparent Carbon Nanotube Coatings," *Applied Surface Science*, 252, pp. 425–429.
- [78] M. D. Lima, M. J. de Andrade, C. P. Bergmann, and S. Roth, 2008 "Thin, conductive, carbon nanotube networks over transparent substrates by electrophoretic deposition," *Journal of Materials Chemistry*, 18, pp. 776-779.
- [79] X. Mei, J. Ouyang, 2011, "Highly conductive and transparent single-walled carbon nanotube thin films fabricated by gel coating," *J. Mater. Chem.*,
- [80] M. A. Meitl, Y. Zhou, A. Gaur, S. Jeon, M. Usrey, M.S. Strano, J.A. Rogers, 2004, "Solution Casting and Transfer Printing Single-Walled Carbon Nanotube Films," *Nano Letters*, 4, pp. 1643-1647.
- [81] N. P. Armitage, J.C.P. Gabriel, G. Gruner, 2004, "Quasi-Langmuir–Blodgett thin film deposition of carbon nanotubes," *J. Appl. Phys.*, 95, pp. 3228-3230.
- [82] E. C. Venancio, P. C. Wang, N. Consolin-Filho, A. G. MacDiarmid, 2009, "Flexible Thin Films of Single-Walled Carbon Nanotubes Deposited on Plastic Substrates," *Journal of Nanoscience and Nanotechnology*, 9, pp. 567-571.
- [83] T. Hasan, V. Scardaci, P. Tan, A. G. Rozhin, W. I. Milne, A. C. Ferrari, 2007, "Stabilization and "Debundling" of Single-Wall Carbon Nanotube Dispersions in N-Methyl-2-pyrrolidone (NMP) by Polyvinylpyrrolidone (PVP)," *J. Phys. Chem. C*, 111, pp. 12594-12602.
- [84] M. Majumder, C. Rendall, M. Li, N. Behabtu, J. A. Eukel, R. H. Hauge, H. K. Schmidt, M. Pasquali, 2010, "Insights into the Physics of Spray Coating of SWNT Films," *Chemical Engineering Science* 65, pp. 2000–2008.
- [85] H. Jung, N. V. Quy, N. D. Hoa, D. Kim, 2010, "Transparent Field Emission Device from a Spray Coating of Single-Wall Carbon Nanotubes," *Journal of The Electrochemical Society*, 157, pp. J371-J375.
- [86] Y. Maeda, K. Komoriya, K. Sode, J. Higo, T. Nakamura, M. Yamada, T. Hasegawa, T. Akasaka, T. Saito, J. Lu, S. Nagase, 2011, Preparation and Characterization of Transparent and Conductive Thin Films of Single-Walled Carbon Nanotubes," *Nanoscale*, 2011, 3, p. 1904.
- [87] A. Schindler, J. Brilla, N. Fruehaufa, J. P. Novak, Z. Yaniv, 2007, "Solution-Deposited Carbon Nanotube Layers for Flexible Display Applications," *Physica E*, 37, pp.119–123.

- [88] V. Scardaci, R. Coull, J. N. Coleman, 2010, "Very Thin Transparent, Conductive Carbon Nanotube Films on Flexible Substrates," *App. Phys. Lett.*, 97, pp. 023114.
- [89] Q. Liu, T. Fujigaya, H. Cheng, N. Nakashima, 2010, "Free-Standing Highly Conductive Transparent Ultrathin Single-Walled Carbon Nanotube Films," *J. Am. Chem. Soc.*, 132, pp. 16581–16586.
- [90] R. C. Tenent, T. M. Barnes, J. D. Bergeson, A. J. Ferguson, B. To, L. M. Gedvilas, M. J. Heben, J. L. Blackburn, 2009, "Ultrasoother, Large-Area, High-Uniformity, Conductive Transparent Single-Walled-Carbon-Nanotube Films for Photovoltaics Produced by Ultrasonic Spraying," *Adv. Mater.*, 21, pp. 3210–3216.
- [91] M. A. Seo, J. H. Yim, Y. H. Ahn, F. Rotermund, D. S. Kim, 2008, "Terahertz Electromagnetic Interference Shielding Using Single-Walled Carbon Nanotube Flexible Films," *App. Phys. Lett.*, 93, p. 231905.
- [92] J. H. Yim, Y. S. Kim, K. H. Koh, and S. Lee, 2008, "Fabrication of Transparent Single Wall Carbon Nanotube Films with Low Sheet Resistance," *Journal of Vacuum Science and Technology B: Microelectronics and Nanometer Structures*, 26, pp. 851-855.
- [93] Q. Cao, J. A. Rogers, 2009, "Ultrathin Films of Single-Walled Carbon Nanotubes for Electronics and Sensors: A Review of Fundamental and Applied Aspects," *Adv. Mater.*, 21, pp. 29–53.
- [94] Z. Wu, Z. Chen, X. Du, J. M. Logan, J. Sippel, M. Nikolou, K. Kamaras, J. R. Reynolds, D. B. Tanner, A. F. Hebard, and A. G. Rinzler, 2004 "Transparent, Conductive Carbon Nanotube Films," *Science*, 305, pp. 1273-6.
- [95] M. W. Rowell, 2011, "Carbon Nanotube Transparent Electrodes for Photovoltaic Applications," PhD. Thesis, Stanford University, pp. 24.
- [96] Y. Zhou, L. Hu, G. Grüner, 2006 "A Method of Printing Carbon Nanotube Thin Films," *Applied Physics Letters*, 88, p. 123109.
- [97] M. Brumbach, P. A. Veneman, F. S. Matrikar, T. Schulmeyer, A. Simmonds, W. Xia, P. Lee, N. R. Armstrong, 2007 "Surface Composition and Electrical and Electrochemical Properties of Freshly Deposited and Acid-etched Indium Tin Oxide Electrodes," *Langmuir*, 23, pp. 11089-11099.
- [98] H.E. Unalan, P. Hiralal, D. Kuo, B. Parekh, G. Amaratunga, M. Chhowalla, 2008 "Journal of Materials Chemistry, 18, p. 5909.
- [99] H. E. Unalan, G. Fanchini, A. Kanwal, A. Du Pasquier, M. Chhowalla, 2006, "Design Criteria for Transparent Single-Wall Carbon Nanotube Thin-Film Transistors," *Nano Lett.*, 6, pp. 677- 682.
- [100] D. Johnston, M. F. Islam, A. G. Yodh, A. T. Johnson, 2005, "Electronic devices based on purified carbon nanotubes grown by high-pressure decomposition of carbon monoxide," *Nat. Mater.*, 4, p.589-592.

- [101] L. Hu, G. Gruner, D. Li, R.B. Kaner, J. Cech, 2007 “Patternable Transparent Carbon Nanotube Films for Electrochromic Devices,” *Journal of Applied Physics* 101, p. 016102.
- [102] A. Behnam, J. Johnson, Y. Choi, L. Noriega, M.G. Ertosun, Z. Wu, A.G. Rinzler, P. Kapur, K.C. Saraswat, A. Ural, 2008, “Metal-Semiconductor-Metal Photodetectors Based on Single-Walled Carbon Nanotube Film–GaAs Schottky Contacts,” *Journal of Applied Physics*, 103, pp. 114315.
- [103] R. K. Jackson, 2009, “Development of Single Wall Carbon Nanotube Transparent Conductive Electrodes for Organic Electronics,” PhD. Thesis, Georgia Institute of Technology.
- [104] D. C. Giancoli, *Physics for Scientists & Engineers* (Prentice Hall, New Jersey, 2000).
- [105] M. Gupta and E. W. W. Leong, *Microwaves and Metals* (Wiley, 2007).
- [106] IPAC, *Infrared Windows*, (Infrared Processing and Analysis Center, California, 2010).
- [107] G.Gurer, 2008, “Design and Characterization of Electromagnetic Wave Absorbing Structural Composites,” MSc. Thesis, Middle East Technical University, pp.6 -43.
- [108] R. C. Che, C. Y. Zhi, C. Y. Liang, X. G. Zhou, 2006, “Fabrication and Microwave Absorption of Carbon Nanotubes/CoFe₂O₄ Spinel Nanocomposites,” *Appl. Phys. Lett.* 88,p. 033105.
- [109] E. F. Knott, J. F. Shaeffer, M. T. Tuley, 1993, *Radar Cross Section*, SciTech Publishing.
- [110] Z. P. Wu, M. M. Li, Y. Y. Hu, Y. S. Li, Z. X. Wang, Y. H. Yin, Y. S. Chena, X. Zhoua, 2011, “Electromagnetic Interference Shielding of Carbon Nanotube Macrofilms,” *Scripta Materialia*, 64, p.809-812.
- [111] C. Xiang, Y. Pan, X. Liu, X. Sun, X. Shi, 2005, “Microwave Attenuation of Multiwalled Carbon Nanotube-Fused Silica Composites,” *Appl. Phys. Lett.* 87, p.123103.
- [112] N.Li, Y.Huang, F. Du, X. He, X. Lin, H. Gao, Y. Ma, F. Li, Y. Chen, P. C. Eklund, 2006, “Electromagnetic Interference (EMI) Shielding of Single-Walled Carbon Nanotube Epoxy Composites,” *Nano Letters*, 6, P.1141-1145.
- [113] W. Callister, *Materials Science and Engineering: An Introduction* (Wiley, 2006).
- [114] J. F. Shackelford, *Introduction to Material Science for Engineers* (Prentice Hall, New Jersey, 2005).
- [115] P. S. Neelakanta, *Handbook of Electromagnetic Materials*, 1995, CRC Press, Washington D.C.
- [116] L. F. Chen, C. K. Ong, C. P. Neo, V. V. Varadan and V. K. Varadan, 2004, “*Microwave Electronics Measurement and Characterization*,” John Wiley & Sons Ltd.

- [117] J. Huo, L. Wang and H. Yu, 2009, "Polymeric Nanocomposites for Electromagnetic Wave Absorption", *Journal of Materials Science*, 44, pp. 3917-3927.
- [119] D. Ebbing and S. D. Gammon, 2001, *General Chemistry*, Houghton Mifflin Company, New York.
- [120] C. K. Yuzcelik, 2003, *Radar Absorbing Materials Design*, MSc Thesis, Naval Postgraduate School, Systems Engineering.
- [121] W. Mingzhong, 2000, "Electromagnetic and microwave absorbing properties of iron fibre-epoxy resin composites," *Journal of Physics D: Applied Physics*, 33, p. 2398.
- [122] J. Daintith, 2005, *A dictionary of science "Oxford paperback reference"*, Oxford University Press, Oxford.
- [123] D. Pozar, *Microwave Engineering*, 2004, Wiley.
- [124] Y. Qing, W. Zhou, F. Luo, D. Zhu, 2009, "Microwave- absorbing and Mechanical Properties of Carbonyl-iron/epoxy-silicone resin coatings," *Journal of Magnetism and Magnetic Materials* 321, p. 25-27.
- [125] J. Li, J. Huang, Y. Qin, F. Ma, 2007, "Magnetic and Microwave Properties of Cobalt Nanoplatelets," *Materials Science and Engineering B: Solid-State Materials for Advanced Technology* 138, p.199-204.
- [126] Y. Fan, H. Yang, X. Liu, H. Zhu, G. Zou, 2008, "Preperation and Study on Radar Absorbing Materials of Nickel-Coated Carbon Fiber and Flake Graphite", *Journal of Alloys and Compounds*, 461, p.490-494.
- [127] N. Gagnon, 2002, "Design and Study of a Free - Space Quasi Optical Measurement System," PhD. Thesis, University of Ottawa.
- [128] D. K. Ghodgaonkar, V. V. Varadan, V. K. Varadan, 2009, "Free-space Measurement of Complex Permittivity and Permeability of Magnetic Materials at Microwave Frequencies," *IEEE Transactions on Instrumentation and Measurement*, 39, p. 387.
- [129] P. Saini, M. Arora, 2012, "Microwave Absorption and EMI Shielding Behavior of Nanocomposites Based on Intrinsically Conducting Polymers, Graphene and Carbon Nanotubes, *New Polymers for Special Applications*," 112, p.45.
- [130] I. S. Seo, W. S. Chin, D. G. Lee, 2004, "Characterization of Electromagnetic Properties of Polymeric Composite Materials with Free Space Method," *Composite Structures*, 66, p.533-542.
- [131] F. Borondics, K. Kamaras, M. Nikolou, D. B. Tanner, Z. H. Chen, A. G. Rinzler, 2006, "Charge Dynamics in Transparent SWNT Thin Films from Optical Transmission Measurements," *Phys. Rev. B*, 74, p.045431.
- [132] D.D.L. Chung, 2001, "Electromagnetic Interference Shielding Effectiveness of Carbon Materials," *Carbon*, 2, p. 279-285.

- [133] M. A. Seo, J. H. Yim, Y. H. Ahn, F. Rotermund, D. S. Kim, 2008, "Terahertz Electromagnetic Interference Shielding Using Single-Walled Carbon Nanotube Flexible Films," *Appl. Phys. Lett.* 93,p. 231905.
- [134] Y. Yang, M.C. Gupta, 2005, "Novel Carbon Nanotube-Polystyrene Foam Composites for Electromagnetic Interference Shielding," *Nano Letters*, 5, p. 2131-2134.
- [135] Z.Liu, G. Bai, Y. Huang, Y. Ma, F. Du, F. Li, 2007, "Reflection and Absorption Contributions to the Electromagnetic Interference Shielding of Single-Walled Carbon Nanotube/Polyurethane Composites," *Carbon*, 45, p. 821-827.
- [136] Z. Wu, Z. Chen, X. Du, J. M. Logan, J. Sippel, M. Nikolou, K. Kamaras, J. R. Reynolds, D. B. Tanner, A. F. Hebard, A. G. Rinzler, 2004, *Science*, 305, p. 1273.
- [137] H. Xu, S. M. Anlage, L. Hu, G. Gruner, 2007, "Microwave Shielding of Transparent and Conducting Single-Walled Carbon Nanotube Films," *Applied Physics Letters*, 90, p. 183119.
- [138] M. S. Pinho, M. L. Gregori, R. C. R. Nunes, B. G. Soares, 2002, " Performance of Radar Absorbing Materials by Waveguide Measurements for X- and Ku-band Frequencies," *European Polymer Journal*, 38, p. 2321- 2327.
- [139] K. K. Chawla, 2008, *Composite Materials: Science and Engineering*, Springer London London.
- [140] T. F. Wallenberger, J. C. Watson and H. Li, 2001, "ASM Metals Handbook", edited by A. I. H. Committee, ASM International, p. 77.
- [141] METYX Glass Fiber Reinforcement Catalog, (Last Visited on: 12.02.2013).